DAMAGE OF CONCRETE WITH EPOXY COATED REINFORCEMENT DUE TO CORROSION, FREEZE-THAW AND FATIGUE WITH APPLICATION TO BRIDGE DECKS

By

Matthew Garratt

A THESIS

Submitted to
Michigan State University
in partial fulfillment of the requirements
for the degree of

MASTER OF SCIENCE

Civil Engineering

2011

ABSTRACT

DAMAGE OF CONCRETE WITH EPOXY COATED REINFORCEMENT DUE TO CORROSION, FREEZE-THAW AND FATIGUE WITH APPLICATION TO BRIDGE DECKS

By

Matthew Garratt

The deterioration of reinforced concrete bridge decks due to corrosion of the steel bars is a common problem. Epoxy coated reinforcement (ECR) is known to perform better than plain (black) steel, but the appropriate maintenance schedule for ECR bridge decks is not well established. The goal of this project was to compare damage of concrete reinforced with ECR and black steel due to corrosion, freeze-thaw, and fatigue loading for application to bridge decks.

Concrete specimens with ECR and black steel reinforcement were artificially aged using freeze-thaw cycling and accelerated corrosion to simulate the varying ages of bridge decks. These specimens were repaired and then simultaneously subjected to fatigue loading, freeze-thaw cycles, and continued accelerated corrosion to simulate the loading on bridge decks.

Two methods were used to compare the deterioration of specimens with black steel and ECR. The first method was based on corrosion data. It was found that the corrosion rate was about 2.5 times lower for ECR than for black steel, implying that the effects of corrosion-induced damage appear more slowly in ECR. The second method utilized X-ray tomography to obtain images of internal cracking in the specimens. Image-processing software was used to compute the volume of cracks inside the specimens. It took about 4 times longer for the ECR specimens to have the same volume of cracks as black steel specimens. The damage was insensitive to the type of repair performed.

ACKNOWLEDGMENTS

First and foremost, I give thanks to the Lord Jesus Christ. This thesis would not have been possible without the strength and knowledge given to me by Him.

I also want to thank my advisor, Dr. Ron Harichandran for giving me the opportunity work on this research. I cannot thank him enough for his financial support for graduate school, advice on this project, and guidance for this thesis. I would also like to thank Dr. Rigoberto Burgueño for his advice and suggestions on this research. His passion and professionalism in the classroom as a teacher encouraged me to want to pursue an advanced degree and to become involved in research.

The Michigan Department of Transportation provided funding for this research. Their support is gratefully acknowledged. My fellow colleague Dr. Gang Zhang and I collaborated in completing this project. I thank him for his advice and help in conducting this research. Finally, I want to thank Siavosh Ravanbakhsh for his help in the lab conducting the experiments throughout this project. His expertise was invaluable to this research and his humor made those tough times in the lab tolerable.

TABLE OF CONTENTS

LIST OF TABLES	V
LIST OF FIGURES	vii
CHAPTER 1: INTRODUCTION	
CHAPTER 2: SPECIMEN PREPARATION 2.1 Specimen Design and Casting Preparation 2.2 Accelerated Freeze-Thaw Test 2.3 Accelerated Corrosion 2.4 Specimen Repair	18 25 27
CHAPTER 3: EXPERIMENTAL DESIGN. 3.1 Fatigue Testing. 3.2 Static Testing.	37
CHAPTER 4: EXPERIMENTAL TEST RESULTS	47
CHAPTER 5: X-RAY COMPUTED TOMOGRAPHY 5.1 X-Ray Scanning 5.2 Image Processing.	54
CHAPTER 6: INTERPRETATION OF RESULTS AND CONCLUSIONS 6.1 Corrosion Damage 6.2 Image-Based Damage Results 6.3 Summary and Conclusions 6.4 Final Remarks	61 66 68
APPENDIX A: STIFFNESS DATA	73
APPENDIX B: X-RAY IMAGES AND PROCESSED CRACK IMAGES	77
APPENDIX C: CORROSION CHARGE DATA	85
REFERENCES	9.4

LIST OF TABLES

Table 2.1: Test Matrix	20
Table 2.2: Corrosion Charge for Different Damage Levels	29
Table 3.1: List of Groups of Specimens	39
Table 4.1: Survival Under Fatigue Loading	52
Table 5.1: Image-Based Damage	60
Table 6.1: Estimates of Time in the Field for Black Steel	62
Table 6.2: Time Scale Factors from Image-Based Damage	67
Table A.1: Black Level 0	73
Table A.2: Epoxy Level 0 Unrepaired	73
Table A.3: Black Level 1 Unrepaired	73
Table A.4: Epoxy Level 1 Unrepaired	73
Table A.5: Black Level 1 Repaired	74
Table A.6: Epoxy Level 1 Repaired	74
Table A.7: Black Level 2 Unrepaired	74
Table A.8: Epoxy Level 2 Unrepaired	74
Table A.9: Black Level 2 Repaired	74
Table A.10: Epoxy Level 2 Repaired	74
Table A.11: Black Level 3 Unrepaired	75
Table A.12: Epoxy Level 3 Unrepaired	75
Table A.13: Black Level 3 Repaired	75
Table A.14: Epoxy Level 3 Repaired	75
Table A.15: Black Level 4 Unrepaired	75
Table A.16: Epoxy Level 4 Unrepaired	75
Table A.17: Black Level 4 Repaired	76
Table A.18: Epoxy Level 4 Repaired	76
Table C.1: B-0 Corrosion Data	85

Table C.2: E-0 Corrosion Data	
Table C.3: B-1-N Corrosion Data	85
Table C.4: E-1-N Corrosion Data	86
Table C.5: B-1-R Corrosion Data	86
Table C.6: E-1-R Corrosion Data	86
Table C.7: B-2-N Corrosion Data	86
Table C.8: E-2-N Corrosion Data	87
Table C.9: B-2-R Corrosion Data	87
Table C.10: E-2-R Corrosion Data	88
Table C.11: B-3-N Corrosion Data	88
Table C.12: E-3-N Corrosion Data	89
Table C.13: B-3-R Corrosion Data	89
Table C.14: E-3-R Corrosion Data	90
Table C.15: B-4-N Corrosion Data	90
Table C.16: E-4-N Corrosion Data	91
Table C.17: B-4-R Corrosion Data	91
Table C 18: E-4-R Corrosion Data	92

LIST OF FIGURES

Figure 2.1: Specimen Configuration.	19
Figure 2.2: ECR with Damage in Coating	21
Figure 2.3: Dimensions and Reinforcement Layouts of Pilot Beams	22
Figure 2.4: Load-Displacement Response of Pilot Test Beams	23
Figure 2.5: Failure Patterns of Pilot Test Beams	24
Figure 2.6: Molds before Casting	25
Figure 2.7: Specimens after Freeze-Thaw Test	26
Figure 2.8: Accelerated Corrosion Test Setup	28
Figure 2.9: Corrosion Curves for BSR and ECR	29
Figure 2.10: Specimen after Level 1 Corrosion	30
Figure 2.11: Specimen after Level 2 Corrosion	30
Figure 2.12: Specimen after Level 3 Corrosion	31
Figure 2.13: Specimen after Level 4 Corrosion	31
Figure 2.14: Specimen Repaired with Epoxy Overlay	32
Figure 2.15: Oversized Shallow Concrete Overlay	33
Figure 2.16: Specimen with Shallow Concrete Overlay	34
Figure 2.17: Specimen with Waterproofing and HMA Overlay	35
Figure 2.18: Oversized Deep Concrete Overlay	35
Figure 2.19: Specimen with Deep Concrete Overlay	36
Figure 3.1: Environmental Chamber	38
Figure 3.2: Fatigue Test Setup	39
Figure 3.3: Corrosion Setup	41
Figure 3.4: Static Test Setup	43
Figure 3.5: Smooth Surface for LVDT	43
Figure 3.6: Data Obtained from Multiple Static Tests	45

Figure 3.7:	Schematic of Static Test	.45
Figure 3.8:	Typical Load-Displacement Graph	.46
Figure 4.1:	Normalized Stiffness Values (Level 0 Unrepaired)	.48
Figure 4.2:	Normalized Stiffness Values (Level 1 Unrepaired)	.48
Figure 4.3:	Normalized Stiffness Values (Level 1 Repaired)	.49
Figure 4.4:	Normalized Stiffness Values (Level 2 Unrepaired)	.49
Figure 4.5:	Normalized Stiffness Values (Level 2 Repaired)	.50
Figure 4.6:	Normalized Stiffness Values (Level 3 Repaired)	.50
Figure 4.7:	Normalized Stiffness Values (Level 4 Unrepaired)	.51
Figure 4.8:	Normalized Stiffness Values (Level 4 Repaired)	.51
Figure 4.9:	Charge vs. Fatigue Cycles	.53
Figure 5.1:	X-Ray Scanning Setup	.55
Figure 5.2:	Example of X-Ray Scan	.55
Figure 5.3:	Photograph of Scanned Specimen	.56
Figure 5.4:	Crack Cropped from Image	.57
Figure 5.5:	Crack with Inverted Colors	.57
Figure 5.6:	Crack with Enhanced Brightness and Contrast	.58
Figure 5.7:	Crack after Applying Bandpass Filter	.58
Figure 5.8:	Crack after Applying Threshold	.59
Figure 5.9:	3D Rendering of Crack	.60
Figure 6.1:	Charge vs. Time for Phase 1 and Phase 2	.63
Figure 6.2:	Residual and Weighted Residual Plots for Black Steel	.64
Figure 6.3:	Residual and Weighted Residual Plots for ECR	.64
Figure 6.4:	Early Stage of Accelerated Corrosion for ECR	.65
Figure 6.5:	Image-Based Damage vs. Time	.67
Figure 6.6:	Residual Plot with All Points Included	.68
Figure B.1:	B-0 X-Ray Image and Crack after Applying Threshold	.77

Figure B.2: E-0 X-Ray Image with No Crack	77
Figure B.3: B-1-N X-Ray Image and Crack after Applying Threshold	78
Figure B.4: E-1-N X-Ray Image with No Crack	78
Figure B.5: B-1-R X-Ray Image and Crack after Applying Threshold	79
Figure B.6: E-1-R X-Ray Image with No Crack	79
Figure B.7: E-2-N X-Ray Image and Crack with No Crack	80
Figure B.8: B-2-R X-Ray Image and Crack after Applying Threshold	80
Figure B.9: E-2-R X-Ray Image and Crack after Applying Threshold	81
Figure B.10: B-3-N X-Ray Image and Crack after Applying Threshold	81
Figure B.11: E-3-N X-Ray Image and Crack after Applying Threshold	82
Figure B.12: B-3-R X-Ray Image and Crack after Applying Threshold	82
Figure B.13: E-3-R X-Ray Image and Crack after Applying Threshold	83
Figure B.14: B-4-R X-Ray Image and Crack after Applying Threshold	83
Figure B.15: E-4-R X-Ray Image and Crack after Applying Threshold	84

CHAPTER 1

INTRODUCTION

The highway system in the United States is very complex and plays an important role in its economics. Bridges are built to span a valley, road, body of water, or other physical obstacles and account for a substantial component in highway infrastructure. In bridge construction, concrete has the advantages of being a durable, versatile, and economical material and is of great interest for transportation agencies and bridge owners. Although the deterioration of structures over time is normal, concrete was thought to be a relatively low maintenance material before the first use of de-icing salts in the 1950s. However, when de-icing salts began to be applied in northern locations in the winter, reinforcement corrosion in concrete bridges increased rapidly [1]. Bridges in coastal locations have also been severely corroded, due to seawater or spray exposure. A recent study [2] showed that 14 percent of the nation's concrete bridges were rated structurally deficient, and the primary cause of the deficiency was corrosion of the reinforcing steel. The study determined that the annual cost of corrosion to all bridges (including steel bridges) is \$8.29 billion, including indirect costs incurred by bridge closures.

Due to the severity of the problem, researchers have attempted to develop corrosion protection methods. Early research by the National Bureau of Science (now National Institute of Standards and Technology) and the Federal Highway Administration (FHWA) indicated that epoxy coated reinforcement (ECR) performed well in concrete contaminated by salts [3] and provided protection such that the premature deterioration of concrete due to expansive corrosion is minimized. However, field investigations found that even though ECR generally performs better than traditional bare steel reinforcement (BSR), some bridges constructed using ECR are

now starting to show indications of surface damage and repairs are needed to prevent the progress of the damage. It is not clear whether the repair options used for bridges with black (or bare) steel reinforcement should be applied to bridges with ECR. It is therefore necessary to investigate the frequency and type of repair that should be performed for ECR bridge decks.

This section first introduces the corrosion mechanism of reinforcement in bridge decks and commonly used corrosion control methods. Research on the performance and applications of ECR, including laboratory tests and field investigations, is then summarized. Research on the repair of ECR bridge decks is also included.

1.1 Corrosion Mechanism of Reinforced Concrete Bridge Decks

The corrosion of steel reinforcement is an electro-chemical process in which the steel reacts with the surrounding environment and the metal is converted into a metal oxide compound. For this process to occur there has to be a current flow, which results from a potential difference between two nodes, typically on the same reinforcing bar. The water inside the concrete is usually alkaline and this protects the steel because a protective oxide (passive) film forms under this condition. The exact product may vary with the pH value and can be expressed in a general form as [4]:

$$m \cdot \text{Fe(OH)}_2 + n \cdot \text{Fe(OH)}_3 + p \cdot \text{H}_2\text{O}$$
 (1.1)

This film effectively protects the steel so that the corrosion rate is negligible, allowing decades of relatively low maintenance [5].

However, when there is a change in the environment, for example, a decrease in the pH value, corrosion of the steel will start. Two mechanisms commonly induce corrosion in the steel

reinforcement. One mechanism is carbonation, where carbon-dioxide dissolved in the water reacts with calcium ions in the cement and produces calcium carbonate:

$$Ca(OH)_2 + CO_2 \longrightarrow CaCO_3 + H_2O$$
 (1.2)

The loss of OH⁻ reduces the pH of the water in the concrete. When the pH reduces to a certain level, the steel is no longer passive and will start reacting with the oxygen dissolved in the water. The associated reactions are:

At anode:

$$3\text{Fe} + 8\text{OH}^{-} \longrightarrow \text{Fe}_{3}\text{O}_{4} + 4\text{H}_{2}\text{O} + 8\text{e}^{-}$$
 (1.3)

At cathode:

$$O_2 + 2H_2O + 4e^- \longrightarrow 4OH^- \tag{1.4}$$

The rate of this type of corrosion depends on factors including the availability of water and oxygen and the surface area exposed. The amount of oxygen in the concrete depends on the diffusion rate and is affected by the water saturation in the concrete. When fully saturated, the diffusion rate is low. When the concrete is dry, the oxygen can move freely in the pores, but the reactions cannot take place due to the lack of water. Wet and dry cycles accelerate the corrosion process as it allows oxygen to diffuse and the water to act as an electrolyte.

A second mechanism of corrosion in concrete reinforcement is chloride-induced corrosion in which chloride ions from de-icing salts or marine environments can penetrate the concrete through cracks and destroy the passive film on the steel. The product of the chemical reaction is a soluble iron-chloride complex [6]. The corrosion reaction at the anode is:

$$Fe \longrightarrow Fe^{2+} + 2e^{-} \tag{1.5}$$

The reaction at the cathode is the same as that in carbonation-induced corrosion. If the supply of water and oxygen is sufficient, the iron-chloride will react with oxygen and become Fe₂O₃ or Fe₃O₄ and release the chloride to continue the corrosion process. A low concentration of 0.6 kilograms per cubic meter (concrete weight basis) can compromise steel passivity [5]. Considerable efforts have focused on identifying a chloride threshold for initializing corrosion. However, a unique value for this parameter has remained unavailable because many factors such as cement type, concrete mix design, environmental factors, and reinforcement composition can influence this value.

Figure 1.1 shows corroded reinforcing bars in concrete. The volume of corrosion products for both types of corrosion is approximately 3-6 times the volume of the original steel. Tensile stresses will develop due to the corrosion-induced expansion and results in cracks, delaminations, and spalls in concrete due to its low tensile strength. This further accelerates the corrosion process by providing more pathways for water, oxygen, and chloride ions.



Figure 1.1: Steel Corrosion in Concrete. For interpretation of the references to color in this and all other figures, the reader is referred to the electronic version of this thesis.

1.2 Corrosion Control Methods

To prevent or reduce the damage caused by corrosion, different corrosion control methods have been investigated and developed. This section briefly describes the commonly used methods.

One method is to use stainless steel or stainless steel-clad reinforcement. Stainless steel differs from regular black steel. A passive film of chromium oxide forms on stainless steel which prevents further surface corrosion and blocks the spread of the corrosion into the internal structure [7]. The corrosive threshold of stainless steel in concrete is about 10 times higher than that for traditional black steel [8]. Field investigations have found that bridge decks using stainless-reinforcement had no corrosion induced cracks after 9 years of service. This makes stainless steel an attractive material to reduce corrosion in highway and bridge infrastructure. However, the cost of stainless steel is a major concern for owners. The use of stainless steel in a

bridge deck increases the initial cost by 5.5 to 15.6 percent [9], and is therefore typically considered to protect only critical and hard-to-repair structures.

Another method to control or reduce corrosion of reinforcing bars in concrete is cathodic protection. In cathodic protection, an external current is supplied to the protected metal by an auxiliary anode. As a result, corrosion is reduced or stopped. Two methods are used to supply external current. In one method, the protected metal is connected to a more active sacrificial metal, for example, zinc. In the second method, an external current source is applied [10]. This method is effective in reducing the corrosion of steel in concrete, but it has several drawbacks. If an external power source is used, the power source needs to be charged and replaced regularly. The wiring and connections also induce additional cost. If an active metal is used, the cost of obtaining and replacing the sacrificed metal can also be high.

Epoxy-coated reinforcing bars is one of the most widely used anti-corrosion methods. The epoxy coating reduces corrosion by [11]:

- Resistance inhibition: providing electrical resistance to limit current transfer between anodic and cathodic sites.
- Oxygen deprivation: excluding oxygen and thereby impeding the cathodic reaction.
- Inhibition or aestivation: introducing material into the interfacial environment to stimulate the development of passive or inhibitive surface films.

Even though the cost of ECR is higher than that of regular black steel, the benefit of ECR is obvious and it is cost-effective in the long run. Ideally, bridge decks with ECR should not suffer from corrosion-induced damage. However, in reality, corrosion of ECR does occur. For example, when the adhesion between the epoxy coating and the reinforcement is lost, the surface of the

steel will be exposed to the environment and corrosion is likely to occur. Water absorption properties of the coating can influence the de-bonding of the coating. Another cause for corrosion of ECR is damage to the coating during manufacture, fabrication, transportation, or construction. Small regions of steel exposed to the surrounding environment can corrode. Even though these problems can be reduced by proper design of the coating and proper handling during the transportation and construction process, they cannot be completely eliminated and the signs of ECR corrosion have been observed in both field investigations and laboratory experiments.

1.3 Corrosion Performance of Epoxy Coated Reinforcement

Extensive research has been conducted in the past decade in order to understand the performance of ECR. This section summarizes the results of previous research and is divided into two sub-sections: performance of ECR in laboratory tests and field performance of ECR in concrete structures.

1.3.1 Corrosion Performance of ECR in Laboratory Tests

To compare the corrosion performance of different types of bars, the FHWA [12] evaluated the corrosion of organic, ceramic, inorganic, and metallic clad and solid metallic bars. Corrosion tests of the bars themselves, as well as tests of the bars in concrete, were performed. The results showed that black bars exhibited very poor corrosion performance. Galvanized bars had a better performance than black steel bars when such bars were used for the entire structure. The corrosion rate of copper clad bars was 95 percent lower than that of black steel bars. The corrosion rate of Type 304 stainless steel bars varied with the cathode: if the cathode was stainless the corrosion rate was 99.8 percent lower than that of the black steel bars, while the rate

became 90-95 percent if black steel bars were used as cathodes. Type 316 stainless steel showed no sign of corrosion and had the best performance. For ECR, the presence of cracks in the concrete and the amount of damage to the bars played a significant role in the performance. The corrosion rate of ECR was 100 times less than that of black steel bars when both top and bottom layers were ECR. The type of coating also played a role but the difference reduced if all bars were epoxy coated. According to the results of the report, ECR is a good corrosion protection system but several requirements are needed to maximize its performance. First, ECR needs to be used for the entire structure. Second, the cracks in the concrete need to be repaired. Third, the damage to the coating needs to be minimized.

Researchers at Wiss, Janney, Elstner Associates, Inc. (WJE) [13] conducted an accelerated corrosion test to compare the performance of ECR, iron chromium alloy, galvanized bars, and stainless steel bars. They found that ECR performed very well and corroded at drilled holes as shown in Figure 1.2. ECR removed from a 15-year old deck performed well during the test. Corrosion was minor and only occurred at drilled holes or at existing defects in the coating. They also observed that bars with poor coat bond still performed well, indicating that the effect of coat bonding may not affect the corrosion performance significantly.

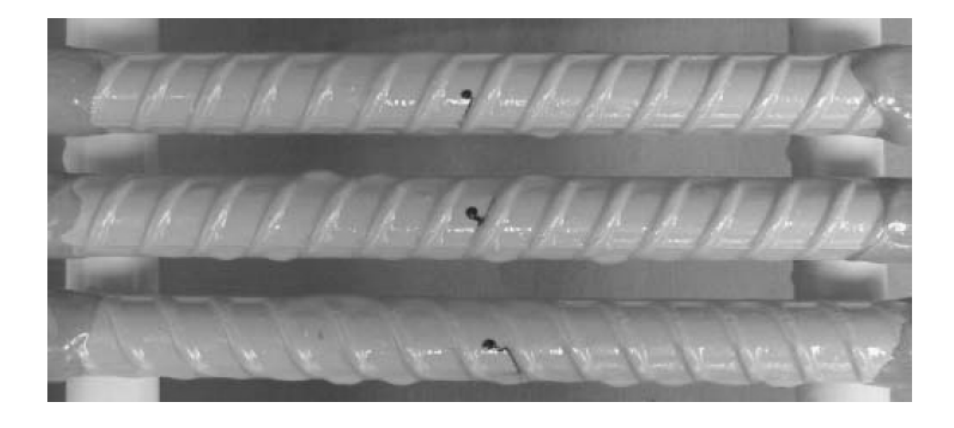


Figure 1.2: ECR after Corrosion

NFESC (Naval Facilities Engineering Service Center) performed a test to compare the performance of ECR, zinc-galvanized bars, and plain rebar in a marine environment [14]. Concrete specimens with different types of rebar were prepared and exposed to an inter-tidal zone for corrosion when the age of concrete was 9 months. Visible surface staining and cracking were observed in black steel specimens after 42 months of exposure. However, such staining was not observed for ECR and zinc-galvanized specimens. This indicated that ECR can delay the initialization of corrosion and provided a longer service life with little or no maintenance.

Investigations on the durability of different steel reinforcement were also conducted in the UK. In research conducted by Swamy [15], concrete specimens with uncoated black steel, zinc-galvanized steel, and epoxy coated steel were cast and exposed to a natural marine environment as well as an accelerated corrosion environment. The research concluded that uncoated steel bars corroded extensively under natural marine conditions. A concrete cover as thick as 70 mm could not prevent corrosion. Galvanized bars showed improved performance under both marine conditions and accelerated corrosion conditions. However, progressive corrosion was observed under the natural environment. ECR had the best performance among the three tested bars and survived corrosion in both marine conditions and accelerated corrosion conditions, even with a shallow concrete cover of 20 mm. The corrosion of ECR with artificial surface damage was also negligible and far less than uncoated and galvanized bars. The research concluded that ECR had the best performance.

1.3.2 Corrosion Performance of ECR in Concrete Bridge Decks

Field investigation of twelve sites in Virginia showed that ECR bridge decks [16] revealed a significant number of transverse cracks often extending through the entire depth of the deck after

15-20 years in service, but these cracks resulted from mechanisms other than corrosion. The use of ECR did not prevent these cracks, but significantly reduced the corrosion-induced cracks. Bridge decks not using ECR presented widely varying percentages of delamination from 60-80 percent, although 5-20 percent was more common. Bridge decks using ECR did not reveal much delamination. ECR was found to be the main reason for the lack of delamination in bridge decks.

A limited field survey carried out in Minnesota [17] showed that bridges with ECR showed no signs of distress after almost 20 years of service and no corrosion was observed on the epoxy coated bar.

The advantage of ECR under field conditions was also verified by an investigation of eleven bridges with bare reinforcement and eleven bridges with ECR [18]. The investigation observed that the decks with bare reinforcement were in the initial stages of corrosion deterioration while decks with ECR showed no signs of corrosion, indicating that ECR delayed the initiation of corrosion.

A two year investigation on the effectiveness of ECR in concrete bridge decks indicated that the condition of bridge decks using ECR in Pennsylvania and New York performed very well [19]. The occurrence of progressive corrosion was less than 3 percent in Pennsylvania but coating adhesion reduction or loss was prevalent. Half of the bridge decks exhibited adhesion reduction of some extent within 6-10 years in service. Coating adhesion loss also occurred with corrosion but it could not be regarded as a predictor of corrosion (i.e., if corrosion occurs there was coating adhesion loss, but coating adhesion loss did not necessarily indicate the occurrence of progressive corrosion). The results of this investigation were based on bridges with a low average age (around 10 years in service).

The Indiana Department of Transportation performed a large scale field investigation on the performance of ECR bridge decks [1]. One hundred twenty three bridges were visually inspected and 44 percent indicated reinforcement corrosion. Six bridge decks (3 decks with black steel and 3 decks with ECR) were selected for detailed surveys. Corrosion of reinforcement was observed in 2 of the 3 ECR bridge decks. Field visits to the construction site showed that the average number of holidays, or defects, created during construction was 9 per foot. Increasing the thickness of the epoxy coating reduced the coating damage during construction. Cracking and insufficient concrete cover decreased the effectiveness of ECR as a corrosion protection method. Laboratory experiments showed that cracking allowed chlorides and oxygen to reach the reinforcement. This provided the necessary conditions for corrosion to occur. Increasing the thickness of the concrete cover also helped prevent the penetration of chloride and oxygen and therefore protected the reinforcement from corrosion. The reason for the better performance of ECR was that it increased the electrical resistance dramatically. Researchers recommended that increasing the thickness of epoxy coating and concrete cover could improve the corrosion resistance of ECR.

Investigation on ECR bridge decks in Iowa [20] concluded that ECR bridges showed no delamination or spalling after 20 years of use and that the concrete cover played an important role in the initiation of corrosion. Most of the ECR corrosion was found in cores displaying concrete cracking.

The FHWA performed a test on the long-term performance of ECR in concrete severely contaminated by salt [21]. Bare steel had poor performance. The performance of ECR depended on the bottom layer. If the bottom layer was black steel, the corrosion of the top layer (ECR) was about 50 percent of that in black steel even when the coating was damaged. If the bottom layer

was ECR, the corrosion was less than 2 percent of that of black steel and approached the performance of stainless steel reinforcement. Cracking reduced adhesion and coating disbondment (or adhesion loss) was found to be the major reason for corrosion of ECR.

Brown [11] investigated bridges in Virginia and concluded that the early age cracking of concrete decks may increase chloride penetration but did not significantly reduce the service life of bridge decks. The use of ECR provided an extension in service life of about 5 years, making ECR not a cost-effective corrosion protection method for bridge decks in Virginia.

Smith and Virmani [22] summarized the results of investigations conducted by different highway agencies on the performance of ECR. A total of 92 bridge decks, 2 bridge barrier walls and 1 noise barrier wall were investigated. ECR provided effective corrosion protection for up to 20 years of service with little or no maintenance and signs of damages related to the corrosion of ECR were not found. The performance of ECR was not good if the concrete was cracked, the concrete cover was small and concrete permeability and chloride concentration was high. The defects and disbondment in the epoxy coating affected the performance of ECR.

Lee and Krauss [23] conducted a 3-year research project on the service life of ECR bridge decks. Phase I of the research investigated 11 bridges with black steel in the bottom layer and ECR in the top layer. Field investigation showed that bridges with ages from 19 - 27 years had an average surface damage of 1.3 percent. Phase II of the research investigated bridges with ECR in both the top and bottom layers. The bridges showed no sign of damage after 9-15 years of use. A statistical model was used to predict the extension of service life brought by the use of ECR. The results showed that bridge decks with ECR in the top layer extended the service life for

about 40 years or more, while bridge decks with ECR in both layers should have a service life extension of more than 82 years.

In addition to bridge decks, ECR has been used in structures as well. An investigation of 12 garage structures [24] showed that ECR is a worthy investment if properly installed. With a few exceptions, most of the ECR performed well. Thus, with improved quality control and construction standards ECR was seen as a valuable corrosion control option.

The performance of ECR, however, was found to be unsatisfactory based on research performed in Florida on marine substructures [25]. Severe corrosion of ECR was observed after 6-10 years and corrosion proceeded underneath the epoxy coating even though the coating was unaffected. The cause of the damage was identified to be mechanical fabrication and possible coating disbondment before and after the placement of epoxy bars in concrete. To confirm this, laboratory experiments with and without coating defects in ECR were performed. After one-month of exposure to corrosive agents (calcium hydroxide and sodium chloride), delaminations around defects and pits with corrosion products were observed and low pH liquid accumulated between the coating and the metal. Exposure of steel to neutral sodium chloride under open circuit conditions caused significant disbondment around existing or introduced coating imperfections, which led to the extensive corrosion in ECR.

1.3.3 Summary of the Section

This section summarized the results of previous research on the performance of ECR. The use of ECR generally seemed to increase the corrosion resistance, although findings were mixed. The effectiveness of the ECR is influenced by several factors such as the existence of concrete cracks, the thickness of concrete cover, the type of steel for the bottom reinforcement, and the

type of the coating. Also, corrosion of ECR was observed in both laboratory environments as well as in field investigations. Possible reasons for the corrosion of ECR are the damage of the coating during the transportation and construction process and the disbondment of the coating from the steel.

1.4 Repair Options for Reinforced Concrete Bridge Decks

As summarized in the previous section, although ECR can significantly increase the corrosion resistance of bridge decks, signs of corrosion were observed in both laboratory experiments and field investigations. Because corrosion-induced deterioration is progressive, inspections for damage assessment must be performed routinely and repairs are needed continually. For example, corrosion-induced concrete spalls occur as potholes in a bridge deck and contribute to poor ride quality. In extreme conditions, structural failure and collapse may occur [10]. Due to the difference in the corrosion mechanism and service life, the inspection and repair schedule for ECR bridges should be different from bridge decks with black steel. However, research on repair protocols for ECR bridge decks is limited.

In 2002, an NCHRP-sponsored project focused on investigating the repair and rehabilitation of bridge components containing ECR. Repair options for different types of damage were evaluated by both field investigation and laboratory tests [26]. The research concluded that neither admixed nor migrating corrosion inhibitors provided any corrosion protection when used to rehabilitate cracks and delaminations on concrete elements reinforced with ECR that were exposed to an aggressive chloride environment. The research also showed that patching the concrete using high resistivity, low permeability, silica fume concrete as well as a combination of epoxy coating and patching provided protection against corrosion in the repair area. This

report also included a decision matrix for the repair of different types of damage such as corrosion induced and non-corrosion induced cracking and corrosion induced delaminations, based on the severity of the damage and the probability of corrosion.

The selection of repair strategies should be based on the following criteria:

- 1. The strategy should be expected to have a direct and positive impact on the future performance of epoxy-coated reinforcing steel.
- 2. Each technique or material should not have any known adverse effects on ECR.
- Emphasis should be placed on strategies which have a history of success on bare reinforcing steel.
- 4. Each strategy should have some probability of success based on current knowledge even if adequate long-term performance information on bare reinforcing steel is not available.

NCHRP report 558-RC "Manual on service life of corrosion-damaged reinforced concrete bridge super-structure elements" [27] describes the commonly used repair options including overlays, membranes, surface coatings, and sealers. Overlays can restore the surface of the bridge deck and increase the effective thickness of concrete cover. The cost of concrete removal and chloride concentration in the concrete below the depth of removal must be considered when determining the extent of material to be removed. The service life of rehabilitation overlays is limited by the rate of diffusion of chloride ions through the overlay and can be significantly influenced by environmental exposure conditions (i.e., chloride concentration and temperature). The membrane can provide a waterproofing barrier to prevent the intrusion of chloride ions into the concrete deck and is usually used in conjunction with an asphalt overlay. Proper application

of an approved membrane can greatly reduce the intrusion of chlorides into the concrete. The advantage of the membrane is that it can be applied relatively quickly to almost any deck geometry and can bridge most moving concrete cracks because of its elastic nature. However, the service life of the membrane may be limited by wearing when exposed to heavy traffic and by the disbondment and shoving under traffic. Concrete sealers and surface coatings can also be used to prevent chloride ions from diffusing into the concrete, but they cannot reduce the chloride that is already in the concrete before the repair. The performance of the concrete sealer or surface coating is also dependent on the environment, including the level of UV (ultra-violet) radiation, moisture, and abrasion. The extension in service life by surface coating is usually limited.

The Michigan Department of Transportation (MDOT) has a developed a repair matrix for bridge decks with black steel reinforcement in which the repair options were selected based on the level of damage (percentage of damaged surface) and has been successfully applying these repair options. However, the influence of these repair options on the performance of bridge decks with ECR needs to be evaluated.

1.5 Summary

This section first provided a brief review on the corrosion mechanism of steel reinforcement in concrete. Different corrosion protection or corrosion control methods were described. ECR was found to be the most cost-effective corrosion control method in most cases. Next, a review of research on the performance of ECR in concrete bridges and other types of structures was provided. From the review, it is apparent that ECR has better corrosion performance than black steel reinforcement. However, some corrosion of ECR was observed both in laboratory tests and

in field investigations. Therefore, inspection and repair of ECR bridge decks is necessary. The last section summarized research on the repair options for structures with ECR.

CHAPTER 2

SPECIMEN PREPARATION

Damage to bridge decks is caused by a combination of mechanical fatigue and environmental loads. Laboratory specimens need to be conditioned to simulate the actual aging effects before being used to evaluate service life. Bridge decks in Michigan are usually subjected to two main types of environmental loads: freeze-thaw effects and the corrosion of steel bars due to the use of de-icing salts during winter. Therefore, the conditioning of specimens in this project included freeze-thaw cycles and corrosion of the steel. After the specimens were conditioned, they were repaired by different methods according to the damage level they experienced. The conditioned and repaired specimens were then used to evaluate the service life and performance of different repair options.

2.1 Specimen Design and Casting Preparation

To simulate the performance of bridge decks under field conditions, large scale testing is needed. However, cost and logistical considerations often limit the number of configurations that can be tested, and typically only one specimen can be tested each time. In this research, small-scale specimens with different configurations were used. To evaluate the relative performance of bridge decks with epoxy coated rebar (ECR), specimens with black steel rebar (BSR) were used for comparison. Each test unit was fabricated with two rebars. For specimens with black steel, both bars in the test unit consisted of black steel. For specimens with ECR, the top bar was epoxy coated but the bottom bar was made of black steel so that it could be used as a cathode in the

accelerated corrosion process. Figure 2.1 shows the sizes and rebar configuration of the proposed specimens.

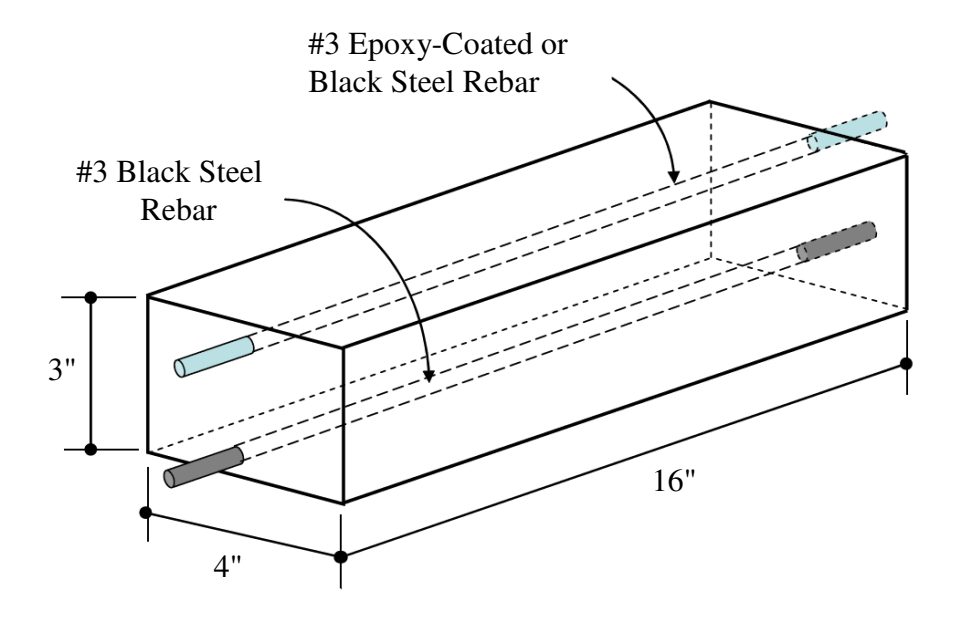


Figure 2.1: Specimen Configuration

To evaluate the performance of the specimens under different damage levels and repair options, a representative sampling of the repair matrix used by the Michigan Department of Transportation (MDOT) was used, as listed in Table 2.1.

The coating of the ECR will inevitably get damaged during construction. Based on previous research and suggestions from the Research Advisory Panel at MDOT, a surface damage of 2 percent was selected. The damage was introduced by lightly drilling the epoxy coated surface of the rebar until the epoxy under the 1/16" drill bit was removed. The location of the damage was randomly selected. One example of the damaged rebar is shown in Figure 2.2.

Table 2.1: Test Matrix

Test ID	Damage Level	Repair Option	Steel Type
B0-N	0	None	BSR
E0-N	0	None	ECR
B1-N	1	None	BSR
E1-N	1	None	ECR
B1-R	1	Epoxy Overlay	BSR
E1-R	1	Epoxy Overlay	ECR
B2-N	2	None	BSR
E2-N	2	None	ECR
B2-R	2	Shallow Concrete Overlay	BSR
E2-R	2	Shallow Concrete Overlay	ECR
B3-N	3	None	BSR
E3-N	3	None	ECR
B3-R	3	HMA Overlay with Waterproofing	BSR
E3-R	3	HMA Overlay with Waterproofing	ECR
B4-N	4	None	BSR
E4-N	4	None	ECR
B4-R	4	Deep Concrete Overlay	BSR
E4-R	4	Deep Concrete Overlay	ECR

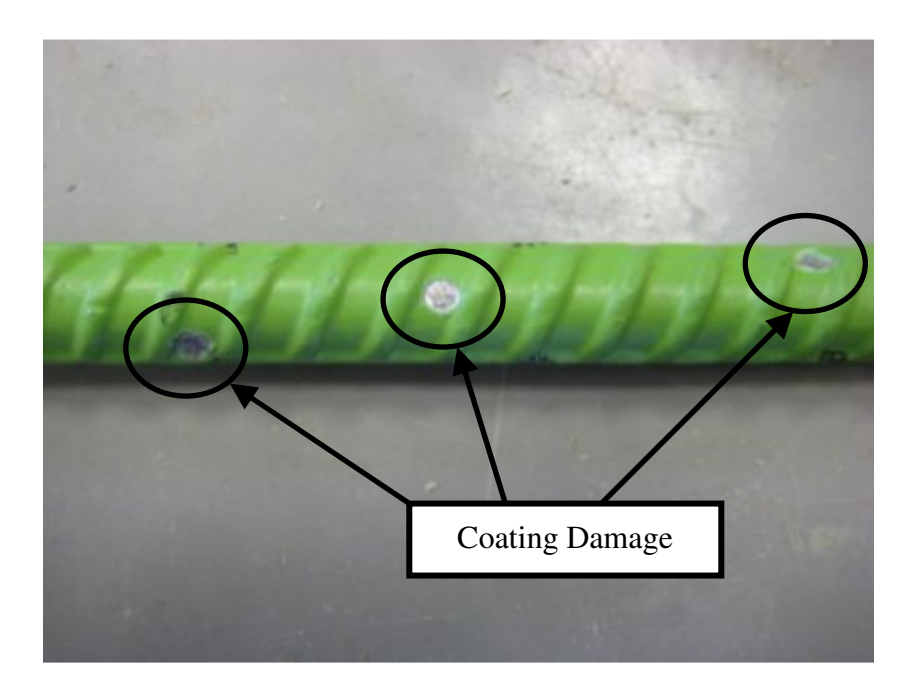


Figure 2.2: ECR with Damage in Coating

Due to the small size of the specimens, it was likely that shear failures would be precipitated by slipping of the tension reinforcement. Once shear cracks initiated, sudden failure would have occurred since the test units had no shear reinforcement. Three pilot test units were thus designed, built, and tested to evaluate if the desired strain levels induced by traffic on bridges could be reached before the onset of shear failure. The first test unit (Beam 1) was only reinforced with two #3 bars at the top and bottom of the test unit. In the second test unit (Beam 2) the tension bar had washers welded at both ends to provide additional mechanical anchorage. The third beam (Beam 3) had no special anchorage detail, but had a steel wire mesh as shear reinforcement. The dimension and reinforcement lay-outs are shown in Figure 2.3.

The beams were loaded in three-point bending to maximize flexural demands and minimize shear demands. The total simply supported span was 16 inches. The beams were loaded monotonically under displacement control until failure. Load, mid-span displacement,

and strain of the tension bar at mid-span were monitored. The average concrete compressive strength when the beams were tested was 6,790 psi.

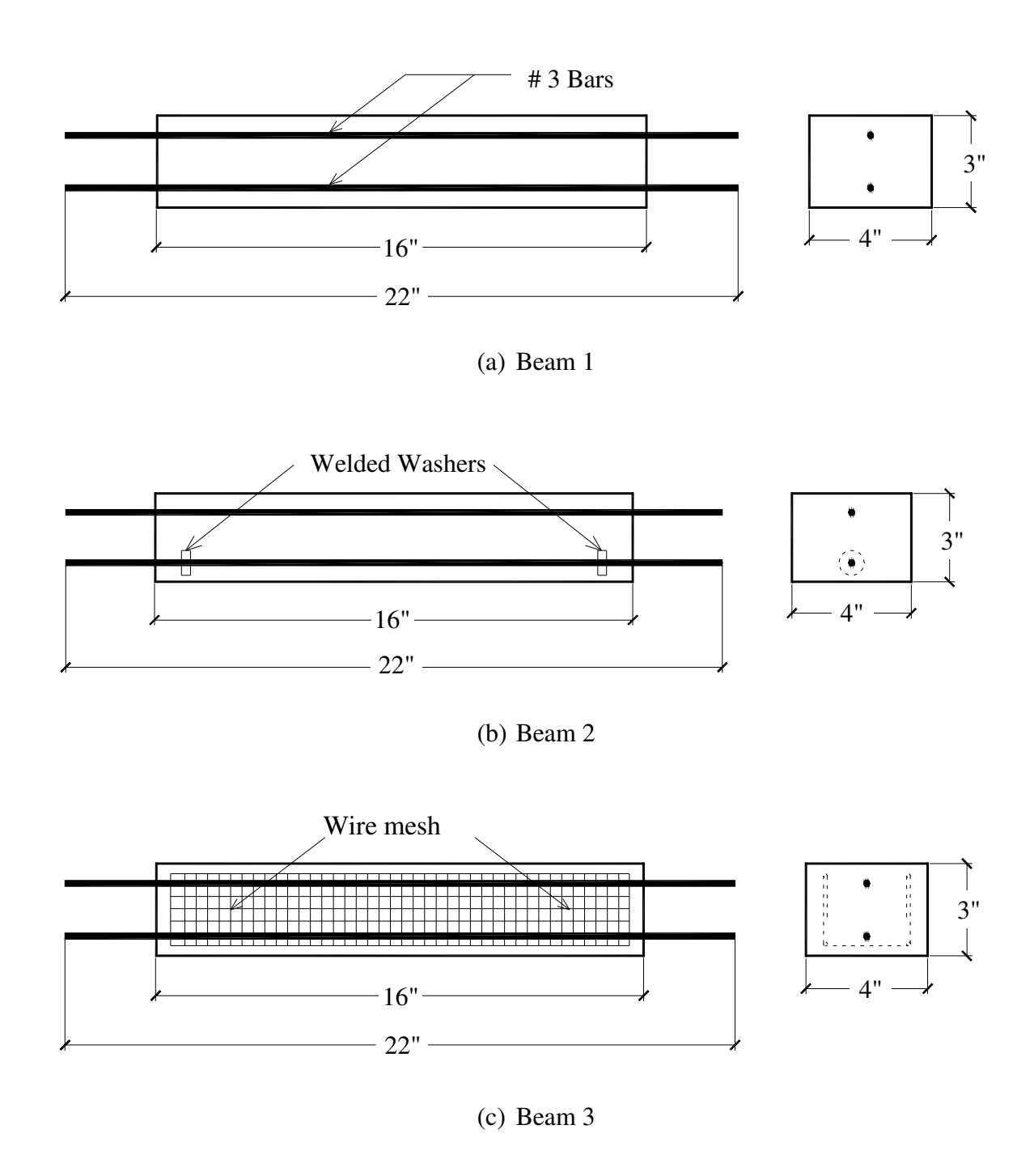


Figure 2.3: Dimensions and Reinforcement Layouts of Pilot Beams

The load-displacement response for all beams is shown in Figure 2.4 and photographs of their failure pattern are shown in Figure 2.5. Beam 1 (without any anchorage enhancement) failed before yielding of the tension rebar. Beam 2 (with welded washer on bottom bar) failed in shear, but the specimen failed after the yielding of the bottom reinforcement. Beam 3 (with wire mesh shear reinforcement) also failed in shear and the tension bar yielded before failure. From the measured responses, observed failure, and crack patterns, Beam 3 performed the best with a rather smooth response up to failure with the tension bar reaching strains well beyond yield. Beam 2 performed the next best and was satisfactory. Since welding washers was much easier than installing the wire mesh, washers were used for fabrication of the project test units. The molds with the steel rebars before casting is shown in Figure 2.6.

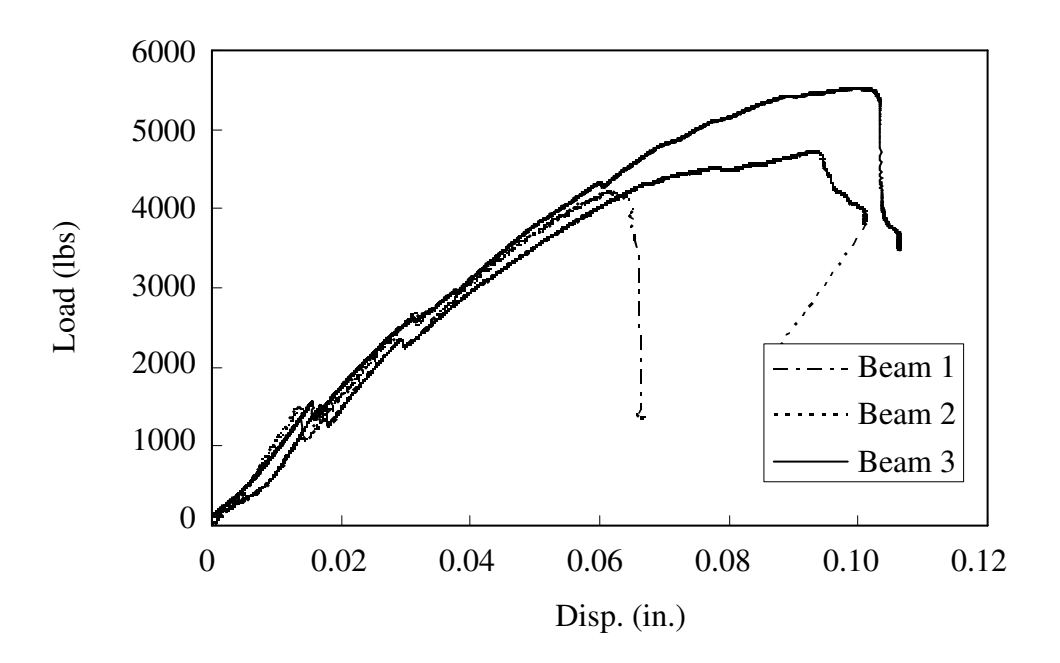
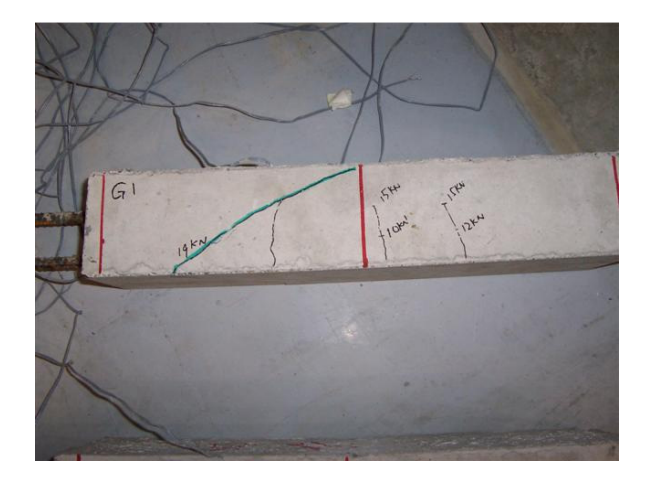


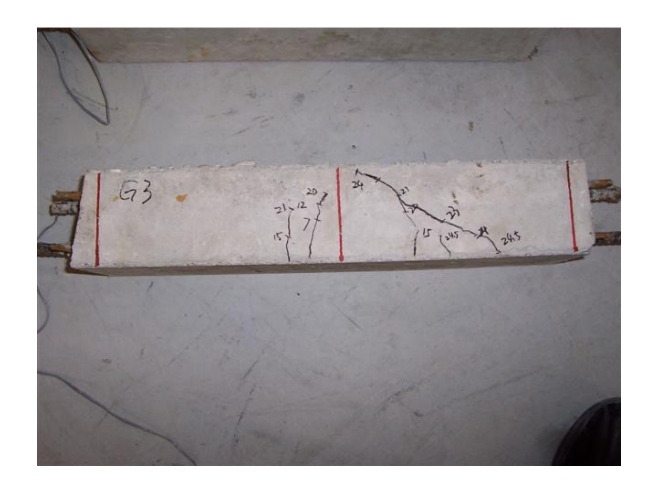
Figure 2.4: Load-Displacement Response of Pilot Test Beams



(a) Beam 1



(b) Beam 2



(c) Beam 3 **Figure 2.5:** Failure Patterns of Pilot Test Beams



Figure 2.6: Molds before Casting

2.2 Accelerated Freeze-Thaw Test

Damage in concrete bridge decks occurs due to a combination of mechanical and environmental loading. All specimens were "aged" by exposing them to freeze-thaw cycling and accelerated corrosion. The initial conditioning imposed was equivalent to approximately 30 years of aging, which corresponded to the approximate age of current ECR decks in Michigan. Based on 3 years of temperature data in the Lansing area, 300 freeze-thaw cycles were used to simulate 30 years of aging. The specimens were subjected to freeze-thaw cycling in MDOT's freeze-thaw machine. ASTM C-666 [28] Procedure B was used in the test. Due to an incorrect mixture design, the first batch of specimens experienced severe damage after the freeze-thaw test as shown in Figure 2.7(a), and could not be used for further testing. The reason for the severe damage was later found to be insufficient air-entrainment in the concrete. The mix design was revised and a second batch of concrete with a measured air-content of 6.1 percent was cast. An average

compressive strength of 4.3 ksi was achieved after 28 days of curing. The specimens from the second batch successfully survived the freeze-thaw test as shown in Figure 2.7(b).



(a) First Batch



(b) Second Batch

Figure 2.7: Specimens after Freeze-Thaw Test

2.3 Accelerated Corrosion

In addition to freeze-thaw, bridge decks in Michigan are also subjected to corrosion induced by the use of de-icing salt. Similar to freeze-thaw, corrosion occurs over a long period of time. In this research, accelerated corrosion using an impressed current was used to simulate field effects after the freeze-thaw test. The top bar was used as an anode and the bottom bar as a cathode. The induced corrosion level was similar to that experienced after 30 years of service and was estimated by monitoring the current through the specimen. The total amount of charge for simulated corrosion is given by:

$$Q = \frac{\Delta m \cdot z \cdot F}{A_m} \tag{2.1}$$

where Δm is the mass loss for a given period of time estimated from field investigations, z is the valency charge of the metal (z = 2 for Fe²⁺), F = 26.8015 Ah is Faraday's constant, and A_m is the atomic weight of the metal (55.85 for steel).

In this project, a corrosion rate of 0.045 mm/year was selected based on previous research [29]. The mass loss over n years can then be calculated as:

$$\Delta m = \frac{\pi}{4} \left[R^2 - (R - 0.045n)^2 \right] \rho L \tag{2.2}$$

where R is the average radius of the rebar, n is the number years, ρ is the density of the steel, and L is the length of the rebar.

The impressed current was measured by a voltage data-logging system (Omega Engineering Inc., AD128-10T2). Three specimens were connected in series and were connected to a 36 V DC power supply to reduce the time of conducting replicate tests. During the accelerated corrosion process the test units were soaked for one hour each day in a 3.5 percent NaCl solution by weight. The circuit used for the corrosion test is shown in Figure 2.8.

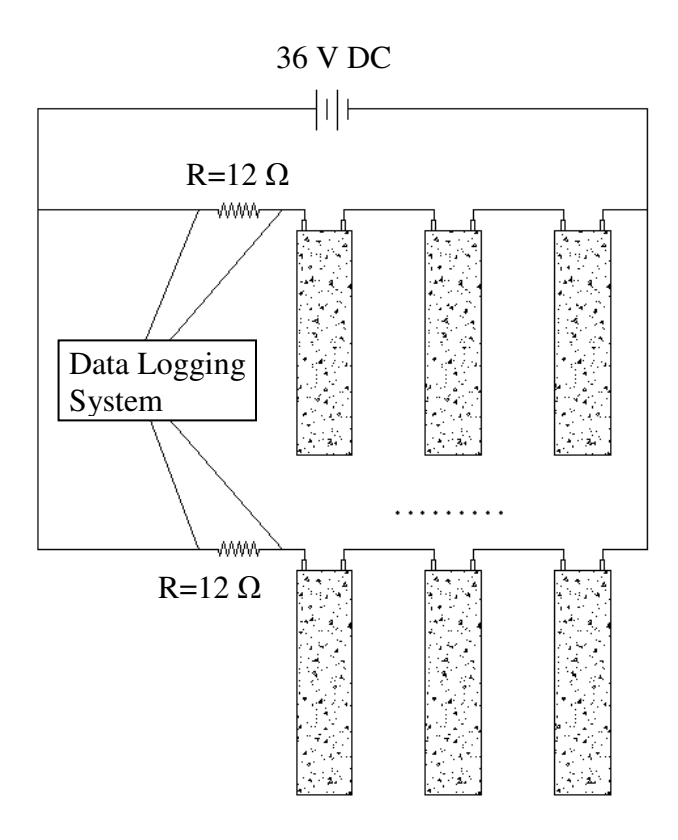


Figure 2.8: Accelerated Corrosion Test Setup

Due to the small size of the specimen, the damage due to corrosion could not be effectively measured in terms of the percent damage to the surface area. Instead, the measured corrosion charge was used as a measure of the damage level. The maximum level of damage (Level 4) was determined to be equivalent to 30 years of field corrosion. The corrosion charge for Level 4 can be calculated using Equation 2.1. The minimum damage level (Level 1) was defined as the charge when the initial crack appears in the specimen and the charge for Level 1 was obtained

through observations during the test. Damage levels 2 and 3 were defined by linear interpolation between the charges Q1 and Q4, corresponding to Level 1 and Level 4 damage. The charge for different levels of damage is shown in Table 2.2.

Table 2.2: Corrosion Charge for Different Damage Levels

Damage Level	1	2	3	4
Corrosion Charge (Ah)	12.57	43.65	74.72	105.79

Figure 2.9 shows an example of the corrosion curve for BSR and ECR specimens. The corrosion rate was much slower for ECR than BSR and the time for ECR specimens to reach the same level of corrosion was approximately 2-3 times longer than for BSR specimens. Therefore, ECR seems to effectively delay the appearance of the corrosion induced damage in concrete bridge decks.

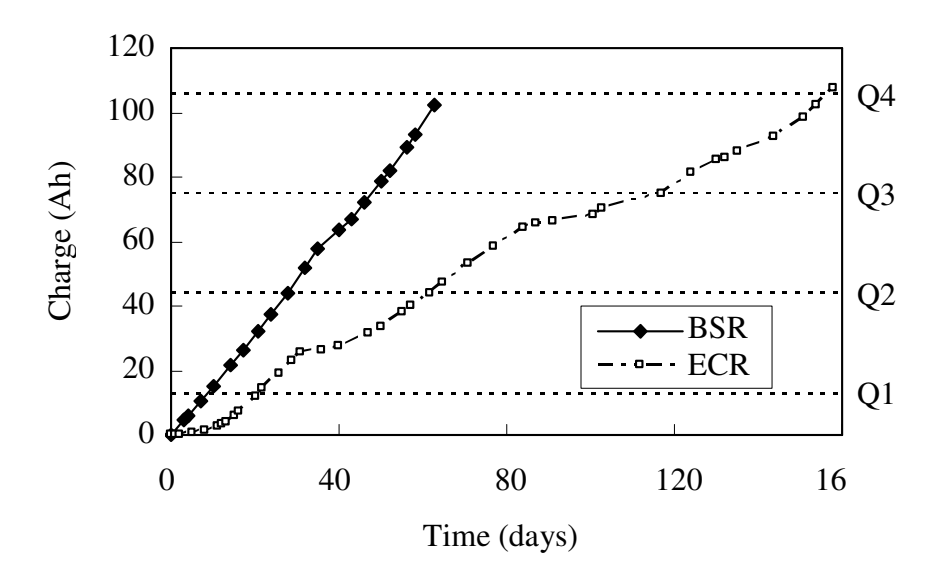


Figure 2.9: Corrosion Curves for BSR and ECR

Figure 2.10 to Figure 2.13 show typical examples of specimens corroded to different levels. Fine cracks were observed in specimens with Level 1 damage and a marker was used to "highlight" the crack in Figure 2.10. It is obvious that the damage increased as the corrosion level increases, as shown in the following figures.



Figure 2.10: Specimen after Level 1 Corrosion



Figure 2.11: Specimen after Level 2 Corrosion



Figure 2.12: Specimen after Level 3 Corrosion



Figure 2.13: Specimen after Level 4 Corrosion

2.4 Specimen Repair

After being corroded to the desired level, specimens were repaired using different options according to the levels of damage. Specimens with Level 1 damage were repaired using an epoxy overlay. According to MDOT Special Provision for Thin Epoxy Polymer Bridge Deck Overlay

[30], epoxy produced by E-bond Epoxies, Inc. was used. The fine aggregate (sand) used in this project was #612 Quartz sand from Best Sand Inc, in Ohio. The surface of the specimen was first roughened by chiseling off the concrete to increase the bond with the applied overlay. According to MDOT's provision, two courses were applied. The epoxy mixture for the first course was 40 ft²/gal and the second course was 20 ft²/gal. Sand was applied such that the surface was covered in excess with no bleed or visible wet spots. A specimen repaired with epoxy overlay is shown in Figure 2.14.



Figure 2.14: Specimen Repaired with Epoxy Overlay

Specimens corroded to Level 2 were repaired with a shallow concrete overlay. When applied on the bridge deck, the concrete cover is removed until the top layer of the reinforcement and the surface is roughened to provide enough bond between the deck and the newly applied overlay. During preparation for the shallow concrete overlay for the test specimens, it was found that the

corrosion cracks developed from the top to the bottom bars. Due to the small size of the specimens, it was easy to break them along the crack and damage them if a chisel was used to roughen the surface (one specimen was damaged due to the impact). To prevent specimen damage, a sander was used to create a rough texture on the surface to provide bonding between the specimen and the overlay. Also due to the penetration of the crack toward the bottom bar (in tension), specimens were prone to be broken in half during the fatigue test. To prevent this, the concrete overlay was applied on both sides and on top of the specimen as shown in Figure 2.15. The confinement provided by concrete on both sides helped prevent the specimen from splitting. Moreover, this over-size repair provided confinement to the damaged specimen and reduced the chance of delamination. The concrete mixture design and material section followed the 2003 Standard Specifications for Construction from MDOT [31]. A typical specimen after repair is shown in Figure 2.16.

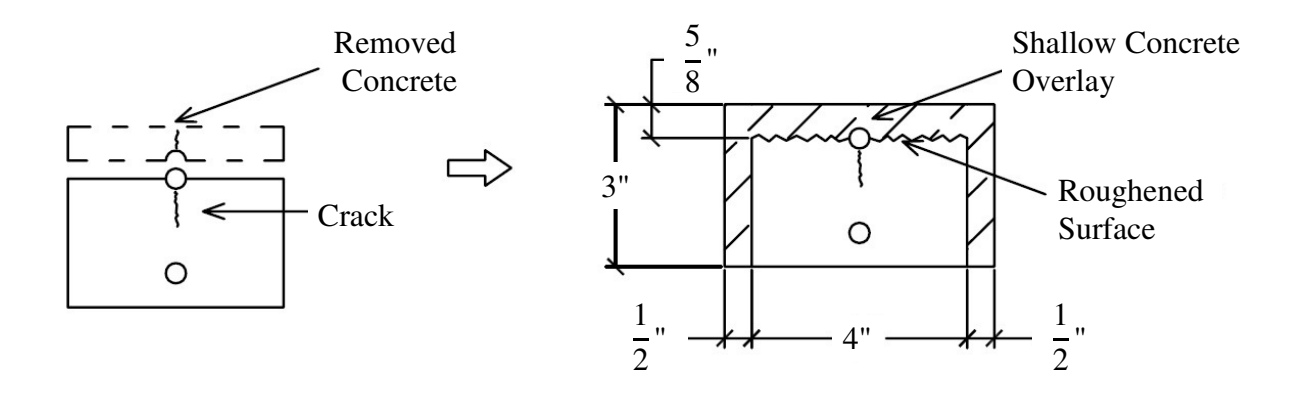


Figure 2.15: Oversized Shallow Concrete Overlay



Figure 2.16: Specimen with Shallow Concrete Overlay

Specimens with Level 3 damage were repaired with a hot mixture asphalt (HMA) overlay and a water-proofing membrane. The HMA mixture and the water proofing were provided by MDOT. The waterproofing was applied according to the 2003 Standard Specifications for Construction [31] provided by MDOT and the asphalt overlay was applied according to the Road Design Manual [32] from MDOT. A typical repaired specimen is shown in Figure 2.17.



Figure 2.17: Specimen with Waterproofing and HMA Overlay

A deep concrete overlay was used to repair specimens with Level 4 damage. Similar to the shallow concrete overlay, an oversize repair method was used due to the small size of the specimens. The mixture design was the same as that used in the shallow concrete overlay. Figure 2.18 shows the size of the deep concrete overlay and Figure 2.19 shows a typical specimen after repair.

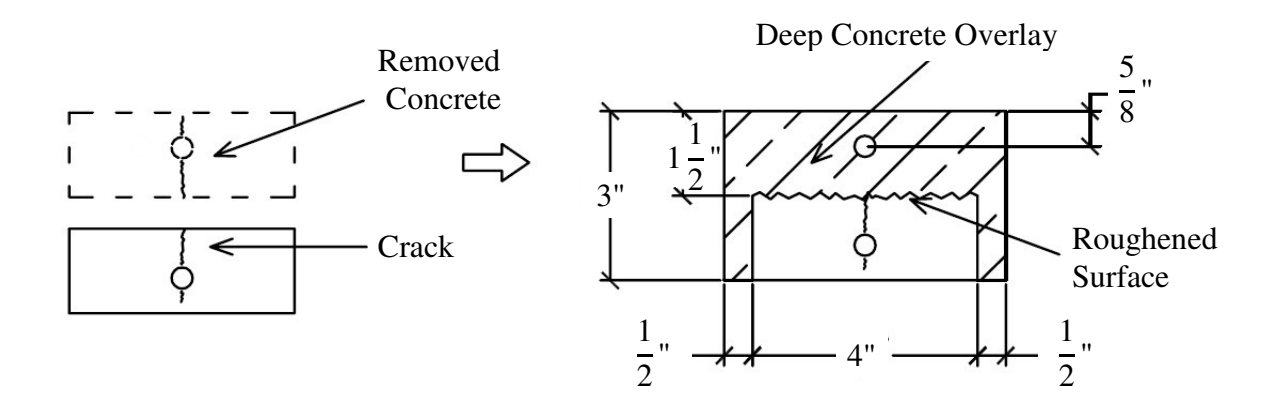


Figure 2.18: Oversized Deep Concrete Overlay



Figure 2.19: Specimen with Deep Concrete Overlay

CHAPTER 3

EXPERIMENTAL DESIGN

An experiment was conducted to determine the service-life performance of concrete bridge decks reinforced with black and epoxy coated steel. This was accomplished by testing small-scale concrete specimens with varying amounts of damage and different repair options for each type of steel. The specimens were subjected simultaneously to cyclic mechanical loads, freeze/thaw cycling, and accelerated corrosion. Periodically, the testing was halted so that the stiffness of the specimens could be measured. The stiffness values obtained throughout the cycling process were used to evaluate the service-life performance of the specimens. These values were used to compare the service-life performance of specimens with black steel and with epoxy coated steel. This chapter provides the detailed experimental design used to accomplish this goal.

3.1 Fatigue Testing

The specimens prepared for this experiment were subjected to loading that simulated the demands that occur on a typical reinforced concrete bridge deck. The types of loads considered were vehicular traffic, freeze-thaw cycling, and corrosion. The service-life of each specimen was determined by simultaneously subjecting the specimens to these loads. In order to reduce the time of this experiment, three specimens were tested at a time in an environmental chamber which is shown in Figure 3.1.



Figure 3.1: Environmental Chamber

Typically, the three specimens being tested at a particular time had the same age and the same method of repair. Since some of the specimens were damaged during the aging process, this was not always the case. Therefore, specimens were placed into groups of three, in which the specimens in each group had similar ages and methods of repair. A list showing the groups is given in Table 3.1.

 Table 3.1: List of Groups of Specimens

Group 1	B-0-1	B-0-2	B-0-3
Group 2	E-0-1	B-1-N-1	E-0-2
Group 3	B-1-R-1	B-2-R-1	B-1-R-2
Group 4	B-2-N-1	B-1-N-2	B-2-N-2
Group 5	E-1-N-1	E-1-N-2	E-1-N-3
Group 6	E-1-R-1	E-1-R-2	E-1-R-3
Group 7	E-2-N-1	E-2-N-2	E-2-N-3
Group 8	B-4-N-1	B-4-N-2	B-4-N-3
Group 9	E-4-N-1	E-4-N-2	E-4-N-3
Group 10	B-3-N-1	B-3-N-2	B-3-N-3
Group 11	E-3-N-1	E-3-N-2	E-3-N-3
Group 12	E-2-R-1	E-2-R-2	E-2-R-3
Group 13	B-3-R-1	B-3-R-2	B-3-R-3
Group 14	E-4-R-1	E-4-R-2	E-4-R-3
Group 15	E-3-R-1		E-3-R-2
Group 16	B-4-R-1	B-4-R-2	B-4-R-3

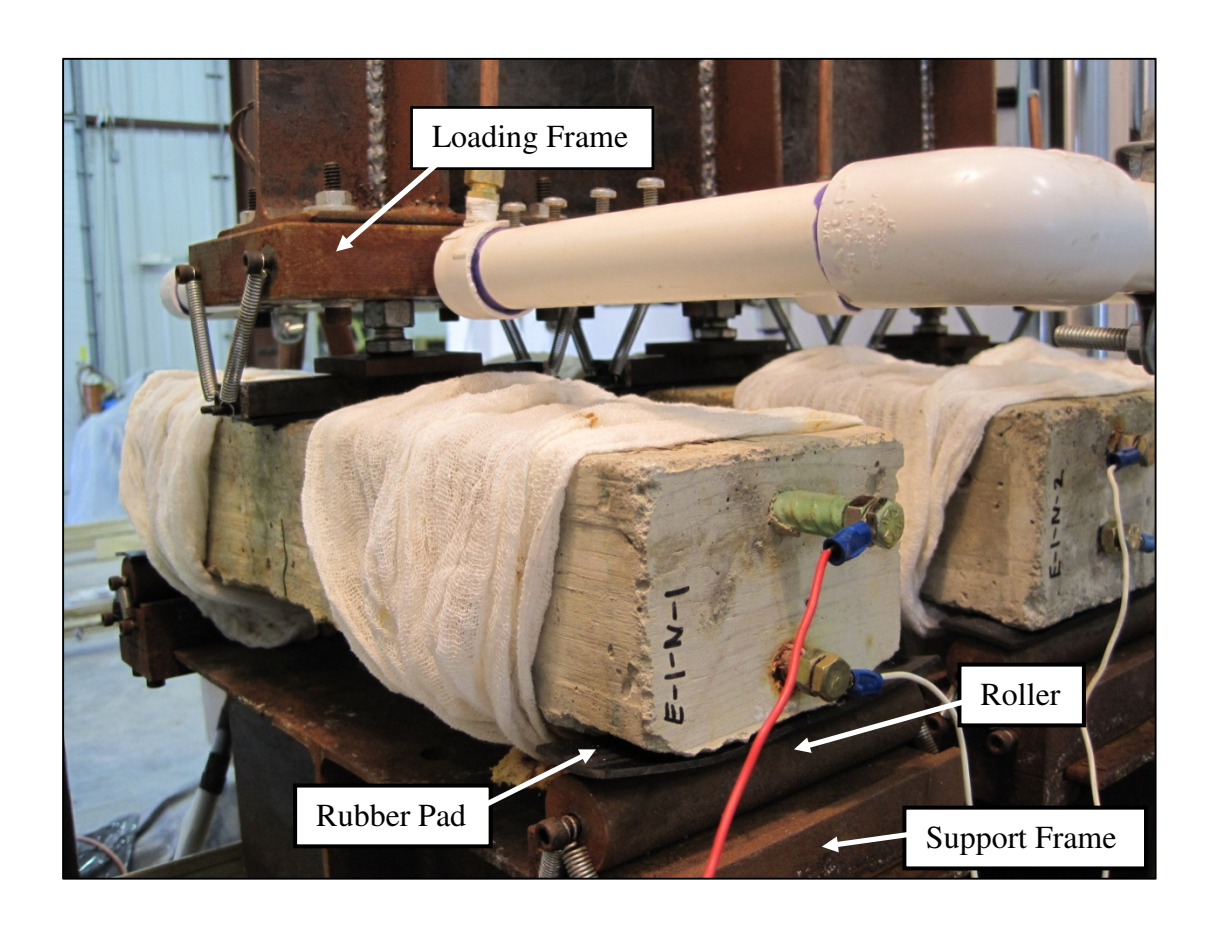


Figure 3.2: Fatigue Test Setup

The vehicular traffic was simulated on the specimens by cyclic flexural loading in a three-point bending setup as shown in Figure 3.2. Rubber pads were placed between the rollers and the specimens in order to ensure even distribution of load throughout the width of the specimens. Two-million cycles of fatigue loading were applied to each specimen throughout this experiment at a rate of 1 Hz. The fatigue loading applied to each group of specimens per cycle varied between 2 kN and 14 kN, therefore applying loads varying from approximately 0.7 kN to 4.7 kN per specimen. A minimum load of 2 kN was maintained in order to ensure that there was no separation between the specimens and loading frame. The maximum load of 14 kN was chosen in order to induce a tensile stress of about $0.45f_y$ in the tension reinforcement. This limit was determined by factoring the upper service steel reinforcement tensile stress limit of $0.6f_y$ by 0.75 for fatigue loading [33], considering that this is what most likely contributes to concrete damage from mechanical loads.

Freeze-thaw cycling was also applied to the specimens. While the fatigue testing was taking place in the environmental chamber, the specimens were wetted using a water drip system. At the same time, the temperature inside the chamber was varied from -3°F to 50°F, thus subjecting the specimens to freeze-thaw cycles. The freeze-thaw cycles took approximately 3-4 hours per cycle. For each specimen, the target number of freeze-thaw cycles was 150. However, the variation in the length of the cycles caused the actual number of freeze-thaw cycles to range between 95 and 146.

The third type of loading applied to the specimens was accelerated corrosion. This was accomplished by impressing current through the steel reinforcement in the specimens, which simulates the corrosion process that occurs in reinforced concrete bridge decks. The setup used

to accomplish this task is shown in Figure 3.3. The applied current was monitored by a voltage data-logging unit and the total corrosion was estimated from these measurements using Faraday's Law.

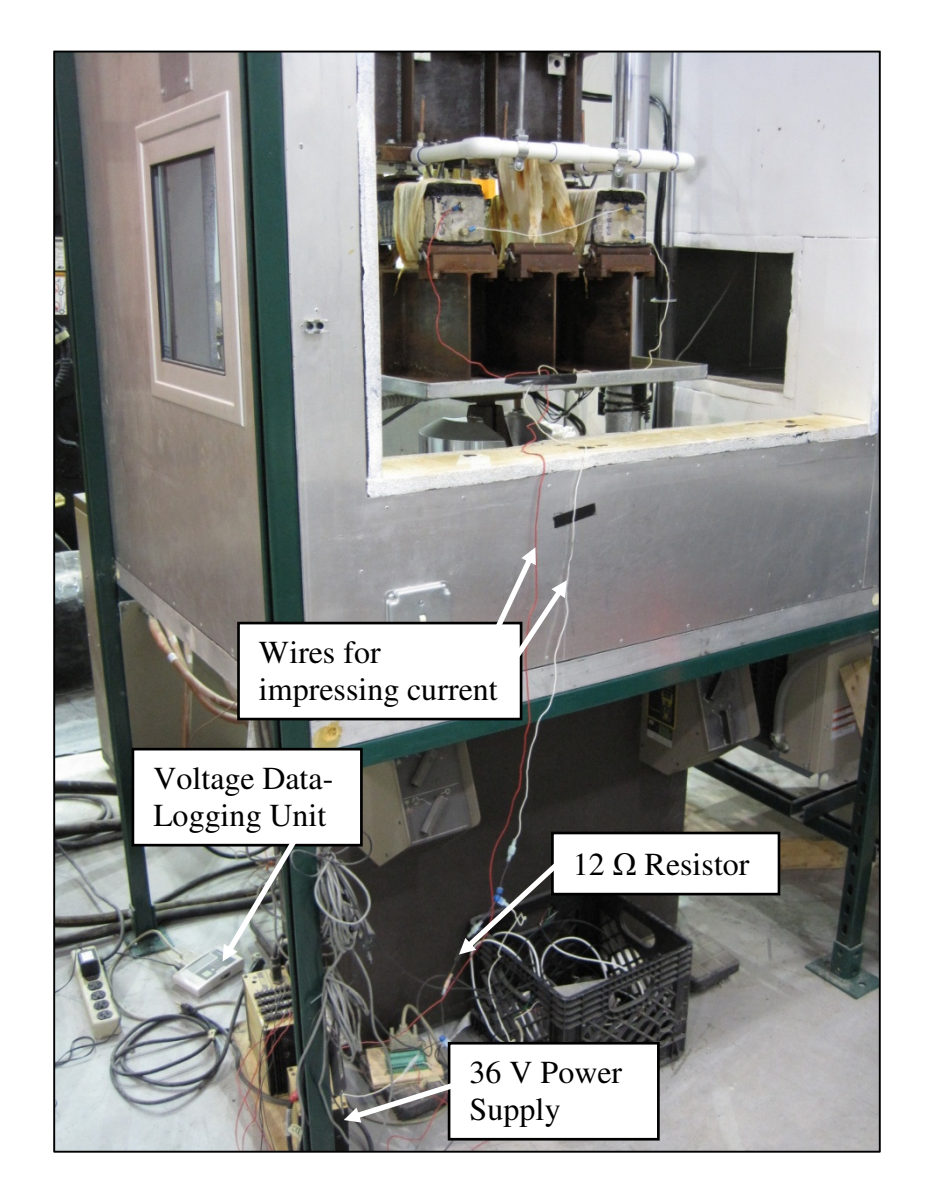


Figure 3.3: Corrosion Setup

3.2 Static Testing

The service-life performance of the specimens was determined by obtaining the stiffness of the specimens at certain times throughout the fatigue testing. This was done by performing static tests during which the load-displacement response of the specimen was measured. The stiffness was then determined by calculating the slope of the resulting load-displacement curve, which will be discussed later.

Periodically, the fatigue test was halted so that the static tests could be performed. These tests were conducted in the same environmental chamber as the fatigue testing, shown in Figure 3.4. Load cells were placed between the specimens and the loading frame to measure the loads applied to each specimen. Linear variable differential transducers (LVDTs) were mounted on the support frame under each specimen to measure their displacements under the load. Small glass plates were glued to the bottoms of the specimens where the LVDTs came into contact with them as shown in Figure 3.5. This was done in order to provide a smooth surface for the LVDTs to rest against so the roughness of the specimens would not interfere with the displacement measurements. The load cells and LVDTs were connected to a computer so that the load and deflection measurements could be recorded. The group of specimens was then subjected to a load in a three-point bending setup that increased from 0 kN to 17 kN at a rate of 4 kN/min. During this loading, data from the load cells and the LVDTs was recorded by the computer. The result of each test was the load-deflection behavior for each of the three specimens.

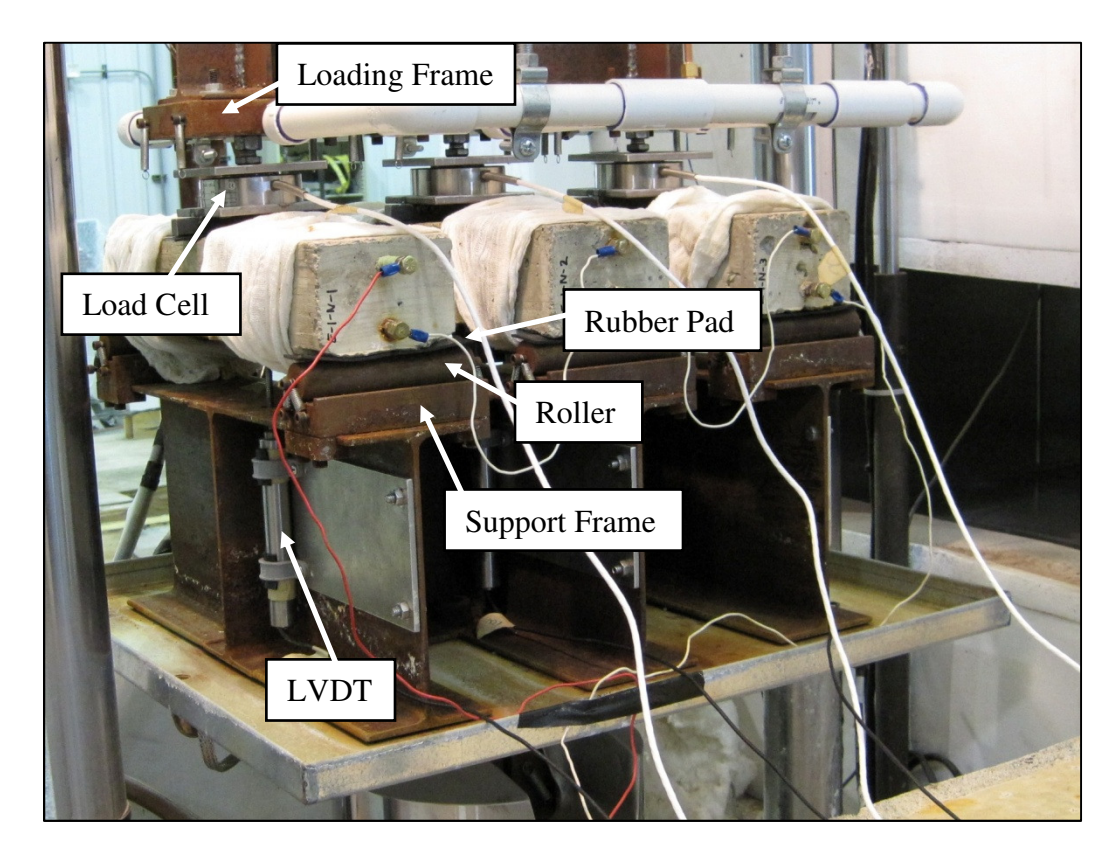


Figure 3.4: Static Test Setup

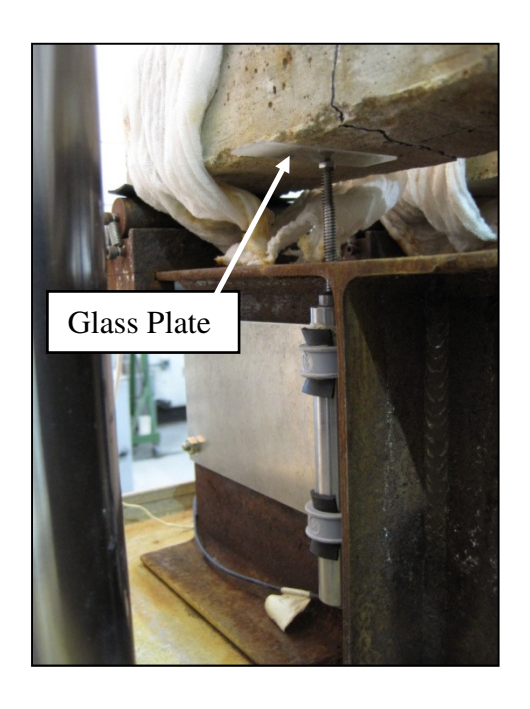


Figure 3.5: Smooth Surface for LVDT

In order to obtain more accurate results, multiple static tests were performed. The first static test was done only to preload the rubber pads, such that the subsequent tests would be performed with the rubber pads having approximately the same amount of deformation. Three static tests were then performed in succession, each one as described before. As shown in Figure 3.6, this resulted in more consistent data, with the latter three tests showing similar load-displacement responses. The nonlinearity in the load-displacement responses during the early stages of loading was due to the nonlinear compressive behavior of the rubber pads used between the rollers and the specimens. The stiffness values obtained from the curves from the latter three tests were averaged for each specimen, obtaining a stiffness value for the specimen after a certain number of fatigue cycles. However, as shown in Figure 3.7, the point where the load was applied and the point where the deflection was measured were not the same. The deflection under the load was estimated by increasing the measured deflection by seven percent as shown in the following calculation:

For a simply supported beam: $\delta(x) = Px/48EI(3L^2 - 4x^2)$

where:

 δ = deflection in the specimen

L =length of specimen

x =distance from edge of specimen

$$\frac{\delta(7.5)}{\delta(5.9)} = \frac{P \cdot 7.5 / 48EI(3 \cdot 15^2 - 4 \cdot 7.5^2)}{P \cdot 5.9 / 48EI(3 \cdot 15^2 - 4 \cdot 5.9^2)} \approx 1.07$$

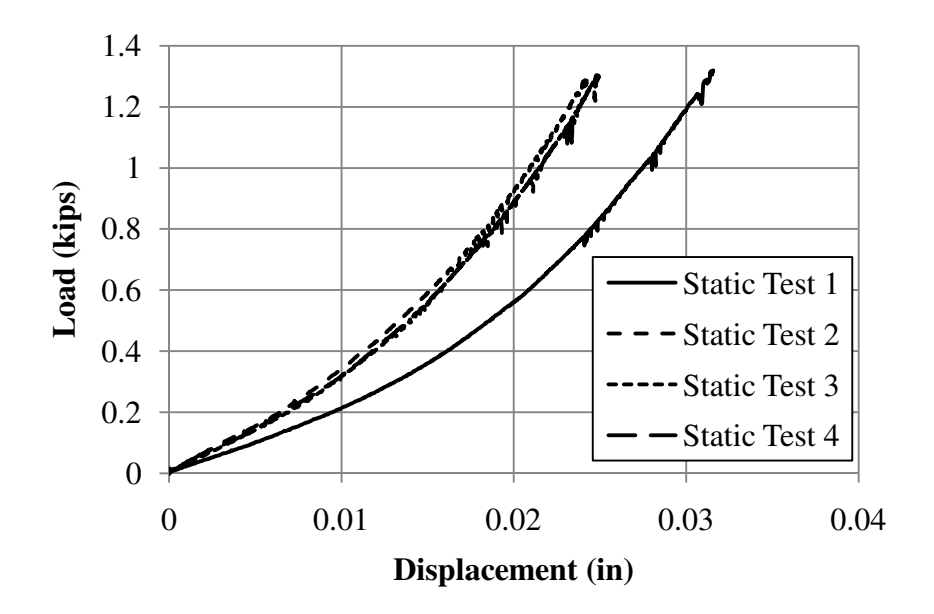


Figure 3.6: Data Obtained from Multiple Static Tests

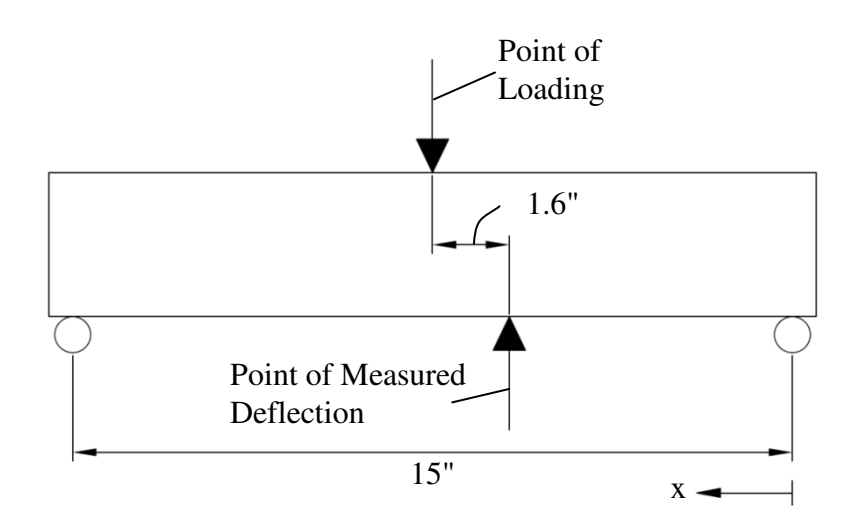


Figure 3.7: Schematic of Static Test

As shown in Figure 3.8, the typical load-displacement graph is non-linear. This is primarily due to the use of the rubber pads between the roller and the specimen, as shown in Figure 3.4. Because of this nonlinearity, the stiffness of the specimens was measured as the slope of the

load-displacement curve when the load was between 0.8 and 1.0 kips. In this range of loading, the rubber pads were significantly compressed and therefore they were not a major factor in the stiffness calculation.

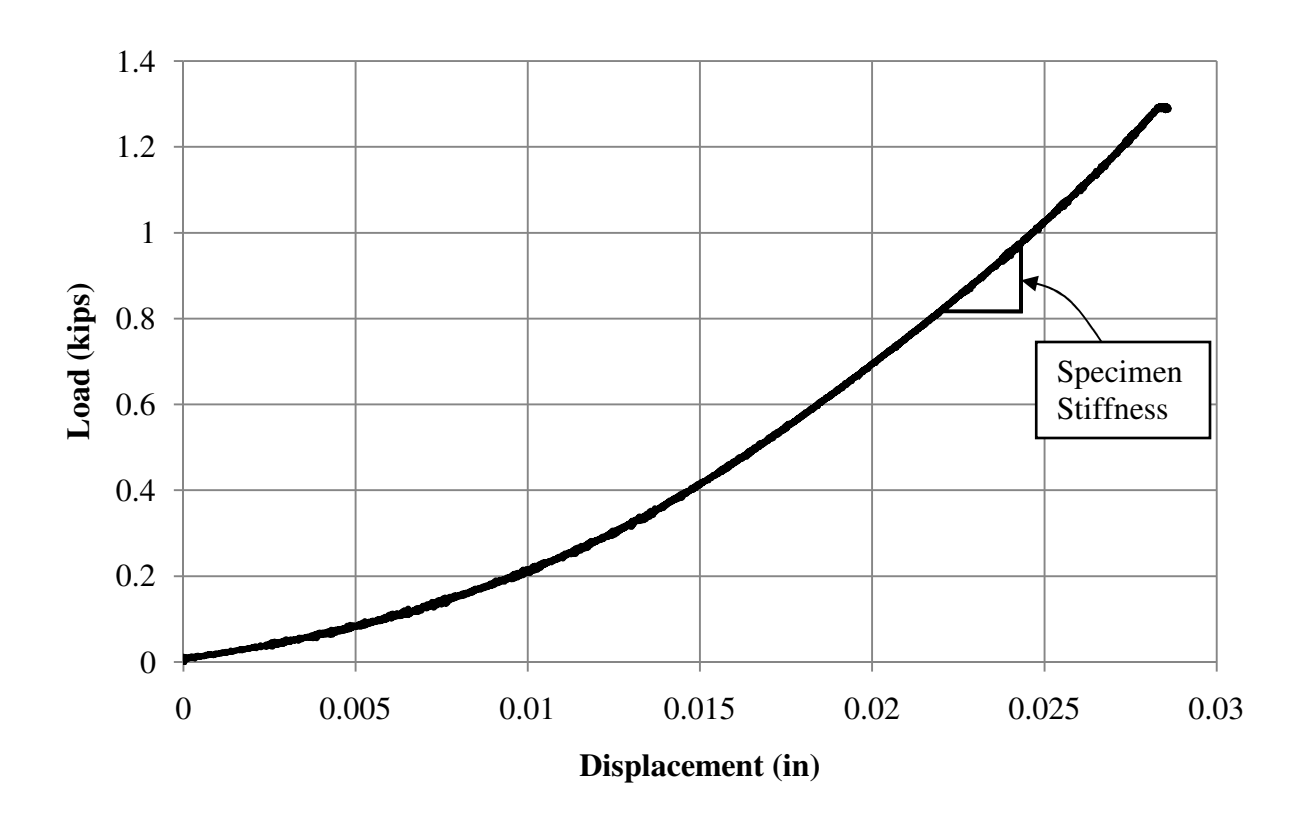


Figure 3.8: Typical Load-Displacement Graph

CHAPTER 4

EXPERIMENTAL TEST RESULTS

The procedures for fatigue and static testing described in Chapter 3 were performed on all repaired and non-repaired specimens and each specimen's stiffness was estimated at specific times during the testing. The expected result was that the stiffness of each specimen would decrease as the fatigue testing progressed. It was envisaged that appropriate repair strategies for ECR decks could be recommended by comparing the stiffness of specimens with black steel with a particular repair option to the stiffness of specimens with ECR with the same repair option.

4.1 Static Test Results

Figures 4.1 to 4.8 show the average stiffness values for each group normalized relative to the initial stiffness measurement for the same group. Figures are not shown for Level 3 unrepaired groups because these specimens failed quickly. The black steel Level 3 unrepaired specimens failed at 0 cycles and the epoxy coated steel Level 3 unrepaired specimens failed at 414,000 cycles. Actual stiffness values are given in Appendix A.

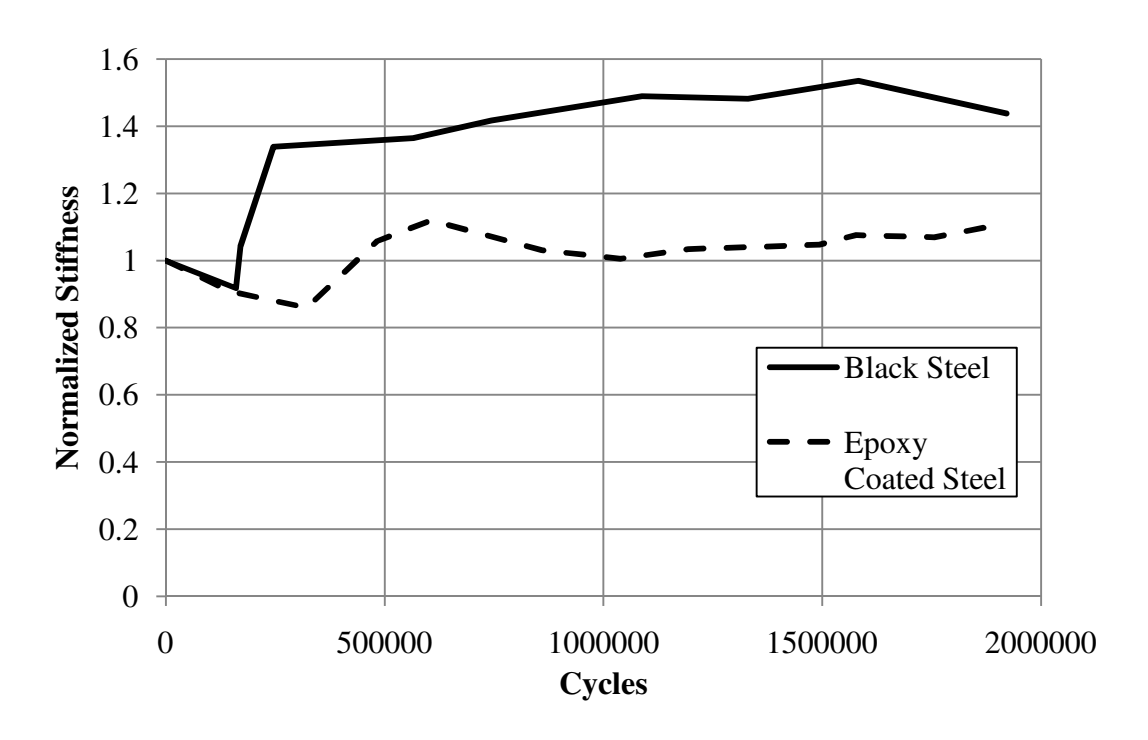


Figure 4.1: Normalized Stiffness Values (Level 0 Unrepaired)

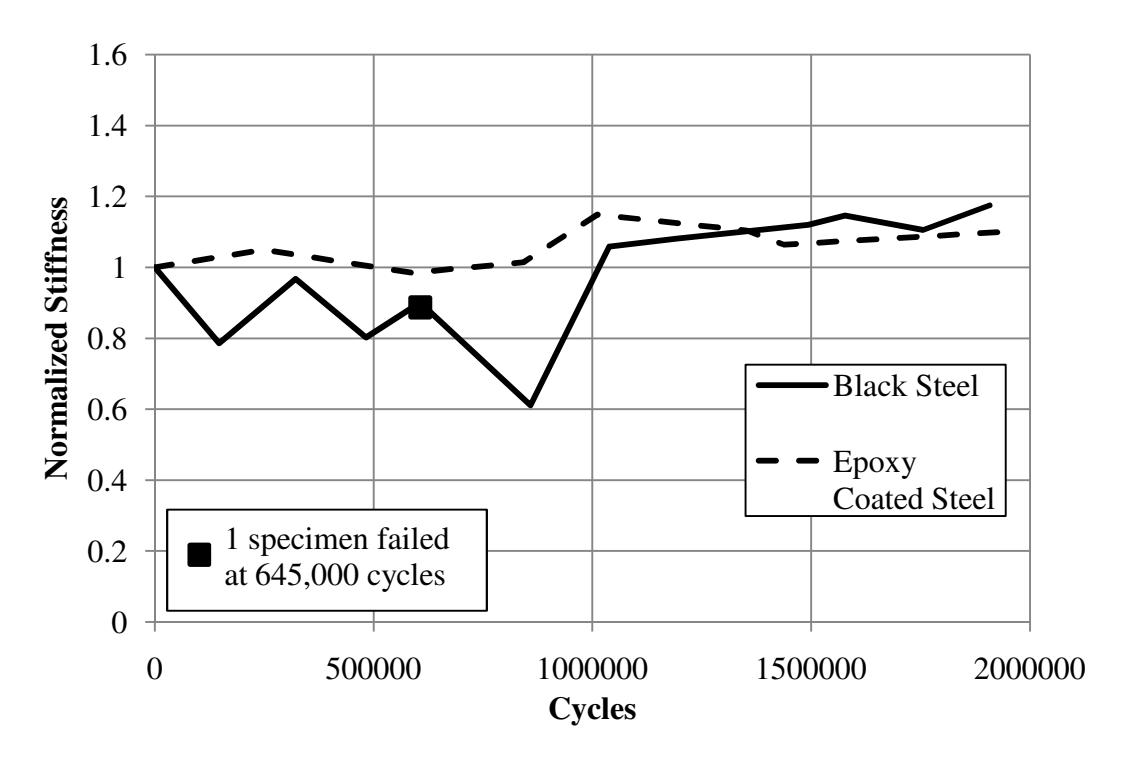


Figure 4.2: Normalized Stiffness Values (Level 1 Unrepaired)

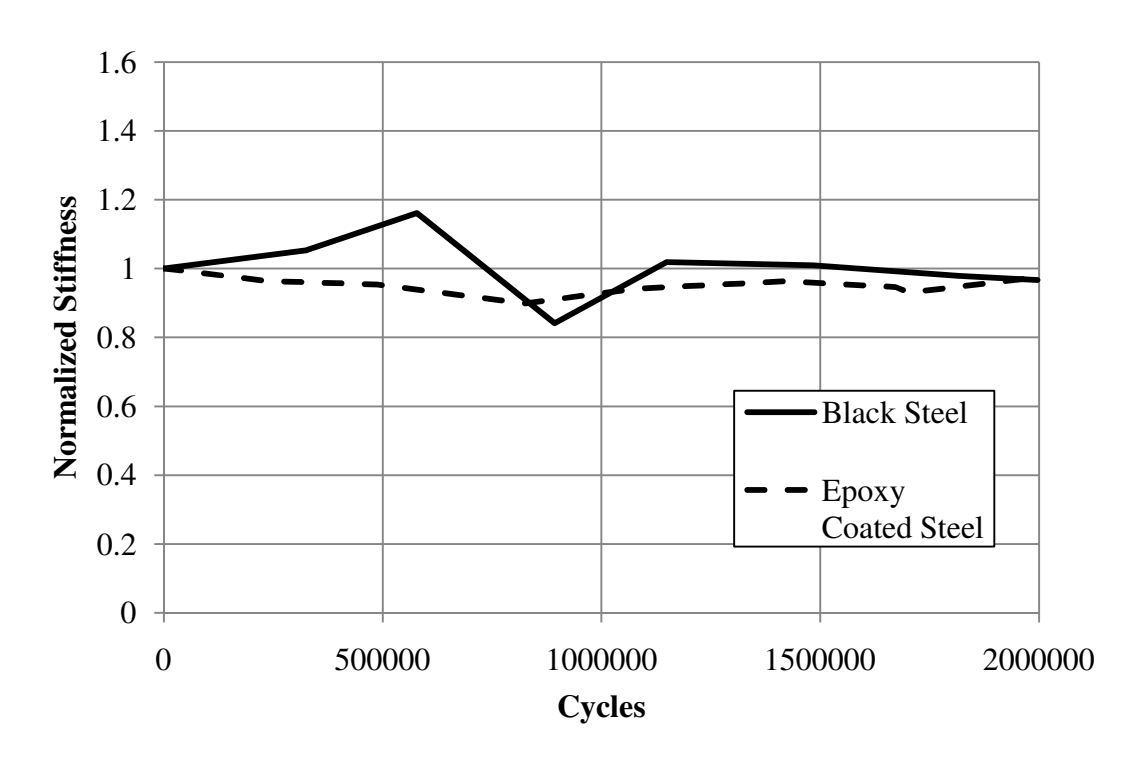


Figure 4.3: Normalized Stiffness Values (Level 1 Repaired)

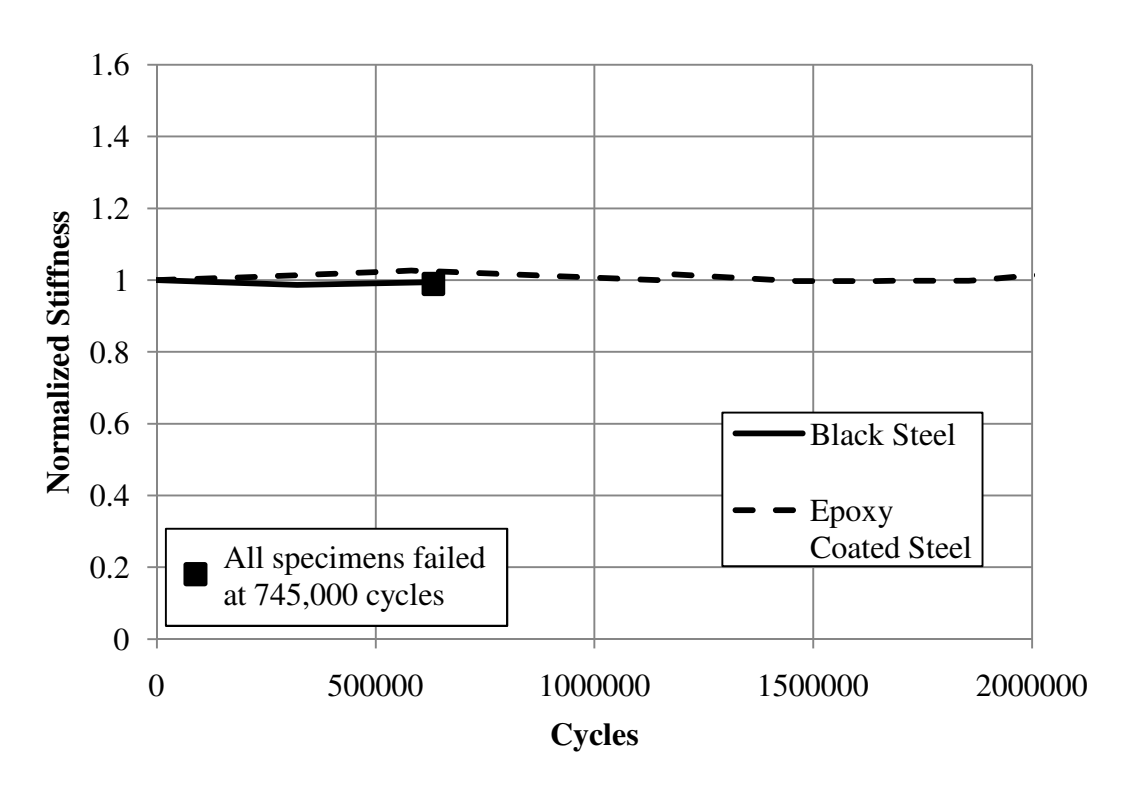


Figure 4.4: Normalized Stiffness Values (Level 2 Unrepaired)

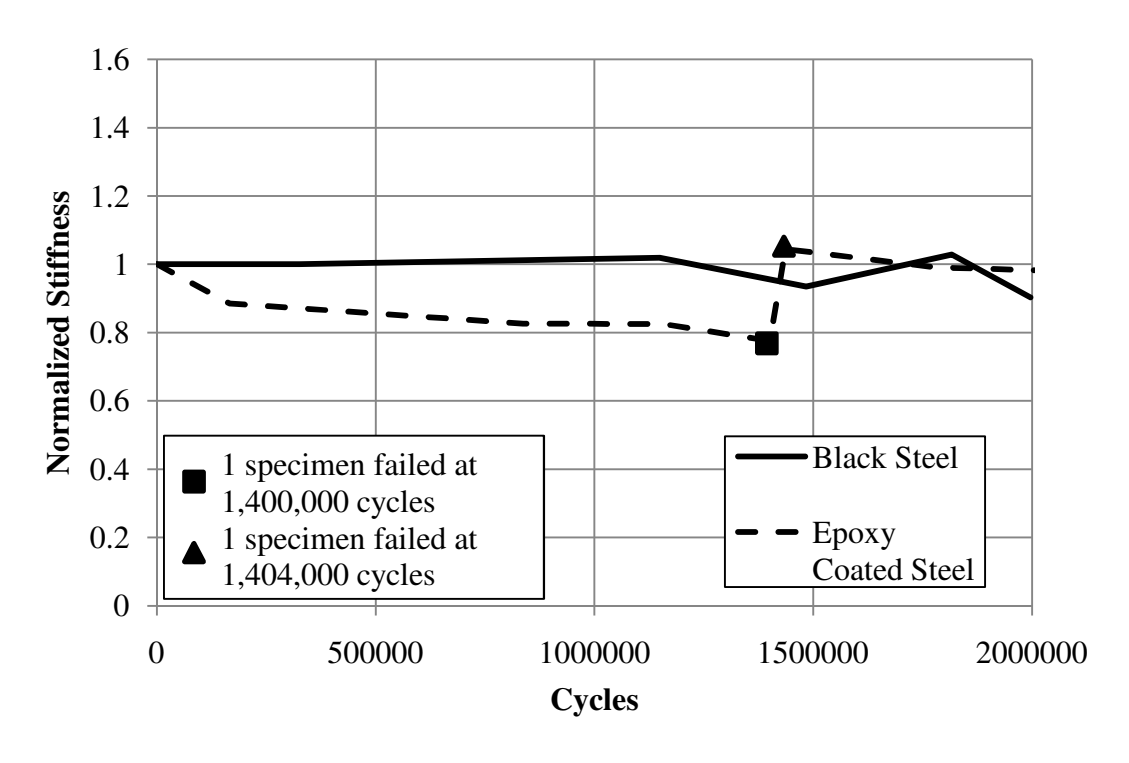


Figure 4.5: Normalized Stiffness Values (Level 2 Repaired)

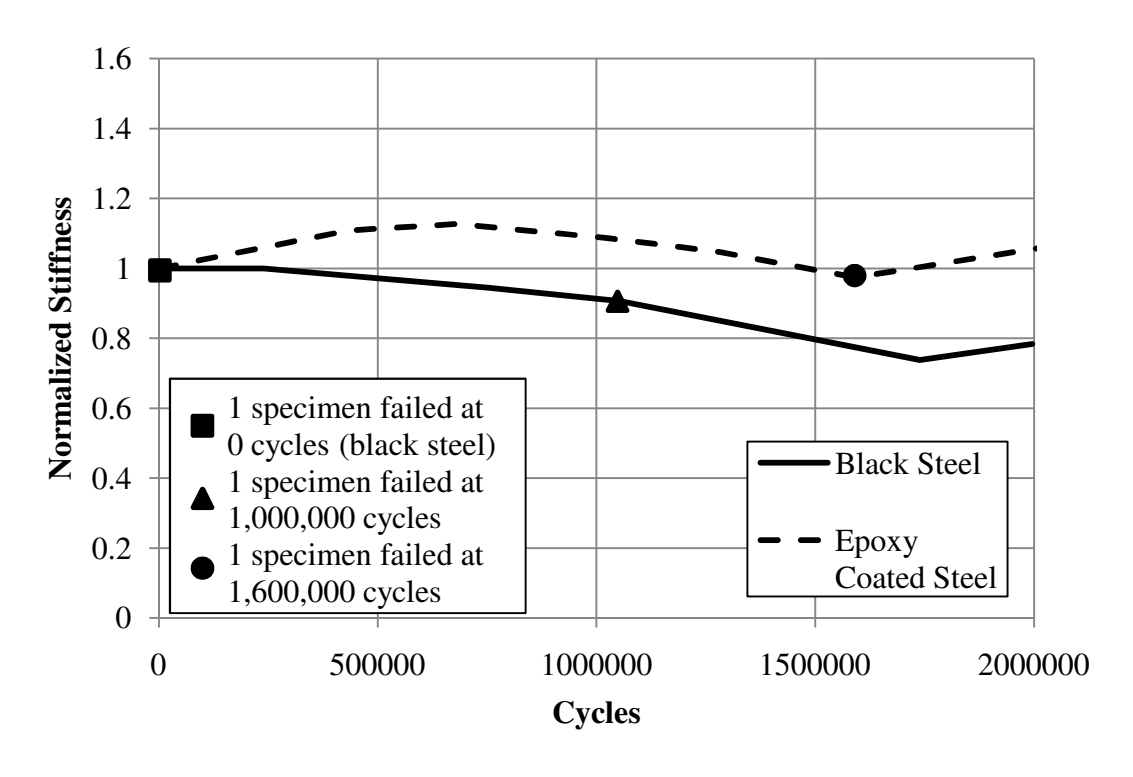


Figure 4.6: Normalized Stiffness Values (Level 3 Repaired)

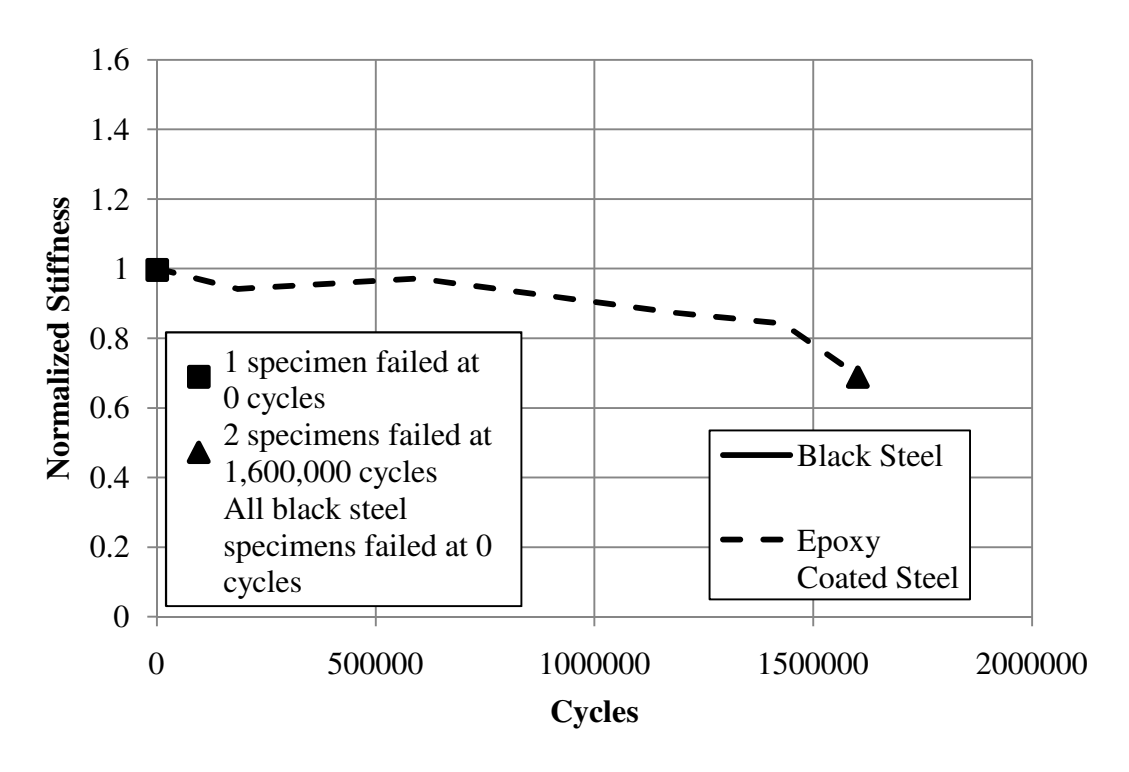


Figure 4.7: Normalized Stiffness Values (Level 4 Unrepaired)

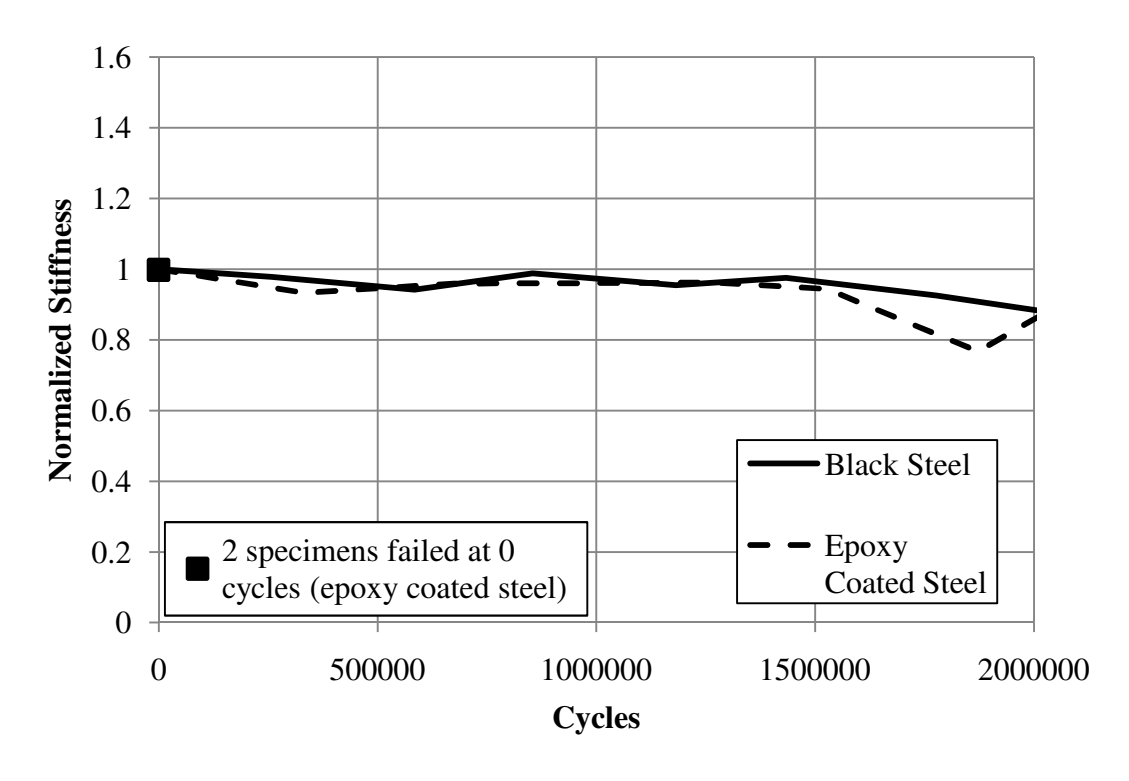


Figure 4.8: Normalized Stiffness Values (Level 4 Repaired)

The stiffness values obtained from the static tests did not show a consistent decreasing trend throughout the fatigue testing as expected. Generally, the stiffness of a given specimen did not change significantly and in many cases, stiffness values increased. Therefore, the stiffness measurements were considered unreliable and not particularly useful.

Some comparisons of the performance between black and epoxy coated steel can be made by examining when some of the specimens failed. Table 4.1 shows the number of cycles to failure for each test specimen. Some specimens were damaged during the repair procedure and hence three replicates were not available for each case. For unrepaired specimens with corrosion levels 0-3, those with black steel always failed before those with epoxy coated steel. Unrepaired specimens with corrosion level 4 all failed when first loaded. Repaired specimens had a more haphazard behavior. In general, epoxy coating helped improve survivability under fatigue loading.

Table 4.1: Survival Under Fatigue Loading

Panair Type/Connecian Lavel	Number of Cycles to Failure*		
Repair Type/Corrosion Level	Black Steel	ECR	
Unrepaired/Level 0	-; -; -	-; -	
Unrepaired/Level 1	-; 644,222	-; -; -	
Unrepaired/Level 2	744,710; 744,710	-; -; -	
Unrepaired/Level 3	0; 0; 0	414,523; 0; 414,523	
Unrepaired/Level 4	0; 0; 0	0; 0; 0	
Epoxy Overlay/Level 1	-; -	-; -; -	
Shallow Concrete Overlay/Level 2	_	-; 1,436,412; 1,401,185	
HMA Overlay/Level 3	-; 0; 1,053,614	-; 1,591,507	
Deep Concrete Overlay/Level 4	-; -; -	0; 0; –	

^{*} The symbol – indicates that a specimen did not fail during the 2 million fatigue cycles

4.2 Corrosion during Fatigue Loading

During fatigue testing the specimens were subjected to accelerated corrosion. This was done by impressing current through the specimens as described in Sections 2.3 and 3.1. The impressed current was measured throughout the fatigue testing, which was then used as a measure of the corrosion-induced damage in the specimens. A typical graph showing the corrosion charge vs. fatigue cycles is shown in Figure 4.9.

The corrosion rate was slower for epoxy coated steel than for black steel by a factor of about 2.5. Therefore, similar to the observations in Section 2.3, epoxy coated steel should effectively delay the appearance of corrosion induced damage compared to black steel. The corrosion data is discussed in more detail in Chapter 6.

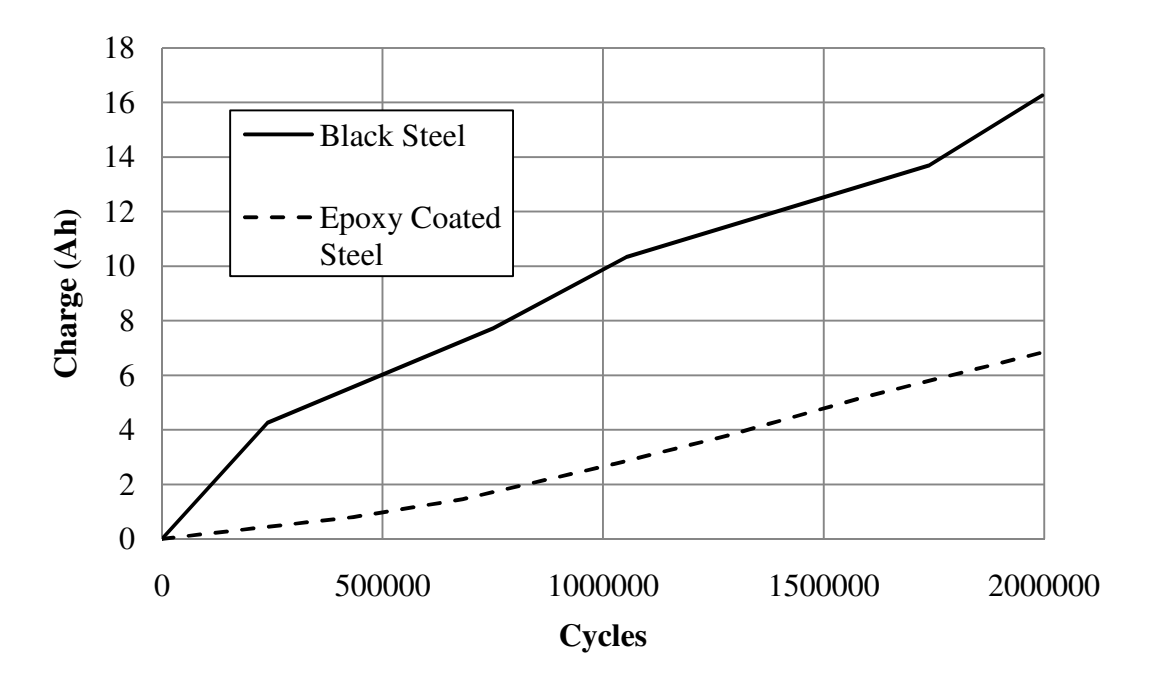


Figure 4.9: Charge vs. Fatigue Cycles

CHAPTER 5

X-RAY COMPUTED TOMOGRAPHY

As discussed in Chapter 4, the stiffness values obtained during the fatigue testing did not provide results that were useful in quantifying the damage done to the concrete specimens with black steel and epoxy coated steel. X-ray tomography had the potential to identify internal damage in concrete specimens. The concrete specimens were scanned with X-rays, resulting in images at specific cross-sections of the specimens. These images showed the cracks inside the specimens, which were used as an indication of the amount of damage done during the fatigue testing.

5.1 X-Ray Scanning

The specimens were scanned at the Center for Quantitative X-Ray Imaging (CQI) at Penn State University [34]. This facility houses the HD600 (OMNI-X) industrial high-resolution X-ray computed tomography (CT) scanner, which was used to scan the specimens [35]. Figure 5.1 shows a photograph of the setup used to do the scanning. A specimen was placed in a tube of sand and rotated on a plate as it was scanned 2400 times in order to produce the best quality image possible at a particular location. Eighty-nine images along the length of the specimen, each with a separation of 0.0046 inches, were taken at four locations in each specimen. Two locations were 1 inch on either side of the mid-length, and the other two locations were 2 inches on either side of the mid-length. Therefore, at each location, images of the cross-sections of the specimen were captured along a 0.409 inch length of the specimen. These images were used to determine the volume of cracks within the four 0.409 inch long segments of each specimen. An

example of an image is shown in Figure 5.2 with a photograph of the specimen shown in Figure 5.3 for comparison.

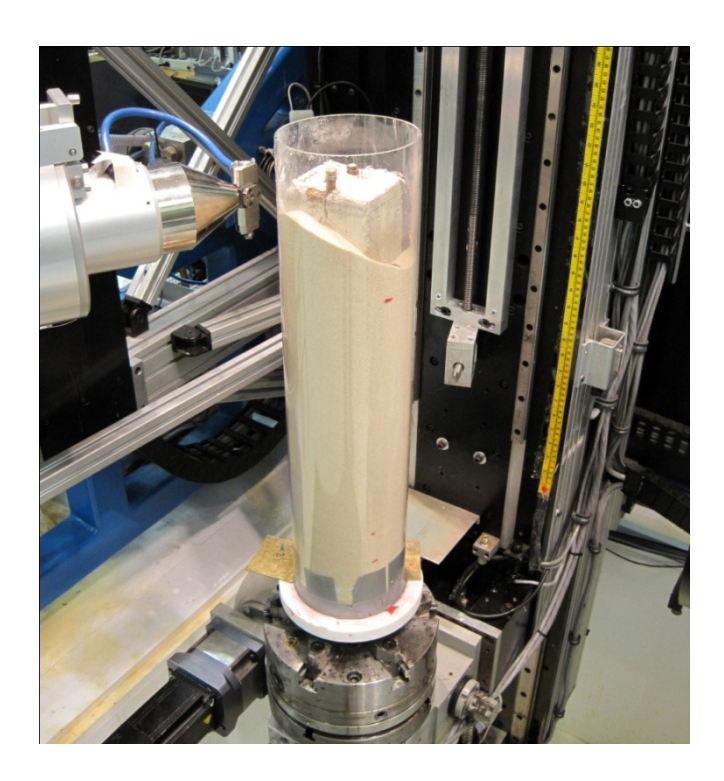


Figure 5.1: X-Ray Scanning Setup

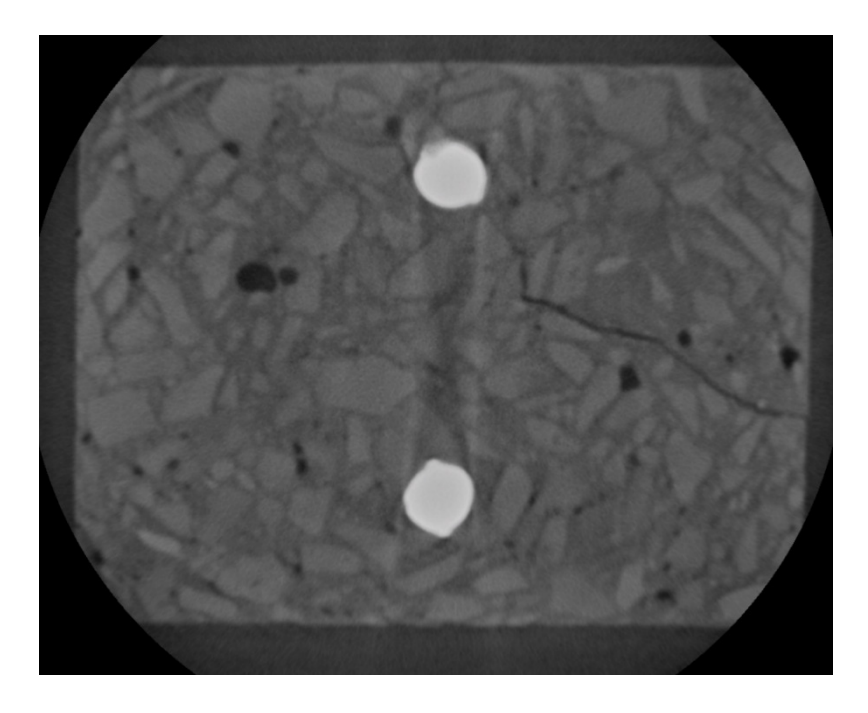


Figure 5.2: Example of X-Ray Scan



Figure 5.3: Photograph of Scanned Specimen

This process was conducted for each specimen that did not break apart during the fatigue testing. A total of 28 specimens were scanned. Images that show a typical scan and its corresponding threshold image from each repair type are shown in Appendix B.

5.2 Image Processing

The main goal of the X-ray scans was to quantify the damage done to each specimen as a result of corrosion, freeze-thaw, and fatigue loading. This was done by computing the volume of the cracks that were visible in the X-ray images. As described in Section 5.1, each specimen had four locations scanned and at each location a thickness of 0.409 in. was scanned 89 times, allowing for the volume of cracks to be calculated. Software was used to compile the images and calculate the volume of cracks [36]. However, before this software was used, a number of steps were performed to process the images so they could be used. The image from Figure 5.2 will be

used as an example to illustrate the process. The software used for the following steps is called "ImageJ" [37].

1. Crop the desired crack from the rest of the image.

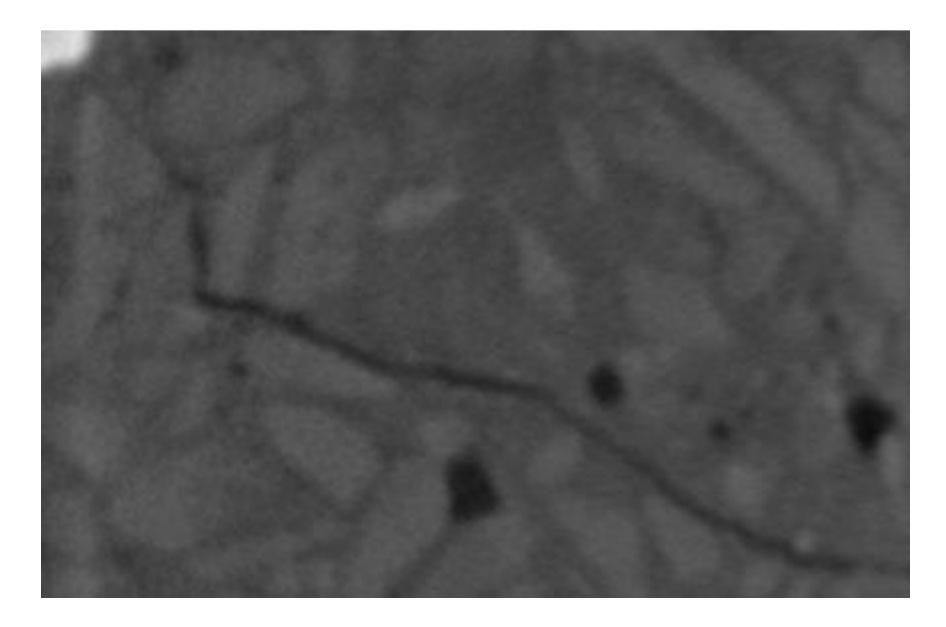


Figure 5.4: Crack Cropped from Image

2. Invert the colors.

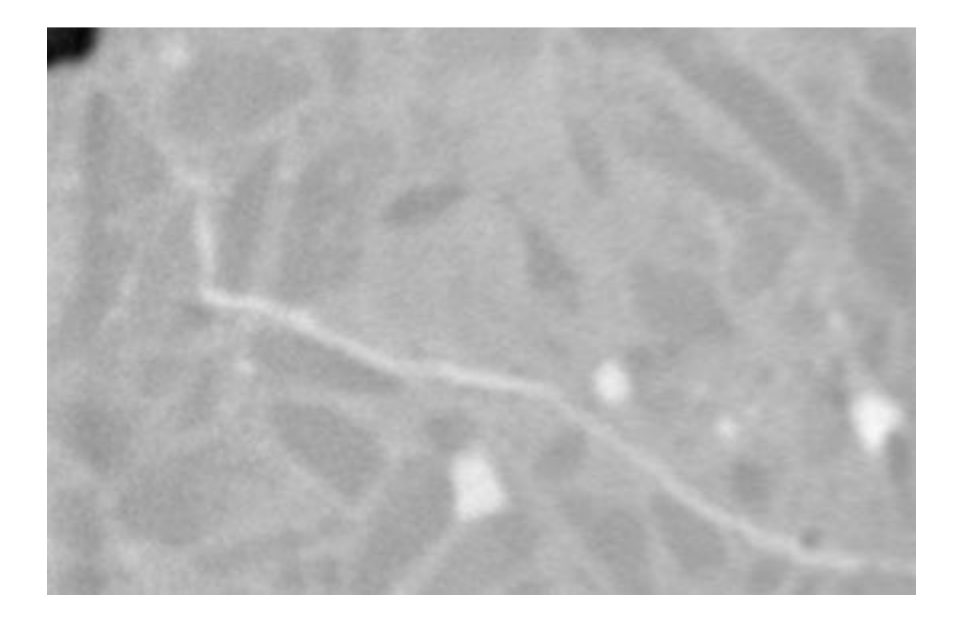


Figure 5.5: Crack with Inverted Colors

3. Adjust contrast and brightness. The values used to adjust these parameters varied between specimens such that the crack was easily shown in each case.

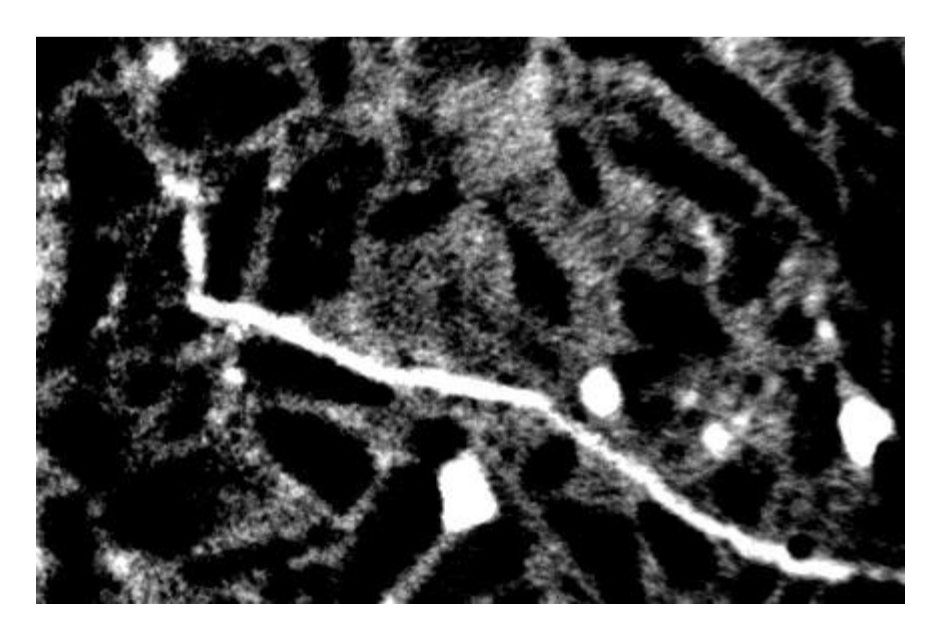


Figure 5.6: Crack with Enhanced Brightness and Contrast

4. Apply a bandpass filter to reduce noise.

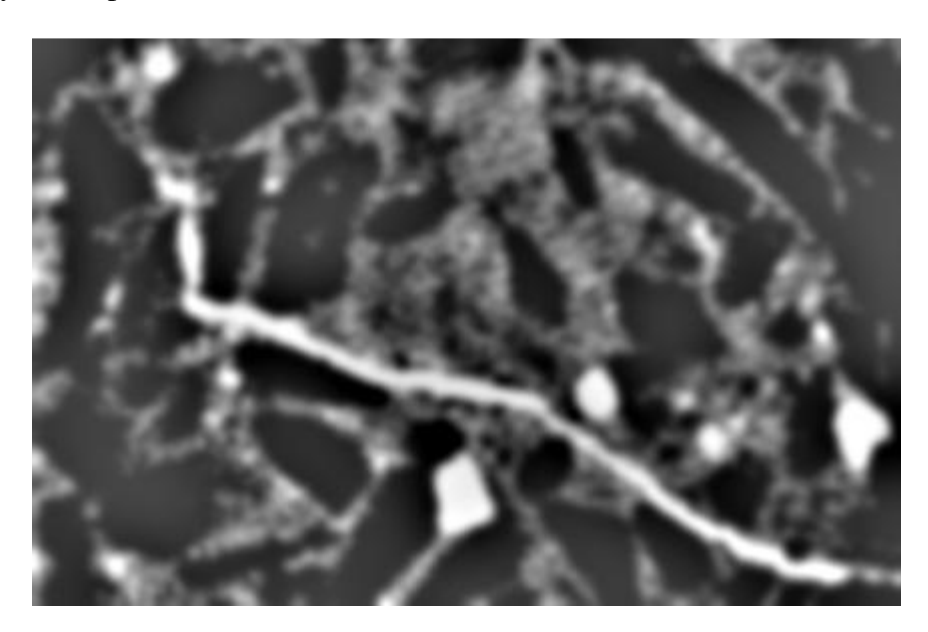


Figure 5.7: Crack after Applying Bandpass Filter

The images were then imported into the XCAT software and a threshold was applied, converting the grayscale images into black and white.

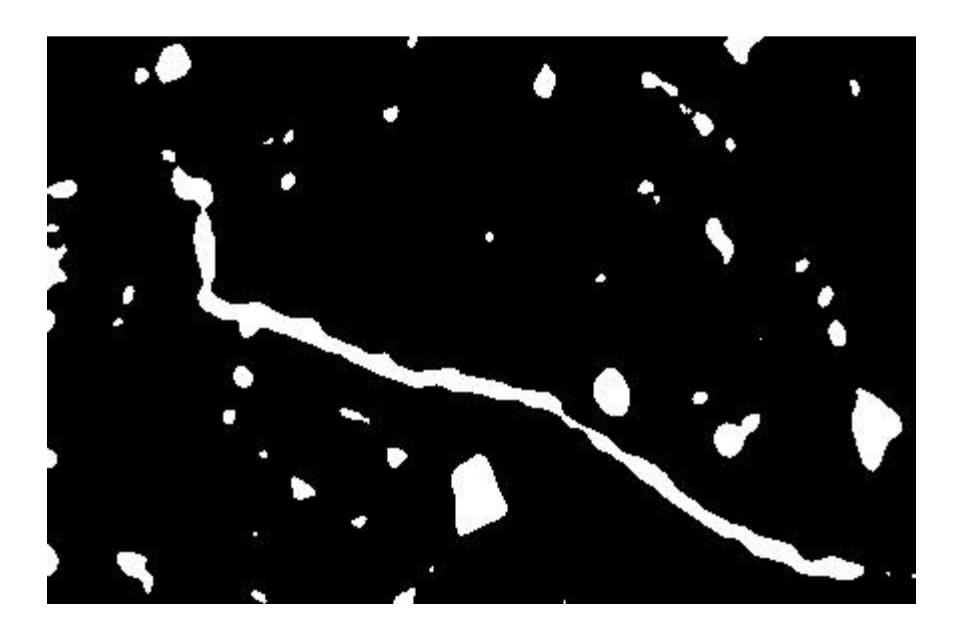


Figure 5.8: Crack after Applying Threshold

This process was done for all 89 images at each location. The XCAT software reconstructed the images at each location and created a 3D rendering of the crack, as shown in Figure 5.9. The software then calculated the volume of the crack in voxels (volumetric pixel). The total volume of cracks in a specimen was used as a measure of the damage done to it by corrosion, freezethaw, and fatigue testing. The results showing the image-based damage for each specimen scanned are shown in Table 5.1 along with the time that each specimen was exposed to accelerated corrosion (initial corrosion for aging plus corrosion during fatigue loading).



Figure 5.9: 3D Rendering of Crack

 Table 5.1:
 Image-Based Damage

Specimen	Image-Based Damage (voxels)	Time (days)
B-0-1	0	23
B-0-2	0	23
B-0-3	89,285	23
B-1-N-1	18,733	35
B-1-N-2	210,555	35
B-1-R-1	1,850,790	35
B-1-R-2	105,660	35
B-2-R-2	1,009,233	54
B-3-N-2	520,482	62
B-3-R-2	1,951,323	79
B-4-R-1	1,165,097	86
B-4-R-2	0	86
B-4-R-3	754,504	86

Specimen	Image-Based Damage (voxels)	Time (days)
E-0-1	0	23
E-0-2	0	23
E-1-N-1	0	44
E-1-N-2	0	44
E-1-N-3	0	44
E-1-R-1	0	67
E-1-R-2	0	67
E-1-R-3	0	67
E-2-N-2	0	147
E-2-N-3	0	147
E-2-R-2	373,500	144
E-3-N-1	757,362	175
E-3-N-3	126,751	175
E-3-R-2	307,464	144
E-4-R-2	15,311	182

CHAPTER 6

INTERPRETATION OF RESULTS AND CONCLUSIONS

The goal of this part of the project was to determine the maintenance schedule for ECR concrete bridge decks. The Michigan Department of Transportation (MDOT) has an established maintenance schedule for concrete bridge decks with black steel based on the amount of surface and underside damage on decks. By comparing the times to equivalent damage levels in ECR and black steel concrete decks, the maintenance schedule for black steel decks could be revised for ECR decks. Damage levels were defined in two ways: (1) by using the corrosion charge impressed during specimen aging described in Section 2.3 (Phase 1) and during the fatigue testing described in Section 4.2 (Phase 2); and (2) by comparing the image-based damage between specimens as described in Section 5.2.

6.1 Corrosion Damage

The cumulative corrosion charge measured during the test was used as a measure of how much the steel corroded as evidenced by the physical appearance (staining, cracking) of the specimen. In other words, how much total charge in Ah was impressed to the specimen at the time of damage observation. A comparison of the corrosion charge for epoxy coated and black steel reinforcement would reveal the relative improvement against corrosion provided by the epoxy coating. Figure 6.1 shows a plot of the corrosion charge as a function of the time for which each specimen experienced accelerated corrosion in the laboratory. Data throughout Phase 1 and Phase 2 are plotted in this figure for all specimens, including repaired and unrepaired. The data displayed in this figure is shown in Appendix C. The approximate field time scale is also

shown on the top (x-axis). This scale was determined by utilizing the fact that a certain amount of charge corresponds to a certain amount of time in the field as described in Section 2.3. The values from Table 2.2 were used where Level 4 damage corresponded to 30 years in the field and Level 1, 2, and 3 damage levels corresponded to 7.5, 15, and 22.5 years in the field, respectively. The time for each group of black steel specimens to reach each level of damage when exposed to accelerated corrosion was averaged and is shown in Table 6.1. This data suggests that the relationship between the time of accelerated corrosion and the corresponding time in the field is linearly related according to Equation 6.1 where t_{field} is the time in the field and t_{ac} is the time exposed to accelerated corrosion (both expressed in the same units).

$$t_{field} = 181.7t_{ac} \tag{6.1}$$

Table 6.1: Estimates of Time in the Field for Black Steel

Time in the	Target Corrosion	Average Time of Accelerated
Field (years)	Charge (Ah)	Corrosion (days)
7.5	12.57	12.8
15	43.65	29.7
22.5	74.72	45.7
30	105.79	60.6

The rate of corrosion charge is higher in black steel than in epoxy coated steel. The data displays considerable scatter, but the type of repair does not seem to have a significant impact on the rate of corrosion during Phase 2. This may be because during fatigue testing moisture could enter the specimens from the sides even though the repair may affect the permeability through the top surface. The behavior may be different in the field where moisture can only penetrate through the top surface.

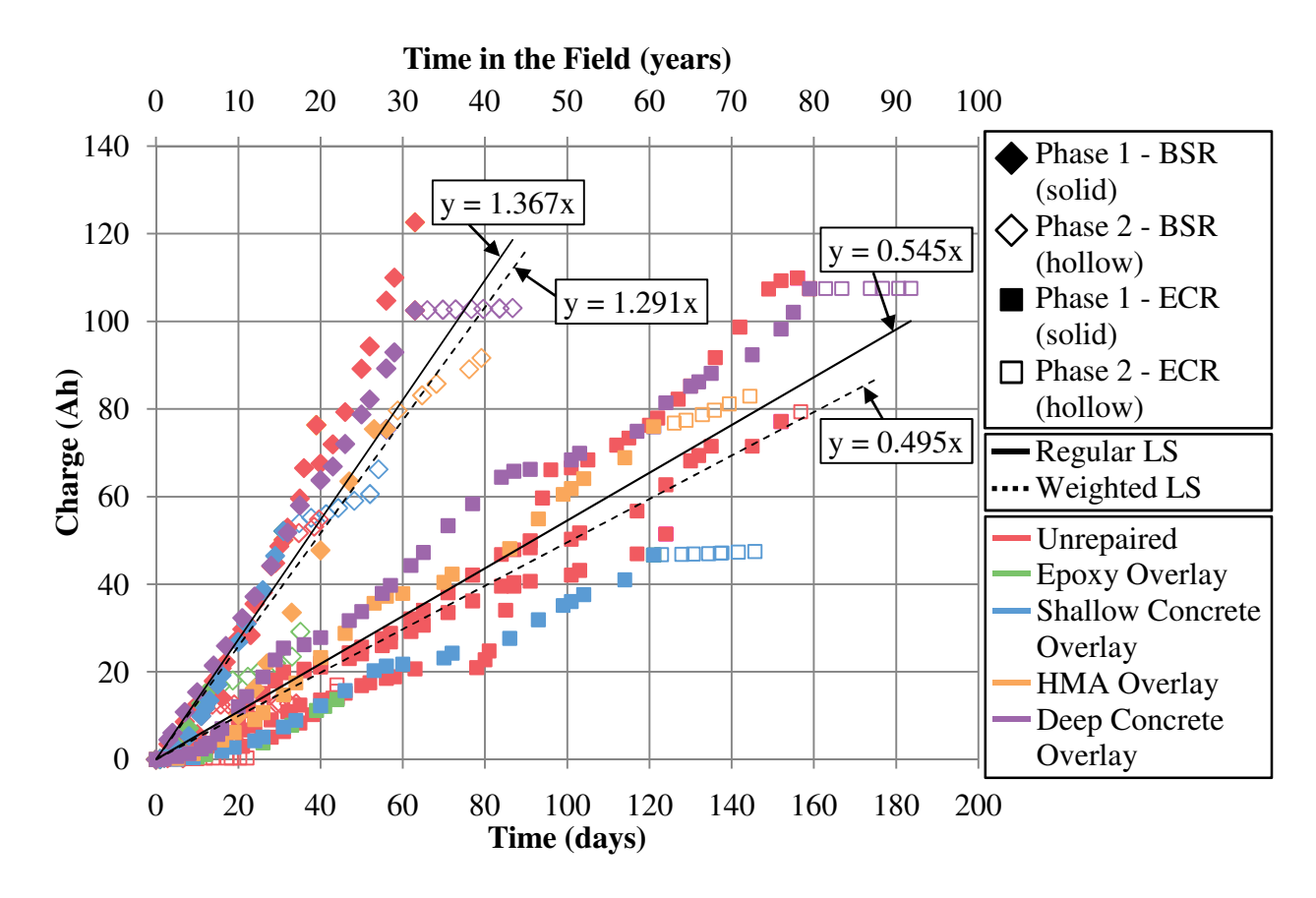


Figure 6.1: Charge vs. Time for Phase 1 and Phase 2

The scatter in Figure 6.1 is non-uniform and the variance increases with time (i.e., scatter is more at larger times). Regression lines fitted to the data should consider the non-constant variance and a weighted least squares fit should be used [38]. Regression lines based on both regular and weighted least squares analysis were fitted for the black steel and the epoxy coated steel and are shown in Figure 6.1. The regular least squares regression lines are shown as solid lines and the weighted least squares regression lines are shown as dotted lines. The difference between the two sets of lines is not large.

The slopes of these lines (i.e., rate of corrosion charge) were used to compare the corrosion rates of the steel bars. Based on the weighted least squares regression lines, the rate of corrosion in epoxy coated steel was about 2.6 times slower than in black steel (i.e., 1.291/0.495 = 2.60). If

the regular least squares regression lines are used, then the rate of corrosion in epoxy coated steel was about 2.5 times slower than in black steel (i.e., 1.367/0.545 = 2.51).

The residuals (measured charge – charge predicted by the regression line) and weighted residuals (residual multiplied by the weight used for each point) for the black steel and ECR are shown in Figure 6.2 and Figure 6.3, respectively. The residuals are heteroscedastic while the weighted residuals are reasonably homoscedastic, indicating that the weights used were appropriate. There were also no significant outliers in the data.

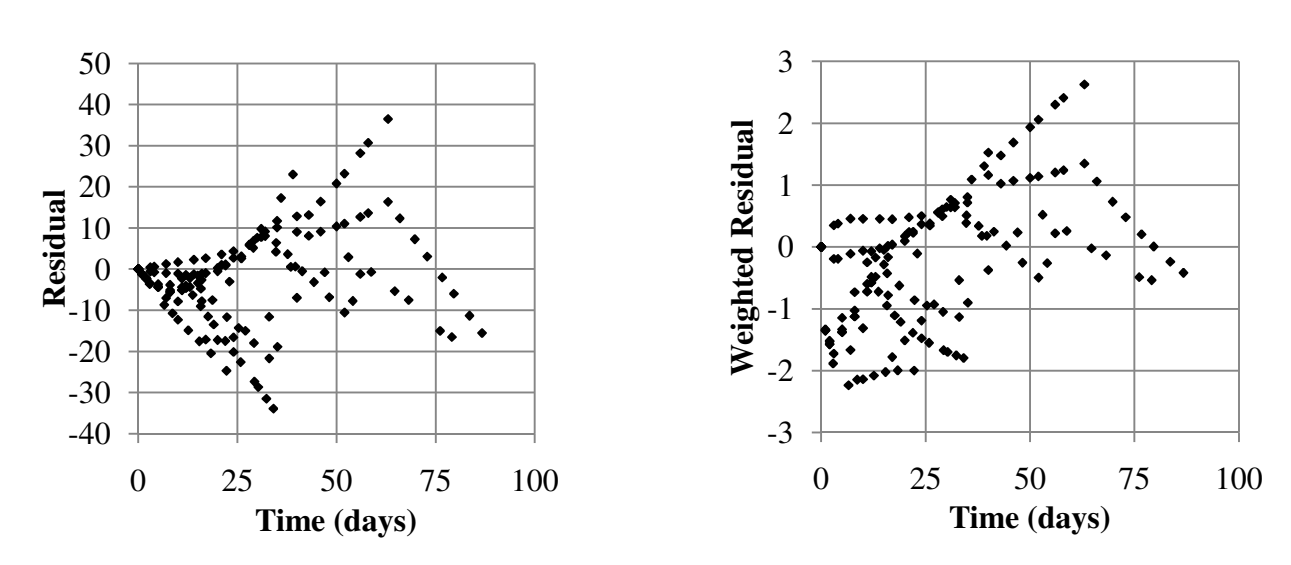


Figure 6.2: Residual and Weighted Residual Plots for Black Steel

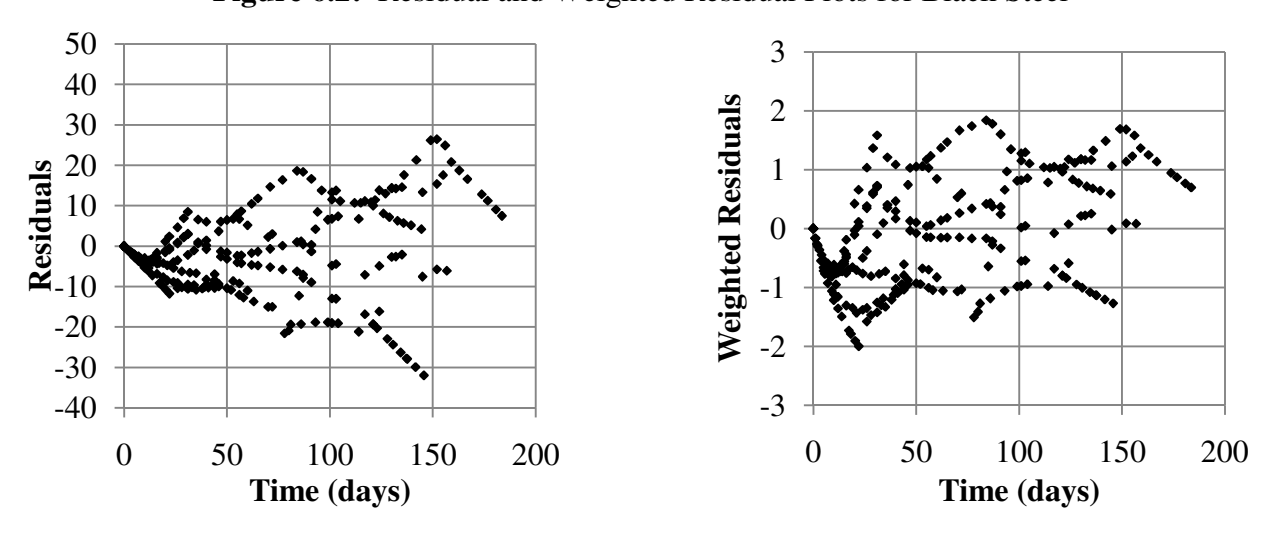


Figure 6.3: Residual and Weighted Residual Plots for ECR

Figure 6.3 shows that the residuals for ECR are mostly negative toward the beginning of the accelerated corrosion testing when using a simple linear regression model. The data in the early stage was examined to see if a better fit could be obtained. Figure 6.4 shows the data in the early stage of accelerated corrosion for ECR. This data seems to indicate a slow progression in the corrosion rate for approximately 12 days (equivalent to about 6 years in the field) after which a higher corrosion rate ensues. A bilinear regression model was used to capture this behavior and provides a better fit for ECR. However, black steel did not show this trend. The bilinear fit indicates that for the first 12 days (6 years in the field) the rate of corrosion in ECR is about 13 times slower than that of black steel. After this the rate of corrosion in ECR is about 2.2 times slower than that of black steel.

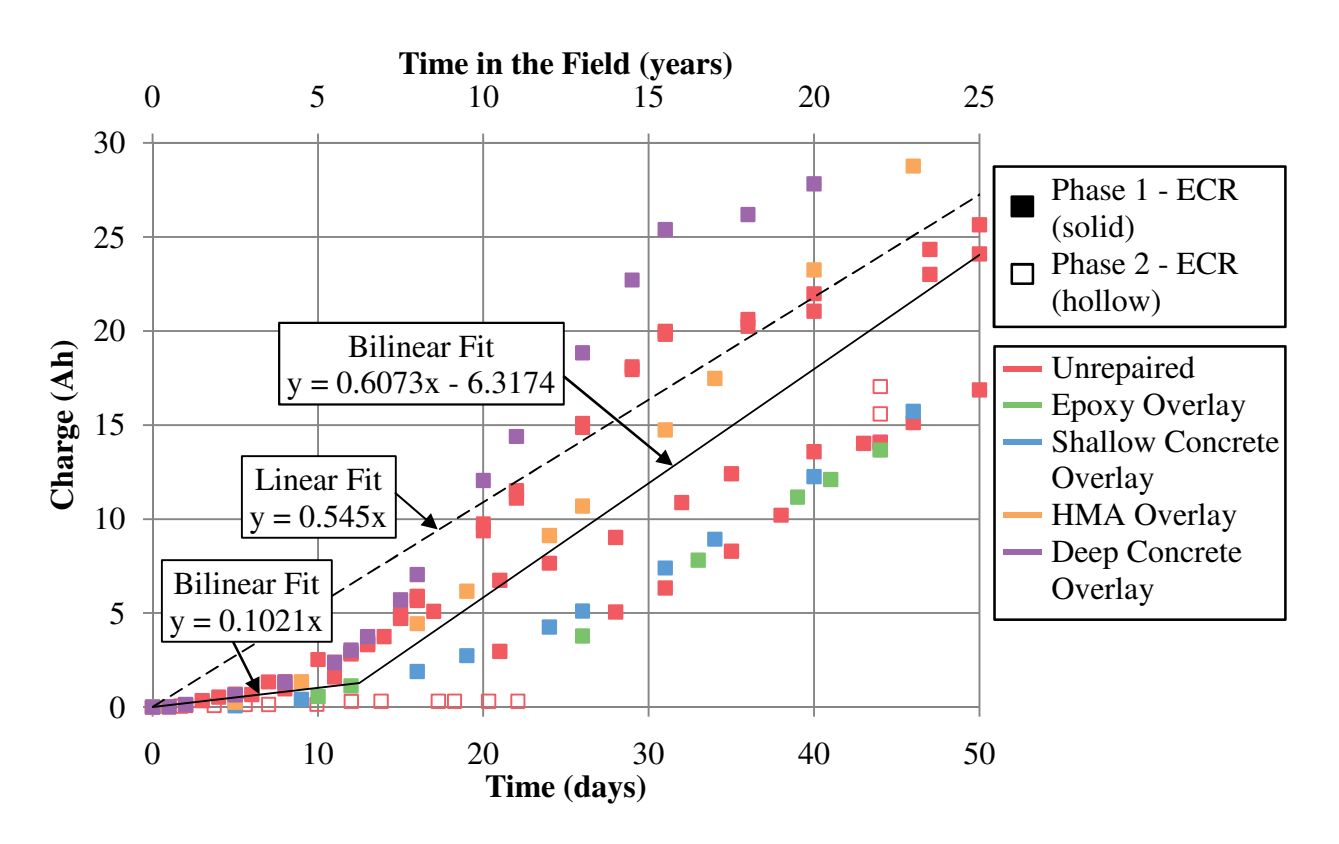


Figure 6.4: Early Stage of Accelerated Corrosion for ECR

6.2 Image-Based Damage Results

The volumes of cracks in the specimens, as described in Section 5.2, were used to assess the damage done to the specimens during Phase 1 and Phase 2. All of the cracks visible in the X-ray images of the specimens were assumed to be due to corrosion only and not from the fatigue loading. The fatigue loading induced flexural cracks, which closed when the specimens were unloaded and were not visible in the X-ray images. The data in Table 5.1 was plotted against the time each specimen was subjected to the accelerated corrosion in Phase 1 and Phase 2. This plot is shown in Figure 6.5, with the image-based damage normalized by dividing by 2,000,000 pixels.

The data from the deep concrete overlay specimens were removed from this plot. In the deep concrete overlay repairs, the damage in the concrete that was removed (upper half of the specimen) was completely repaired and a new ECR bar was used, and therefore the image-based damage data was skewed for that group of specimens. Other than for the deep concrete overlay, the repairs did not significantly affect the corrosion induced cracking.

Although the scatter is quite large, and the number of data points is small, since many specimens did not survive the fatigue testing, polynomial curves were fitted for each type of steel. The residual plot when all points were included in the fit is shown in Figure 6.6. The one outlier identified was excluded when obtaining the fit shown in Figure 6.5. These curves were used to compare the "average" damage in specimens with epoxy coated and black steel.

The times predicted by the curves for attainment of four arbitrary damage levels are shown in Table 6.2. A time scale factor was computed by dividing the time to attain a given damage level for epoxy coated steel by the corresponding time for black steel. For normalized levels of

damage up to 0.2, specimens with epoxy coated steel took about four times longer to attain the same damage state as specimens with black steel.

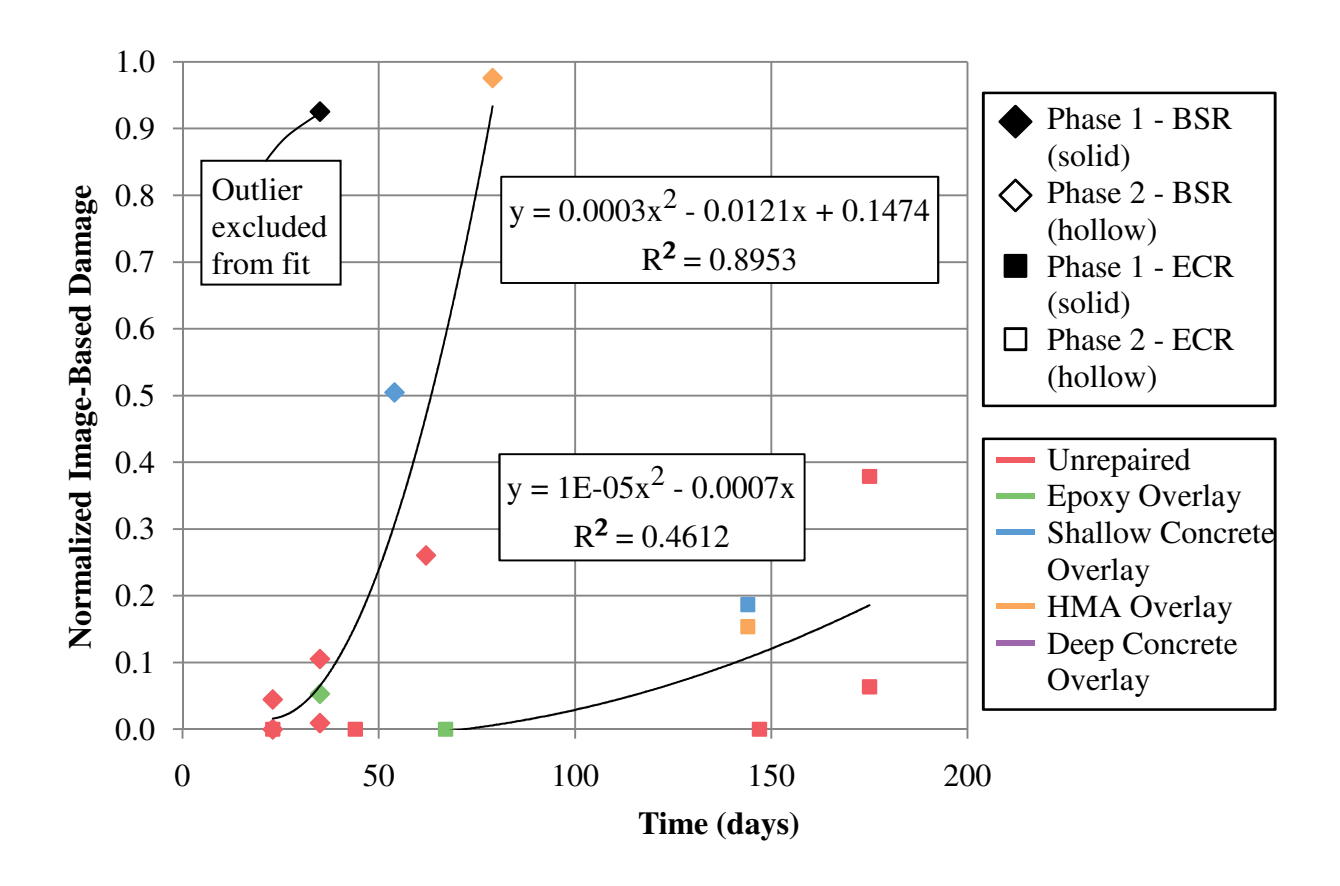


Figure 6.5: Image-Based Damage vs. Time

Table 6.2: Time Scale Factors from Image-Based Damage

Image-Based	Time (days)		Time Scale	
Damage	Black	ECR	Factor	
0.05	29.2	113.9	3.90	
0.1	35.9	140.9	3.92	
0.15	40.5	162.4	4.01	
0.2	44.3	180.7	4.08	

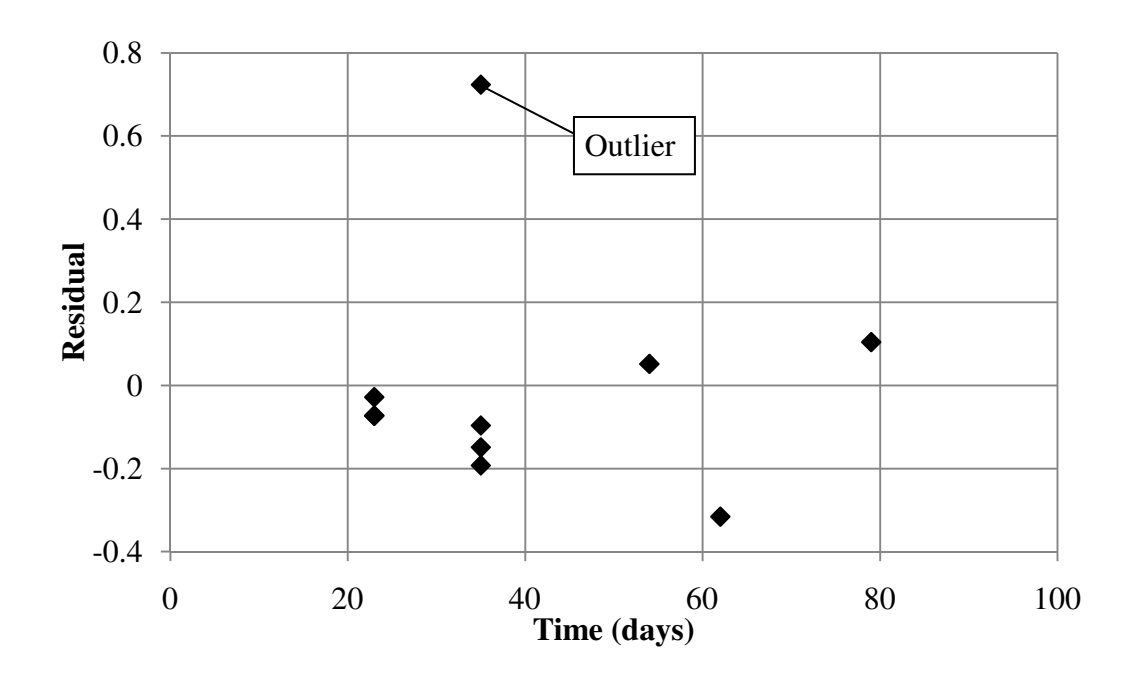


Figure 6.6: Residual Plot with All Points Included

6.3 Summary and Conclusions

Concrete beam specimens were fabricated with an epoxy coated or black steel top bar and a black steel bottom bar. The specimens were aged by subjecting them to 300 freeze-thaw cycles and then accelerated corrosion using an impressed current. Different groups of specimens were subjected to four corrosion levels and four different types of repairs were performed. Level 4 corrosion was taken to be the corrosion experienced over 30 years in the field assuming a reduction in diameter of 0.045 mm/year. Level 1 corrosion was the charge required to induce the first cracks in the specimens. Levels 2 and 3 had corrosion charges equally spaced between the charges required for Levels 1 and 4. Specimens corroded to levels 1, 2, 3, and 4 were repaired with an epoxy overlay, shallow concrete overlay, asphalt overlay with a waterproofing

membrane, and a deep concrete overlay, respectively. The repaired specimens were then subjected to fatigue loading using 3-point bending for 2 million cycles or until failure, combined with freeze-thaw exposure and continued accelerated corrosion. Control specimens that were aged and not repaired and other control specimens that were not aged or repaired were also subjected to the combined fatigue loading, freeze thaw exposure, and accelerated corrosion. Static flexural tests were performed periodically throughout the fatigue loading to measure the flexural stiffness of the beam specimens.

X-ray computed tomography (CT) scans of the specimens that survived the 2 million cycles of fatigue loading were performed. The volume of corrosion-induced cracks at four cross sections, each having a width of 0.409 inches, were computed from the X-ray CT images and used as another measure of damage.

The following conclusions are made based on the test data obtained in this project:

- The impact of damage growth due to corrosion, fatigue cycles at service load levels, and freeze-thaw cycling on the flexural stiffness of repaired and unrepaired beam specimens does not show any consistent trends for specimens with epoxy coated and black steel reinforcement. Stiffness measurements were therefore not useful in quantifying damage.
- The electrical charge impressed to concrete specimens in accelerated corrosion testing indicated that epoxy coated steel with 2 percent surface damage to the coating corroded at a rate that was about 2.5 times slower than black steel. The corrosion rate was not affected significantly by different repairs performed to the concrete surface after initial aging. Fatigue loading also did not have an effect on the corrosion rate.

- The volume of corrosion-induced cracks estimated from X-ray CT scan images indicated that it took about four times longer for specimens with epoxy coated steel to yield crack volumes similar to those of specimens with black steel.
- The damage growth rate between specimens with epoxy coated steel and black steel varied from 2.5 to 4.0 depending on whether the corrosion rate or volume of cracks was taken as the damage measure. In order to be conservative, it is recommended that the estimated life expectancy for decks reinforced with epoxy coated rebar is 2.5 times that of decks reinforced with black rebar.

6.4 Final Remarks

The data in this research suggests that the use of ECR in concrete bridge decks will significantly reduce corrosion induced damage, thereby extending the lifetime of concrete bridge decks reinforced with black steel. However, there has been much debate regarding this topic. As mentioned in Section 1.3.2, much previous research agrees with the findings of this thesis that ECR improves the performance of concrete bridge decks. On the other hand, some research has concluded that ECR does not improve the performance of concrete bridge decks and may even negatively impact performance. Therefore, it is important to view the results of this thesis in the light of a few critical observations on how this research can be applied to concrete bridge decks in the field. First, the small-scale specimens used are not a realistic representation of a concrete bridge deck. The simplified layout of the steel reinforcement did not allow for spalling or delamination of the concrete, which are common in concrete bridge decks. Also, the concrete used in bridge decks in the field is different than the concrete used in this research. The many admixtures used in concrete bridge decks in the field will certainly have an impact on the deck's

ability to resist corrosion induced damage. Furthermore, the amount of damage to the epoxy coating on the steel significantly affects its ability to resist corrosion. A damage amount of 2 percent was used as suggested by the Research Advisory Panel at MDOT. However, this may not be representative of concrete bridge decks in the field. Although environmental and loading conditions were the same for ECR and black steel specimens, the laboratory data reported herein should be validated using field observations.

APPENDICES

APPENDIX A

STIFFNESS DATA

Table A.1: Black Level 0

Cycles	Stiffness (k/in)		
	1	2	3
0	37.8	32.9	28.5
160,000	37.0	31.5	23.3
170,000	41.1	35.7	27.2
245,415	52.6	32.6	46.6
565,279	52.2	33.4	48.4
743,822	53.3	35.1	50.6
1,088,582	52.2	36.5	56.4
1,330,662	57.7	33.0	54.6
1,582,337	57.7	37.8	55.0
1,921,590	52.8	36.3	51.7

Table A.2: Epoxy Level 0 Unrepaired

Cycles	Stiffness (k/in)	
	1	2
0	60.9	67.1
146,935	56.3	59.8
321,980	51.9	58.2
482,885	68.8	66.1
606,165	76.3	66.2
858,481	64.9	66.8
1,038,572	71.4	56.2
1,193,625	65.0	67.1
1,493,625	68.0	65.6
1,577,485	70.9	66.2
1,756,110	69.6	66.8
1,908,408	66.6	75.2

 Table A.3:
 Black Level 1 Unrepaired

Cycles	Stiffness (k/in)	Cycles	Stiffness (k/in)
	1		2
0	57.6	0	57.0
146,935	45.3	320,504	57.3
321,980	53.6	644,222	Failed
482,885	46.2	-	-
606,165	51.9	-	-
858,481	35.2	-	-
1,038,572	61.0	-	-
1,193,625	62.3	-	-
1,493,625	64.5	-	-
1,577,485	66.0	-	-
1,756,110	63.7	-	-
1,908,408	67.7	-	-

Table A.4: Epoxy Level 1 Unrepaired

Cycles	Stiffness (k/in)		
-	1	2	3
0	69.7	62.8	55.4
249,109	75.2	70.7	52.3
588,014	68.7	65.9	50.9
842,443	65.3	72.4	52.8
1,011,581	71.7	89.0	55.5
1,353,276	68.9	82.7	55.7
1,437,992	70.9	72.5	56.5
1,938,583	69.7	80.0	56.9

 Table A.5:
 Black Level 1 Repaired

Cycles	Stiffness (k/in)	
-	1	2
0	67.7	67.4
326,420	72.7	69.6
578,156	72.6	84.2
893,156	73.7	40.0
1,148,889	67.7	69.9
1,483,987	64.3	72.1
1,816,948	60.5	71.7
1,996,324	56.7	73.9

Table A.7: Black Level 2 Unrepaired

Cycles	Stiffness (k/in)	
	1	2
0	58.2	63.6
320,504	76.7	41.7
644,222	71.9	47.9
744,710	Failed	Failed

Table A.9: Black Level 2 Repaired

Cycles	Stiffness (k/in)
-	1
0	53.4
326,420	53.4
578,156	-
893,156	-
1,148,889	54.4
1,483,987	49.9
1,816,948	54.9
1,996,324	48.2

Table A.6: Epoxy Level 1 Repaired

Cycles	Stiffness (k/in)		
	1	2	3
0	79.2	49.3	74.0
236,057	78.9	46.3	70.8
486,801	75.9	46.8	70.6
826,156	70.2	47.9	62.0
1,078,285	77.2	45.7	68.4
1,421,719	75.4	46.9	72.9
1,671,955	75.0	47.4	68.8
1,703,598	72.4	45.1	71.2
2,068,395	75.5	45.7	79.7

Table A.8: Epoxy Level 2 Unrepaired

Cycles	Stiffness (k/in)		
	1	2	3
0	72.8	78.5	74.9
243,446	71.3	77.7	79.5
581,414	69.4	83.0	80.1
1178,510	75.7	71.8	78.0
1178,510	74.3	77.4	78.1
1464,193	74.0	80.6	71.0
1,855,593	70.9	86.1	69.3
2,024,904	66.2	87.5	76.5

Table A.10: Epoxy Level 2 Repaired

Table A.10. Lpoxy Level 2 Repaired			
Cycles	Stiffness (k/in)		
	1	2	3
0	66.9	72.3	67.6
166,188	64.1	70.7	48.6
595,398	-	-	-
836,307	65.2	59.8	45.8
1,156,889	67.3	59.5	43.7
1,401,185	63.6	43.4	Failed
1,436,412	69.9	Failed	-
1,779,847	66.3	-	-
2,130,928	65.4	-	-

Table A.11: Black Level 3 Unrepaired

Cycles	Stiffness (k/in)		
	1	2	3
0	Failed	Failed	Failed

Table A.13: Black Level 3 Repaired

Cycles	Stiffness (k/in)		
-	1	2	3
0	-	Failed	-
239,061	67.1	-	55.1
751,111	62.2	-	53.0
1,053,614	60.8	-	Failed
1,739,217	49.5	-	-
1,995,881	52.6	-	-

Table A.15: Black Level 4 Unrepaired

Cycles	Stiffness (k/in)		
-	1	2	3
0	Failed	Failed	Failed

Table A.12: Epoxy Level 3 Unrepaired

Cycles	Stiffness (k/in)		
	1	2	3
0	95.2	Failed	69.5
414,523	Failed	-	Failed

Table A.14: Epoxy Level 3 Repaired

Cycles	Stiffness (k/in)	
	1	2
0	57.6	55.9
434,020	68.3	57.7
681,744	63.8	64.1
1,024,890	66.3	57.1
1,279,421	66.2	52.8
1,591,507	56.1	Failed
2,025,925	61.1	-

Table A.16: Epoxy Level 4 Unrepaired

Table 11:10: Epoxy Level + Omepaned		
Stiffness (k/in)		
1	2	3
56.2	Failed	74.3
52.5	-	70.5
55.8	-	70.7
50.8	-	62.6
51.7	-	56.8
38.9	-	Failed
Failed	-	-
	Sti 1 56.2 52.5 55.8 50.8 51.7 38.9	Stiffness (k/) 1 2 56.2 Failed 52.5 - 55.8 - 50.8 - 51.7 - 38.9 -

Table A.17: Black Level 4 Repaired

Cycles	Stiffness (k/in)		
-	1	2	3
0	83.5	96.9	95.1
257,041	109.8	61.4	93.7
583,949	99.1	65.8	91.4
854,187	106.1	65.8	96.5
1,181,715	106.9	65.3	86.6
1,433,461	98.7	64.2	102.9
1,775,923	101.9	56.9	92.3
2,048,680	94.9	63.7	79.2

 Table A.18:
 Epoxy Level 4 Repaired

Cycles	Stiffness (k/in)		
-	1	2	3
0	Failed	Failed	78.7
332,288	-	-	73.4
675,110	-	-	75.5
1,275,384	-	-	75.7
1,527,247	-	-	74.3
1,872,321	-	-	60.4
2,123,588	-	-	74.5

APPENDIX B

X-RAY IMAGES AND PROCESSED CRACK IMAGES

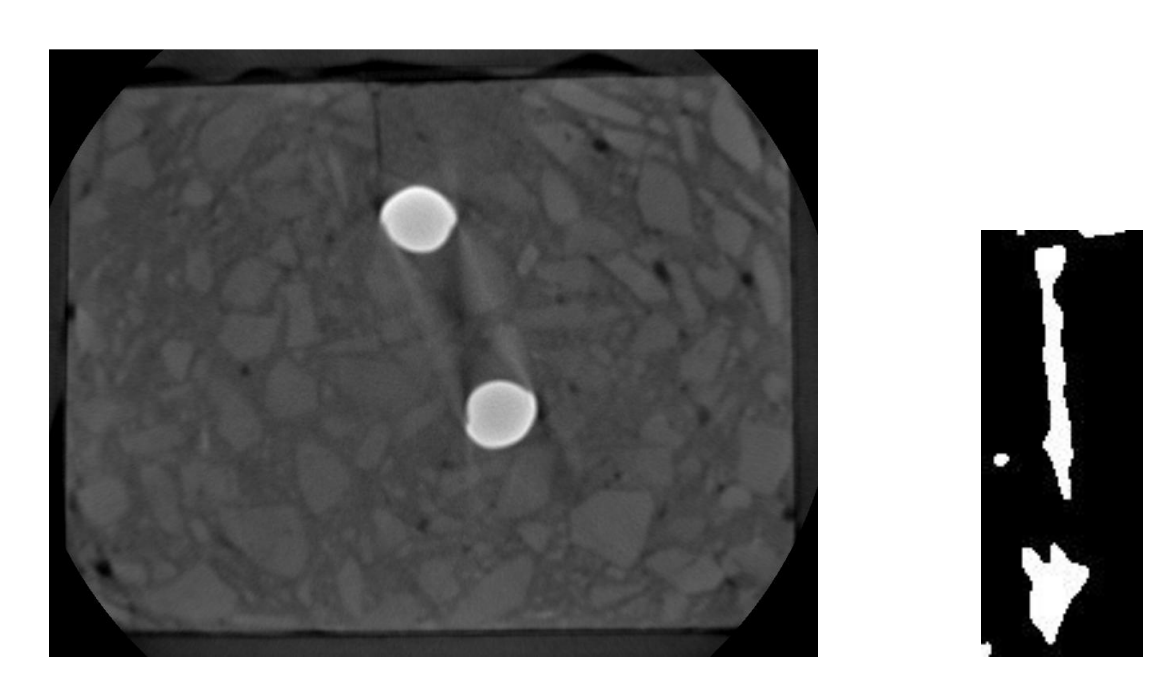


Figure B.1: B-0 X-Ray Image and Crack after Applying Threshold

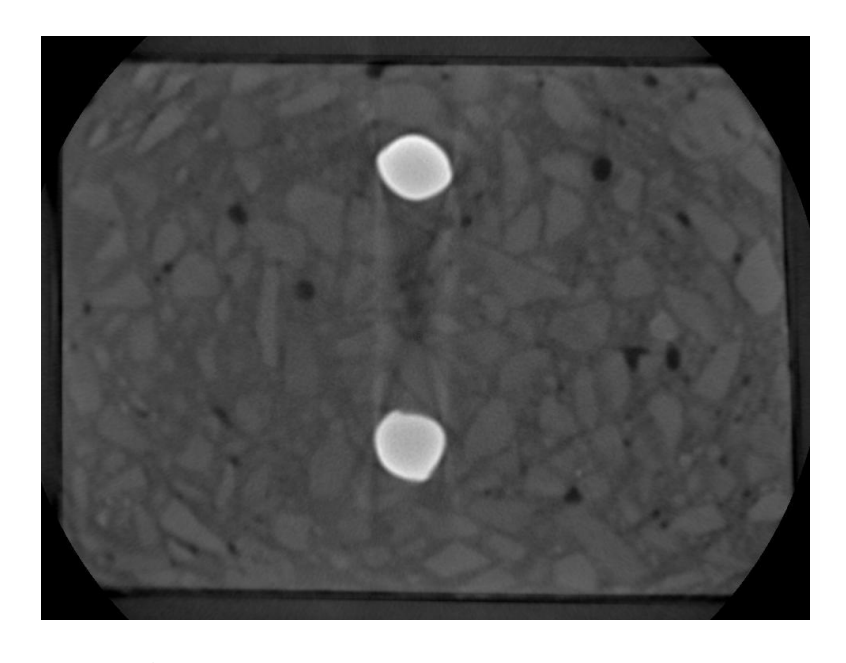


Figure B.2: E-0 X-Ray Image with No Crack

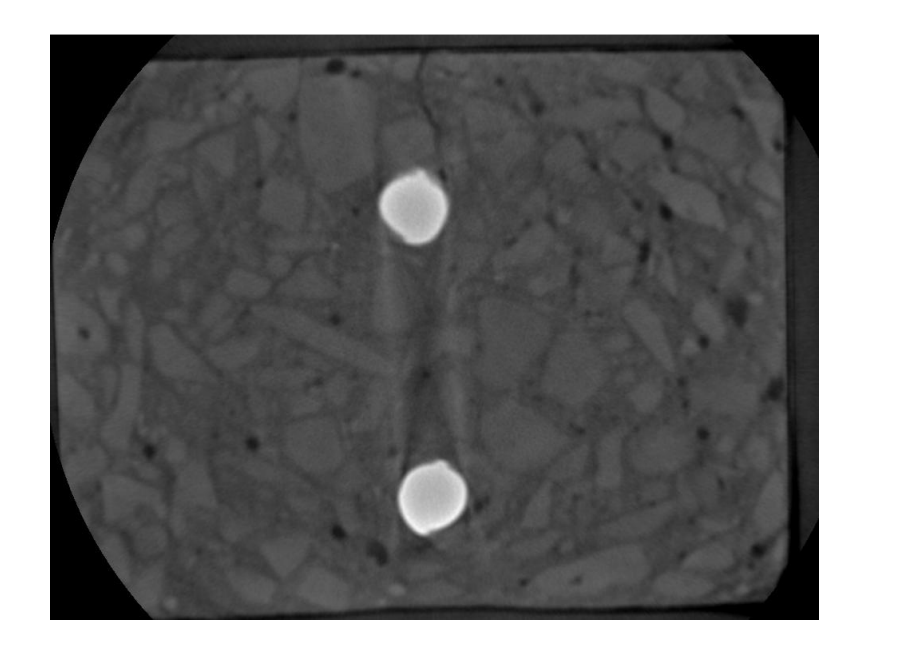




Figure B.3: B-1-N X-Ray Image and Crack after Applying Threshold

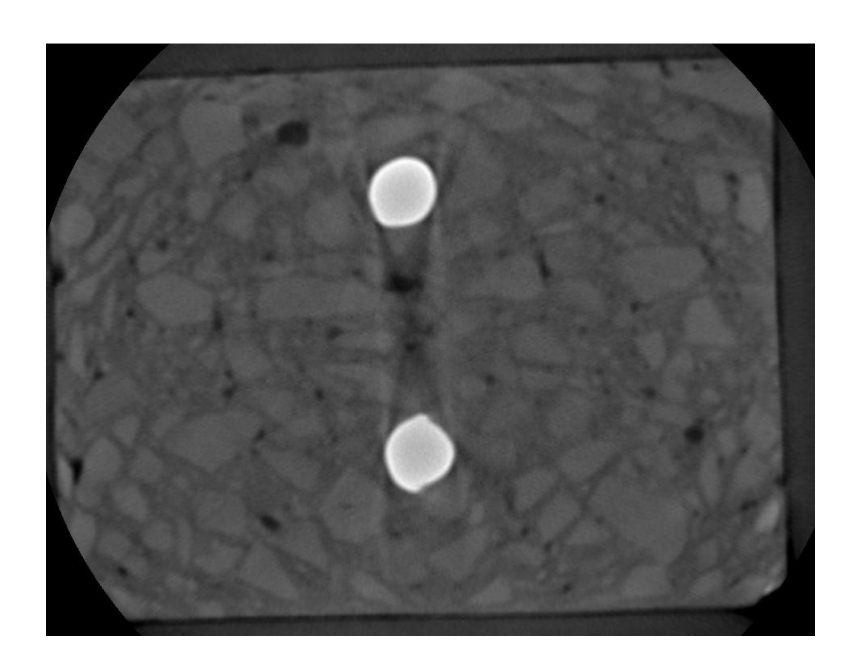


Figure B.4: E-1-N X-Ray Image with No Crack

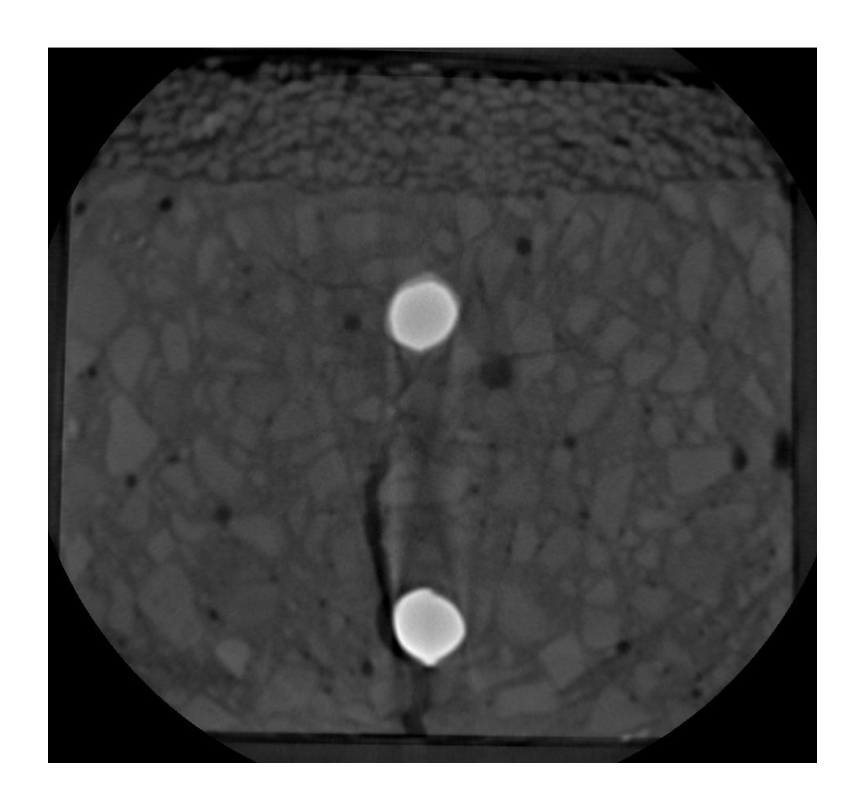




Figure B.5: B-1-R X-Ray Image and Crack after Applying Threshold

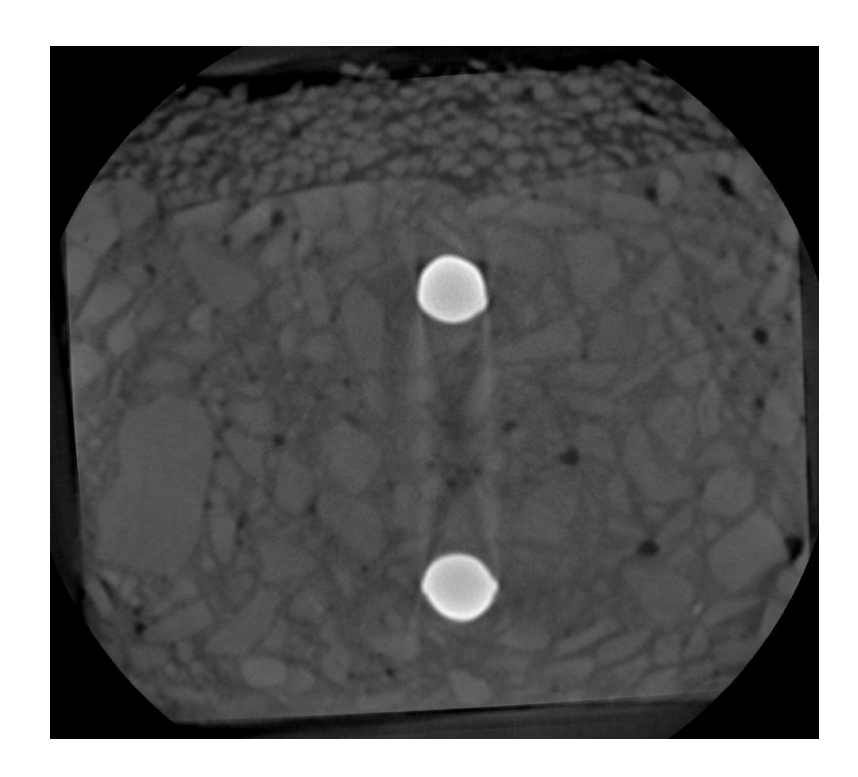


Figure B.6: E-1-R X-Ray Image with No Crack

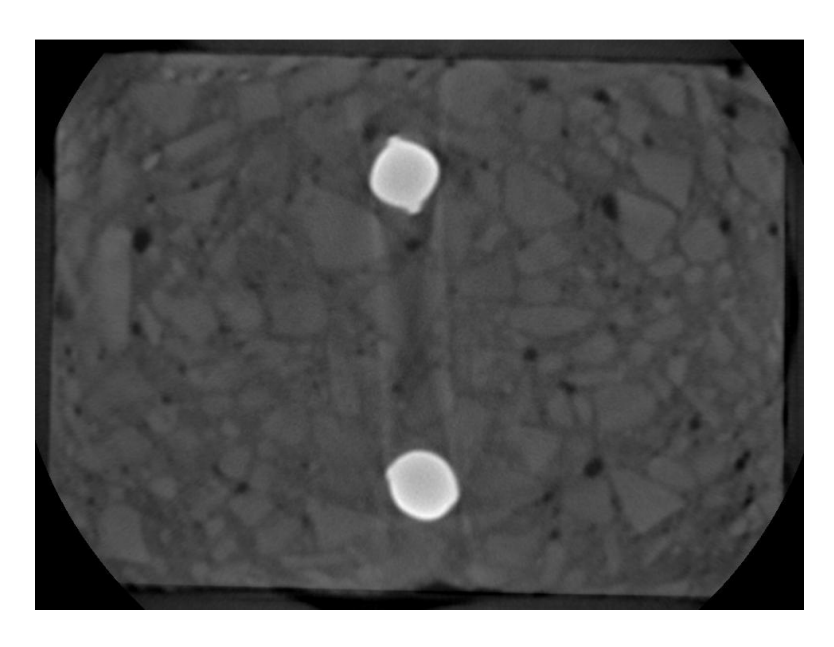


Figure B.7: E-2-N X-Ray Image and Crack with No Crack

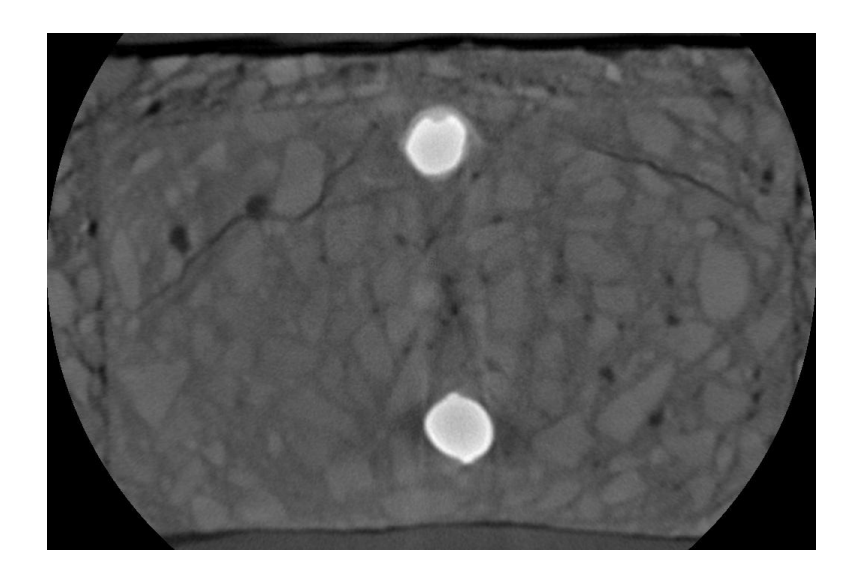
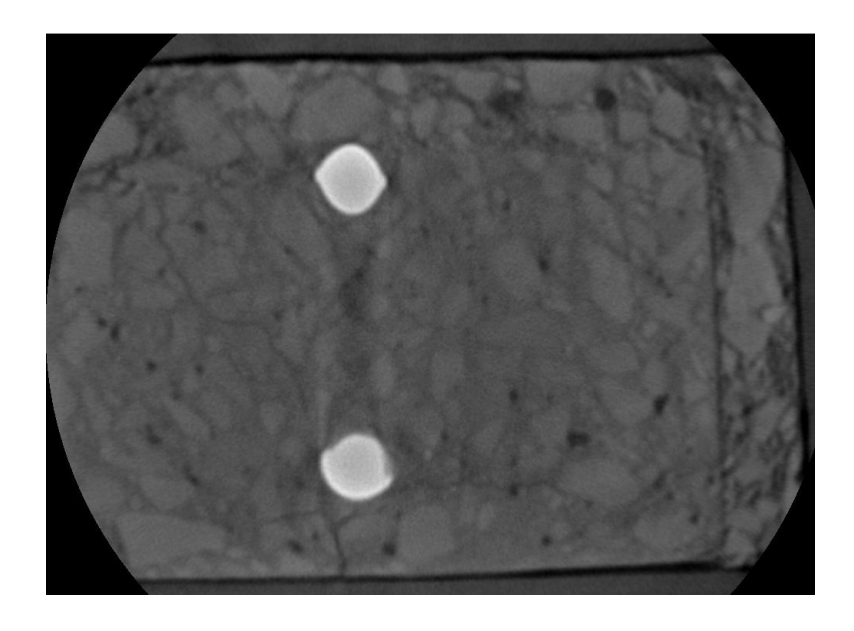




Figure B.8: B-2-R X-Ray Image and Crack after Applying Threshold



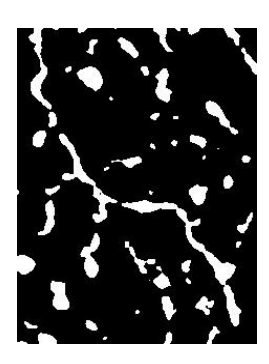
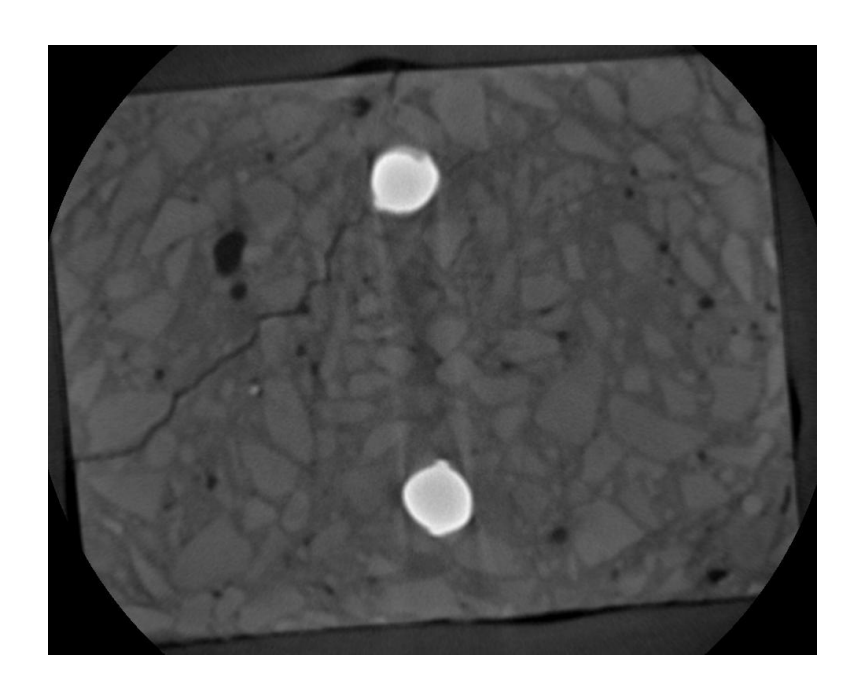


Figure B.9: E-2-R X-Ray Image and Crack after Applying Threshold



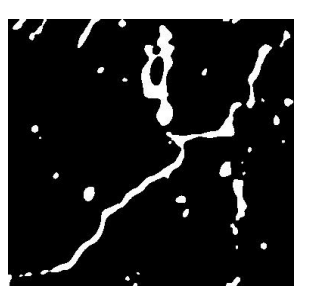


Figure B.10: B-3-N X-Ray Image and Crack after Applying Threshold

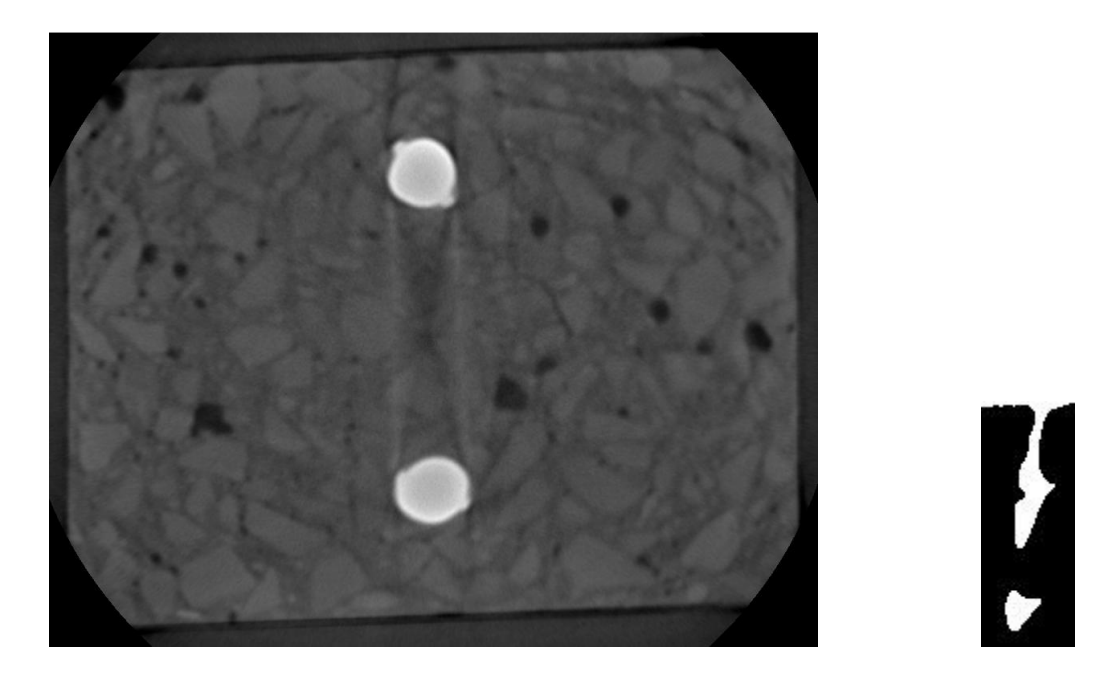


Figure B.11: E-3-N X-Ray Image and Crack after Applying Threshold

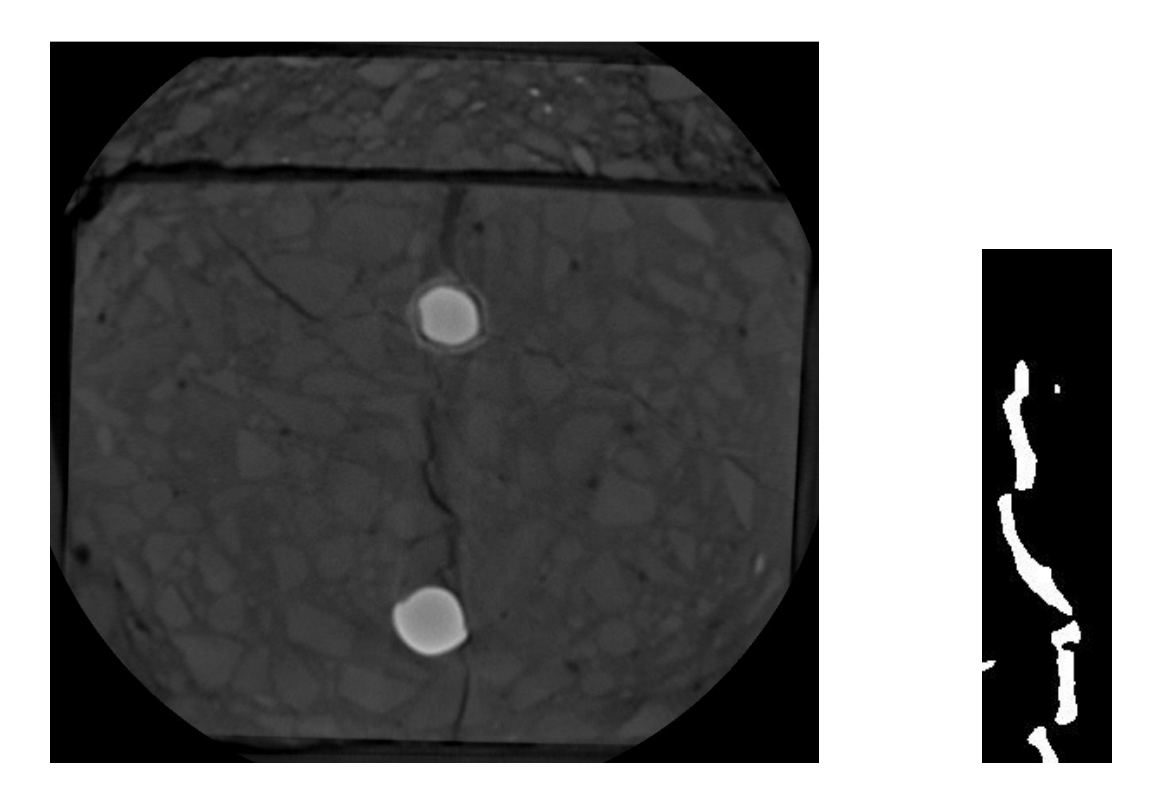


Figure B.12: B-3-R X-Ray Image and Crack after Applying Threshold

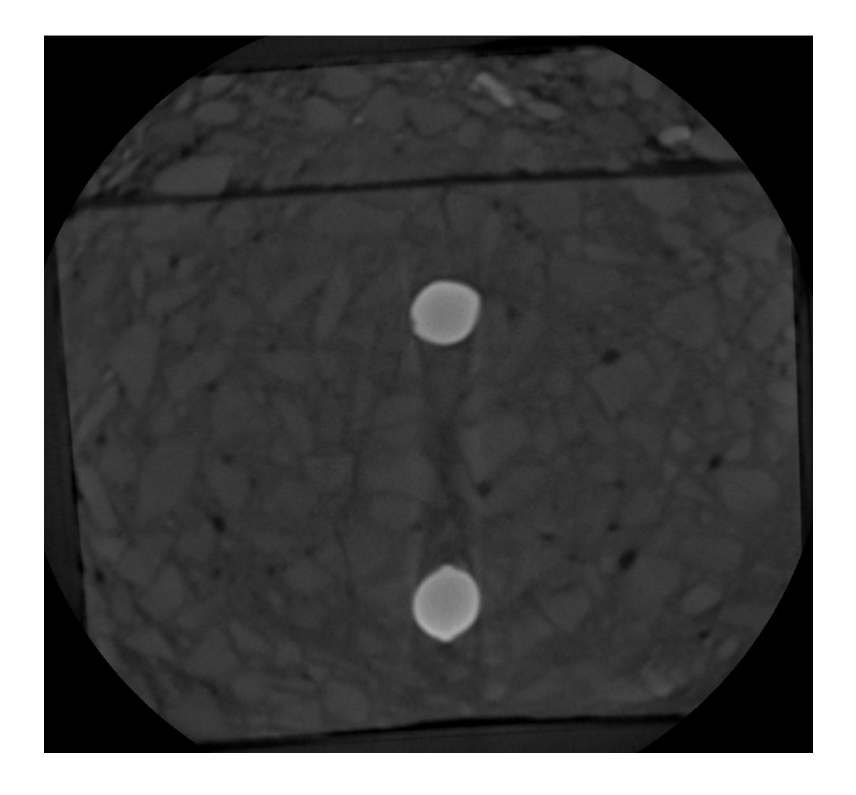




Figure B.13: E-3-R X-Ray Image and Crack after Applying Threshold

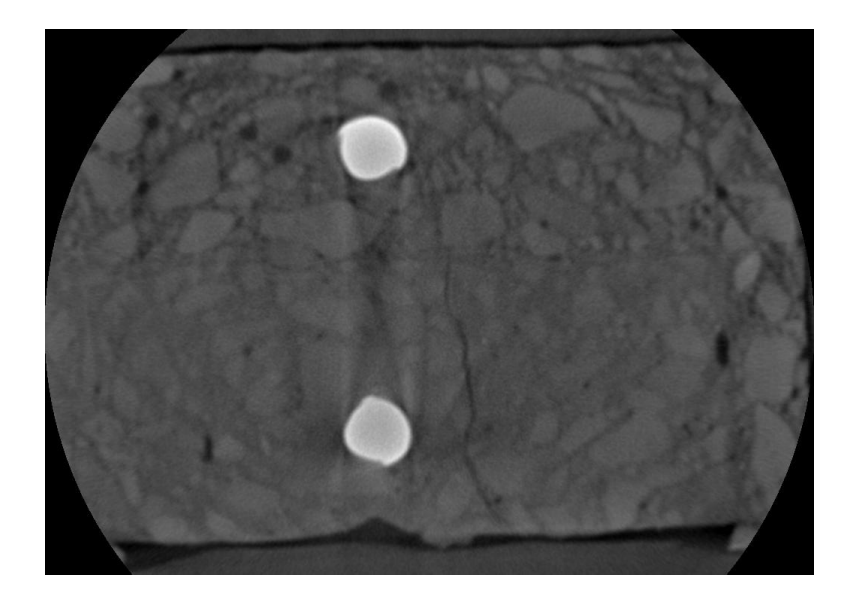




Figure B.14: B-4-R X-Ray Image and Crack after Applying Threshold

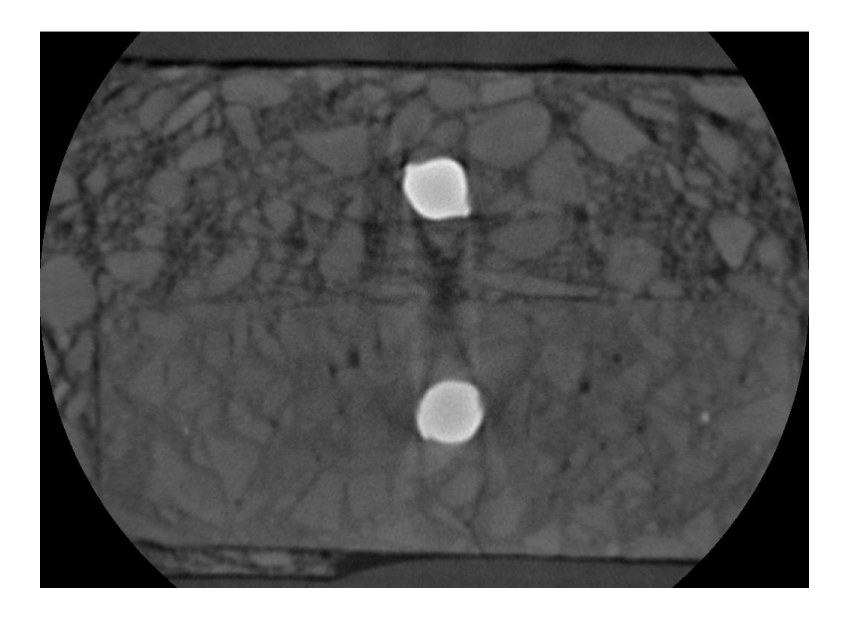




Figure B.15: E-4-R X-Ray Image and Crack after Applying Threshold

APPENDIX C

CORROSION CHARGE DATA

Table C.1: B-0 Corrosion Data

Time (days)	Charge (Ah)
0	0
2.84	0.24
6.54	0.24
8.61	1.03
12.60	2.34
15.40	3.51
18.31	4.58
22.24	5.71

Table C.2: E-0 Corrosion Data

Time (days)	Charge (Ah)
0	0
1.70	0.06
3.73	0.09
5.59	0.14
7.02	0.15
9.94	0.15
12.02	0.30
13.82	0.31
17.29	0.32
18.26	0.32
20.33	0.32
22.09	0.32

Table C.3: B-1-N Corrosion Data

Time (days)	Charge (Ah)
0	0
1.00	0.09
2.00	0.46
5.00	2.59
8.00	5.81
11.00	10.67
12.00	12.38
13.70	12.44
15.73	12.47
17.59	12.52
19.02	12.53
21.94	12.53
24.02	12.68
25.82	12.69
29.29	12.70
30.26	12.70
32.33	12.70
34.09	12.70

Table C.4: E-1-N Corrosion Data

Time (days)	Charge (Ah)
0	0
6.00	0.67
8.00	0.98
11.00	1.59
21.00	2.97
28.00	5.06
31.00	6.33
35.00	8.30
38.00	10.21
44.00	14.08

Table C.5: B-1-R Corrosion Data

Time	Charge	
(days)	(Ah)	
0	0	
1.00	0.08	
2.00	0.45	
5.00	3.13	
800	7.11	
11.00	12.72	
12.00	15.03	
15.78	16.82	
18.69	18.04	
22.34	18.89	
25.30	20.29	
29.18	21.93	
33.03	23.47	
35.11	29.12	

Table C.6: E-1-R Corrosion Data

Time (days)	Charge (Ah)
0	0
10.00	0.57
12.00	1.13
26.00	3.78
33.00	7.81
39.00	11.17
41.00	12.11
44.00	13.68

Table C.7: B-2-N Corrosion Data

Time	Charge
(days)	(Ah)
0	0
1.00	0.08
2.00	0.39
5.00	2.46
8.00	5.38
11.00	9.94
12.00	11.80
13.00	15.59
15.00	18.97
16.00	20.80
20.00	27.60
22.00	31.20
26.00	38.15
29.00	44.82
31.00	50.15
34.71	51.66
38.46	53.12
39.62	54.77

Table C.8: E-2-N Corrosion Data

Time	Charge
(days)	(Ah)
1.00	0.01
2.00	0.12
5.00	0.69
8.00	1.36
11.00	2.40
12.00	2.84
13.00	3.32
15.00	4.72
16.00	5.68
20.00	9.38
22.00	11.12
26.00	14.87
29.00	17.95
31.00	19.82
36.00	20.26
40.00	21.06
47.00	23.01
50.00	24.10
55.00	25.94
57.00	26.85
62.00	29.18
65.00	30.66
71.00	33.52
77.00	36.19
84.00	39.56
87.00	40.38
91.00	40.67
101.00	42.09
103.00	43.15
117.00	46.93
124.00	51.45

Table C.9: B-2-R Corrosion Data

Time	Charge
(days)	(Ah)
0	0
1.00	0.08
2.00	0.39
5.00	2.46
8.00	5.38
11.00	9.94
12.00	11.80
13.00	13.46
15.00	17.12
16.00	19.25
20.00	26.81
22.00	30.95
26.00	38.63
29.00	46.48
31.00	52.15
34.78	53.94
37.69	55.16
41.34	56.01
44.30	57.41
48.18	59.05
52.03	60.59
54.11	66.24

Table C.10: E-2-R Corrosion Data

Time	Charge
(days)	(Ah)
0	0
5.00	0.07
9.00	0.41
16.00	1.89
19.00	2.74
24.00	4.25
26.00	5.11
31.00	7.40
34.00	8.93
40.00	12.25
46.00	15.73
53.00	20.27
56.00	21.33
60.00	21.74
70.00	23.15
72.00	24.27
86.00	27.63
93.00	31.87
99.00	35.16
101.00	36.06
104.00	37.63
114.00	40.99
121.00	46.64
121.04	46.66
122.92	46.73
127.89	46.80
130.68	46.89
134.39	46.97
137.22	47.07
137.63	47.13
141.60	47.30
145.66	47.46

Table C.11: B-3-N Corrosion Data

Time (days)	Charge (Ah)
0	0
3.00	0.60
7.00	2.54
10.00	5.82
16.00	14.09
23.00	28.40
30.00	48.66
36.00	66.51
39.00	76.33

Table C.12: E-3-N Corrosion Data

Time	Charge
(days)	(Ah)
0	0
1.00	0.01
2.00	0.09
5.00	0.63
8.00	1.30
11.00	2.36
12.00	2.89
13.00	3.43
15.00	4.92
16.00	5.89
20.00	9.75
22.00	11.50
26.00	15.09
29.00	18.10
31.00	19.98
36.00	20.62
40.00	21.98
47.00	24.34
50.00	25.65
55.00	27.60
57.00	28.83
62.00	32.10
65.00	34.07
71.00	38.04
77.00	42.10
84.00	46.79
87.00	47.85
91.00	48.29
101.00	50.27
103.00	51.71
117.00	56.70
124.00	62.69
130.00	68.17
132.00	69.38
135.00	71.50
	Cont'd →

145.00	71.50
152.00	77.12
156.80	79.38

Table C.13: B-3-R Corrosion Data

Time (days) Charge (Ah) 0 0 10.00 1.36 17.00 6.11 20.00 10.11 24.00 16.22 27.00 21.93	
0 0 10.00 1.36 17.00 6.11 20.00 10.11 24.00 16.22	
10.00 1.36 17.00 6.11 20.00 10.11 24.00 16.22	
17.00 6.11 20.00 10.11 24.00 16.22	
20.00 10.11 24.00 16.22	
24.00 16.22	
27.00 21.93	
21.00 21.93	
33.00 33.52	
40.00 47.72	
47.00 63.47	
53.00 75.37	
56.00 75.38	
58.77 79.64	
64.69 83.11	
68.19 85.72	
76.13 89.07	
79.10 91.64	

Table C.14: E-3-R Corrosion Data

(days) (Ah) 0 0 5.00 0.25 9.00 1.36 16.00 4.44 19.00 6.16 24.00 9.12 26.00 10.69 31.00 14.74 34.00 17.48 40.00 23.25 46.00 28.77 53.00 35.64 56.00 37.22 60.00 37.88 70.00 40.41 72.00 42.27 86.00 48.10 93.00 54.90 99.00 60.50 101.00 61.83 104.00 64.09 114.00 68.86 121.00 75.96 126.02 76.76 128.89 77.42 135.81 79.74 139.42 81.16	Table C.14. E-3-K Collosion Data		
0 0 5.00 0.25 9.00 1.36 16.00 4.44 19.00 6.16 24.00 9.12 26.00 10.69 31.00 14.74 34.00 17.48 40.00 23.25 46.00 28.77 53.00 35.64 56.00 37.22 60.00 37.88 70.00 40.41 72.00 42.27 86.00 48.10 93.00 54.90 99.00 60.50 101.00 61.83 104.00 64.09 114.00 68.86 121.00 75.96 126.02 76.76 128.89 77.42 135.81 79.74 139.42 81.16	Time	Charge	
5.00 0.25 9.00 1.36 16.00 4.44 19.00 6.16 24.00 9.12 26.00 10.69 31.00 14.74 34.00 17.48 40.00 23.25 46.00 28.77 53.00 35.64 56.00 37.22 60.00 37.88 70.00 40.41 72.00 42.27 86.00 48.10 93.00 54.90 99.00 60.50 101.00 61.83 104.00 64.09 114.00 68.86 121.00 75.96 126.02 76.76 128.89 77.42 135.81 79.74 139.42 81.16	(days)	(Ah)	
9.00 1.36 16.00 4.44 19.00 6.16 24.00 9.12 26.00 10.69 31.00 14.74 34.00 17.48 40.00 23.25 46.00 28.77 53.00 35.64 56.00 37.22 60.00 37.88 70.00 40.41 72.00 42.27 86.00 48.10 93.00 54.90 99.00 60.50 101.00 61.83 104.00 64.09 114.00 68.86 121.00 75.96 126.02 76.76 128.89 77.42 135.81 79.74 139.42 81.16	0	0	
16.00 4.44 19.00 6.16 24.00 9.12 26.00 10.69 31.00 14.74 34.00 17.48 40.00 23.25 46.00 28.77 53.00 35.64 56.00 37.22 60.00 37.88 70.00 40.41 72.00 42.27 86.00 48.10 93.00 54.90 99.00 60.50 101.00 61.83 104.00 64.09 114.00 68.86 121.00 75.96 126.02 76.76 128.89 77.42 135.81 79.74 139.42 81.16	5.00	0.25	
19.00 6.16 24.00 9.12 26.00 10.69 31.00 14.74 34.00 17.48 40.00 23.25 46.00 28.77 53.00 35.64 56.00 37.22 60.00 37.88 70.00 40.41 72.00 42.27 86.00 48.10 93.00 54.90 99.00 60.50 101.00 61.83 104.00 64.09 114.00 68.86 121.00 75.96 126.02 76.76 128.89 77.42 132.86 78.71 135.81 79.74 139.42 81.16	9.00	1.36	
24.00 9.12 26.00 10.69 31.00 14.74 34.00 17.48 40.00 23.25 46.00 28.77 53.00 35.64 56.00 37.22 60.00 37.88 70.00 40.41 72.00 42.27 86.00 48.10 93.00 54.90 99.00 60.50 101.00 61.83 104.00 64.09 114.00 68.86 121.00 75.96 128.89 77.42 132.86 78.71 135.81 79.74 139.42 81.16	16.00	4.44	
26.00 10.69 31.00 14.74 34.00 17.48 40.00 23.25 46.00 28.77 53.00 35.64 56.00 37.22 60.00 37.88 70.00 40.41 72.00 42.27 86.00 48.10 93.00 54.90 99.00 60.50 101.00 61.83 104.00 64.09 114.00 68.86 121.00 75.96 126.02 76.76 128.89 77.42 135.81 79.74 139.42 81.16	19.00	6.16	
31.00 14.74 34.00 17.48 40.00 23.25 46.00 28.77 53.00 35.64 56.00 37.22 60.00 37.88 70.00 40.41 72.00 42.27 86.00 48.10 93.00 54.90 99.00 60.50 101.00 61.83 104.00 64.09 114.00 68.86 121.00 75.96 126.02 76.76 128.89 77.42 132.86 78.71 135.81 79.74 139.42 81.16	24.00	9.12	
34.00 17.48 40.00 23.25 46.00 28.77 53.00 35.64 56.00 37.22 60.00 37.88 70.00 40.41 72.00 42.27 86.00 48.10 93.00 54.90 99.00 60.50 101.00 61.83 104.00 64.09 114.00 68.86 121.00 75.96 126.02 76.76 128.89 77.42 135.81 79.74 139.42 81.16	26.00	10.69	
40.00 23.25 46.00 28.77 53.00 35.64 56.00 37.22 60.00 37.88 70.00 40.41 72.00 42.27 86.00 48.10 93.00 54.90 99.00 60.50 101.00 61.83 104.00 64.09 114.00 68.86 121.00 75.96 126.02 76.76 128.89 77.42 132.86 78.71 139.42 81.16	31.00	14.74	
46.00 28.77 53.00 35.64 56.00 37.22 60.00 37.88 70.00 40.41 72.00 42.27 86.00 48.10 93.00 54.90 99.00 60.50 101.00 61.83 104.00 64.09 114.00 68.86 121.00 75.96 126.02 76.76 128.89 77.42 132.86 78.71 135.81 79.74 139.42 81.16	34.00	17.48	
53.00 35.64 56.00 37.22 60.00 37.88 70.00 40.41 72.00 42.27 86.00 48.10 93.00 54.90 99.00 60.50 101.00 61.83 104.00 64.09 114.00 68.86 121.00 75.96 126.02 76.76 128.89 77.42 135.81 79.74 139.42 81.16	40.00	23.25	
56.00 37.22 60.00 37.88 70.00 40.41 72.00 42.27 86.00 48.10 93.00 54.90 99.00 60.50 101.00 61.83 104.00 64.09 114.00 68.86 121.00 75.96 128.89 77.42 132.86 78.71 135.81 79.74 139.42 81.16	46.00	28.77	
60.00 37.88 70.00 40.41 72.00 42.27 86.00 48.10 93.00 54.90 99.00 60.50 101.00 61.83 104.00 64.09 114.00 68.86 121.00 75.96 126.02 76.76 128.89 77.42 132.86 78.71 135.81 79.74 139.42 81.16	53.00	35.64	
70.00 40.41 72.00 42.27 86.00 48.10 93.00 54.90 99.00 60.50 101.00 61.83 104.00 64.09 114.00 68.86 121.00 75.96 126.02 76.76 128.89 77.42 135.81 79.74 139.42 81.16	56.00	37.22	
72.00 42.27 86.00 48.10 93.00 54.90 99.00 60.50 101.00 61.83 104.00 64.09 114.00 68.86 121.00 75.96 126.02 76.76 128.89 77.42 132.86 78.71 135.81 79.74 139.42 81.16	60.00	37.88	
86.00 48.10 93.00 54.90 99.00 60.50 101.00 61.83 104.00 64.09 114.00 68.86 121.00 75.96 126.02 76.76 128.89 77.42 132.86 78.71 135.81 79.74 139.42 81.16	70.00	40.41	
93.00 54.90 99.00 60.50 101.00 61.83 104.00 64.09 114.00 68.86 121.00 75.96 126.02 76.76 128.89 77.42 132.86 78.71 135.81 79.74 139.42 81.16	72.00	42.27	
99.00 60.50 101.00 61.83 104.00 64.09 114.00 68.86 121.00 75.96 126.02 76.76 128.89 77.42 132.86 78.71 135.81 79.74 139.42 81.16	86.00	48.10	
101.00 61.83 104.00 64.09 114.00 68.86 121.00 75.96 126.02 76.76 128.89 77.42 132.86 78.71 135.81 79.74 139.42 81.16	93.00	54.90	
104.00 64.09 114.00 68.86 121.00 75.96 126.02 76.76 128.89 77.42 132.86 78.71 135.81 79.74 139.42 81.16	99.00	60.50	
114.00 68.86 121.00 75.96 126.02 76.76 128.89 77.42 132.86 78.71 135.81 79.74 139.42 81.16	101.00	61.83	
121.00 75.96 126.02 76.76 128.89 77.42 132.86 78.71 135.81 79.74 139.42 81.16	104.00	64.09	
126.02 76.76 128.89 77.42 132.86 78.71 135.81 79.74 139.42 81.16	114.00	68.86	
128.89 77.42 132.86 78.71 135.81 79.74 139.42 81.16	121.00	75.96	
132.86 78.71 135.81 79.74 139.42 81.16	126.02	76.76	
135.81 79.74 139.42 81.16	128.89	77.42	
139.42 81.16	132.86	78.71	
	135.81	79.74	
	139.42	81.16	
144.45 82.93	144.45	82.93	

Table C.15: B-4-N Corrosion Data

Charge (Ah)
0
3.50
4.70
8.60
12.57
17.91
22.26
29.74
35.52
44.09
52.91
59.56
67.53
71.94
79.31
89.17
94.28
104.74
109.99
122.61

Table C.16: E-4-N Corrosion Data

Time	Charge
(days)	(Ah)
0	0
3.00	0.35
4.00	0.53
7.00	1.34
10.00	2.53
14.00	3.75
17.00	5.09
21.00	6.74
24.00	7.66
28.00	9.02
32.00	10.88
35.00	12.41
40.00	13.58
43.00	14.03
46.00	15.13
50.00	16.87
52.00	17.51
56.00	18.49
58.00	18.88
63.00	20.65
78.00	20.97
80.00	22.74
81.00	24.78
85.00	34.07
87.00	39.57
91.00	49.94
94.00	59.70
96.00	66.12
101.00	66.57
105.00	68.36
112.00	71.73
115.00	73.37
120.00	76.28
122.00	77.93
127.00	82.23
	Cont'd →

130.00	85.24
136.00	91.73
142.00	98.68
149.00	107.38
152.00	109.29
156.00	109.92

Table C.17: B-4-R Corrosion Data

Time (days)	Charge (Ah)
0	0
3.00	4.53
4.00	6.07
7.00	10.81
10.00	15.36
14.00	21.42
17.00	25.91
21.00	32.30
24.00	37.17
28.00	44.22
32.00	51.80
35.00	57.98
40.00	63.74
43.00	66.87
46.00	72.01
50.00	78.74
52.00	82.15
56.00	89.25
58.00	92.93
63.00	102.49

Table C.18: E-4-R Corrosion Data

Tubic citor E	4-R Corrosion Data
Time	Charge
(days)	(Ah)
0	0
1.00	0.01
2.00	0.14
5.00	0.65
8.00	1.33
11.00	2.37
12.00	3.03
13.00	3.74
15.00	5.71
16.00	7.05
20.00	12.05
22.00	14.39
26.00	18.84
29.00	22.71
31.00	25.39
36.00	26.19
40.00	27.82
47.00	31.69
50.00	33.73
55.00	37.89
57.00	39.73
62.00	44.26
65.00	47.23
71.00	53.37
77.00	58.34
84.00	64.42
87.00	65.77
91.00	66.23
101.00	68.35
103.00	69.89
117.00	74.92
124.00	81.41
130.00	85.17
132.00	86.20
	Cont'd →

135.00	88.15
145.00	92.37
152.00	98.24
155.00	102.05
159.00	107.46

REFERENCES

REFERENCES

- [1] Samples, L.M. and Ramirez, J.A., Methods of Corrosion Protection and Durability of Concrete Bridge Decks Reinforced with Epoxy-Coated Bars Phase I. 1999, Purdue University: West Lafayette, IN.
- [2] Koch, G.H., et al., *Corrosion Cost and Preventive Strategies in the United States*. 2002, Turner-Fairbank Highway Research Center: McLean, VA.
- [3] Clifton, J.R., Beeghly, H.F., and Mathey, R.G., *Nonmetallic Coatings for Concrete Reinforcing Bars*. 1974, Federal Highway Administration: Washington, DC.
- [4] Liu, Y. and Weyers, R.E., Modeling the Time-to-Corrosion Cracking in Chloride Contaminated Reinforced Concrete Structures. ACI Materials Journal, 1998. **95**(6): pp. 675-681.
- [5] Hartt, W.H., et al., Critical Literature Review of High-Performance Corrosion Reinforcements in Concrete Bridge Applications. 2004, FHWA: McLean, VA.
- [6] Fraczek, J., Review of Electrochemical Principles as Applied to Corrosion of Steel in a Concrete or Grout Environment. Special Publication, 1987. **102**: pp. 13-24.
- [7] http://en.wikipedia.org/wiki/Stainless_steel; Accessed on Mar. 7, 2010.
- [8] Srensen, B., Jensen, P.B., and Maahn, E., *The Corrosion Properties of Stainless Steel Reinforcement*. Corrosion of Reinforcement in Concrete, 1990: pp. 601-610.
- [9] McDonald, D.B., et al., *Stainless Steel Reinforcing as Corrosion Protection*. Concrete International, 1995. **17**(5): pp. 65-70.
- [10] Weyers, R.E. and Cady, P.D. Cathodic Protection of Concrete Bridge Decks. 1984: ACI.
- [11] Brown, M.C., Corrosion Protection Service Life of Epoxy Coated Renforcing Steel in Virginia Bridge Decks, Ph.D Dissertation, Virginia Polytechnic Institute and State University, 2002
- [12] McDonald, D.B., D.W.Pfeifer, and Sherman, M.R., *Corrosion Evaluation of Epoxy-Coated, Metallic-Clad and Solid Metallic Reinforcing Bars in Concrete*. 1998, Federal Highway Administration: McLean, VA.
- [13] Cui, F. and Krauss, P.D., Corrosion Resistance of Alternative Reinforcing Bars: An accelerated Test. 2006, CRSI: Schaumburg, IL.
- [14] Burke, D.F. Performance of Epoxy-coated Rebar, Galvanized Rebar, and Plain Rebar with Calcium Nitrite in a Marine Environment. in International Conference on Corrosion and Corrosion Protection of Steel in Concrete. 1994. England.

- [15] Swamy, R.N., et al. Durability of Steel Reinforcement in Marine Environment. in 2nd International Conference. 1988. St. Andrews by-the-Sea, Canada.: ACI.
- [16] Evaluation of Bridge Decks using Epoxy Coated Reinforcement. 1994, West Virginia Department of Transportation.
- [17] Gillis, H.J. and Hagen, M.G., *Field Examination of Epoxy-Coated Rebars in Concrete Bridge Decks.* 1994, Minnesota Department of Transportation: St. Paul, MN.
- [18] Weyers, R.E. and Cady, P.D., *Deterioration of Concrete Bridge Decks from Corrosion of Reinforcing Steel*. Concrete International, 1987: pp. 15-20.
- [19] Sohanghpurwala, A.A. and Scannell, W.T., Verification *of Effectiveness of Epoxy-Coated Bars*. 1998, Pennsylvania Department of Transportation: Ashburn, VA.
- [20] Fanous, F., Wu, H., and Pape, J., *Impact of Deck Cracking on Durability*. 2000, Center for Transportation Research and Education, Iowa State University: Ames, IA.
- [21] Lee, S.K. and Krauss, P.D., Long-Term Performance of Epoxy-Coated Reinforcing Steel in Heavy Salt-Contaminated Concrete. 2004, Federal Highway Administration: McLean, VA.
- [22] Smith, J.L. and Virmani, Y.P., *Performance of Epoxy-Coated Rebars in Bridge Decks*. 1996, Federal Highway Administration: McLean, VA.
- [23] Lee, S.K. and Krauss, P., Service Life Extension of Northern Bridge Decks Containing Epoxy-Coated Reinforcing Bars. 2003, Concrete Reinforcing Steel Institute: Schaumburg, IL.
- [24] Brown, D., *Epoxy-Coated Reinforcing Steel in Parking Garages*. Concrete Reinforcing Steel Institute (CRSI), 1997.
- [25] Sagues A.A., Perez-Duran H.M., and Powers R.G. Corrosion Performance of Epoxy-Coated Reinforcing Steel in Marine Substructure Service. in The NACE Annual Conference and Corrosion Show. 1991. Cincinnati, OH.
- [26] Sohanghpurwala, A.A., Scannell, W.T., and Hartt, W.H., *Repair and Rehabilitation of Bridge Components Containing Epoxy-Coated Reinforcement*. 2002, Transportation Research Board: Washington, DC.
- [27] Sohanghpurwala, A.A., *Manual on Service Life of Corrosion-Damaged Reinforced Concrete Bridge Superstructure Elements*. 2006, American Association of State Highway and Transportation Officials and Federal Highway Administration: Washington, DC.
- [28] ASTM-C666, Standard Test Method for Resistance of Concrete to Rapid Freezing and Thawing. 2003, West Conshohocker, PA: ASTM Internatinal.

- [29] Harichandran, R. S., and Baiyasi, M. I. "Repair of corrosion-damaged columns using FRP wraps." *Report No. RC-1386*, Michigan Department of Transportation, Lansing, Michigan. 2000.
- [30] MDOT, Special Provision for Thin Epoxy Polymer Bridge Deck Overlay. 2005, Michigan Department of Transportation: Lansing, MI.
- [31] MDOT, 2003 Standard Specifications for Construction. 2003, Michigan Department of Transportation: Lansing, MI.
- [32] MDOT, *Road Design Manual*. 2002, Michigan Department of Transportation: Lansing, MI.
- [33] AASHTO (2003). *LRFD Bridge Design Specifications*. American Association of State Highway Transportation Officials, Washington, D.C.
- [34] Halleck, Phillip M., Ryan, Timothy, and Stecko, Tim. Penn State University. Center for Quantitative X-Ray Imaging. 2010.
- [35] http://www.cqi.psu.edu/about.html; Accessed on June 14, 2010
- [36] Kutay, M. E. X-ray CT Image 3D Analysis Tool (XCAT). Michigan State University. 2010.
- [37] Rasband, W.S., ImageJ, U. S. National Institutes of Health, Bethesda, Maryland, USA, http://rsb.info.nih.gov/ij/, 1997-2009.
- [38] Ang, A.H-S., and Tang, W.H. *Probability Concepts in Engineering Planning and Design: Volume 1*, Wiley, New York, 1975.